

Number 813



**UNIVERSITY OF
CAMBRIDGE**

Computer Laboratory

Reconstructing compressed photo and video data

Andrew B. Lewis

February 2012

15 JJ Thomson Avenue
Cambridge CB3 0FD
United Kingdom
phone +44 1223 763500
<http://www.cl.cam.ac.uk/>

© 2012 Andrew B. Lewis

This technical report is based on a dissertation submitted June 2011 by the author for the degree of Doctor of Philosophy to the University of Cambridge, Trinity College.

Some figures in this document are best viewed in colour. If you received a black-and-white copy, please consult the online version if necessary.

Technical reports published by the University of Cambridge Computer Laboratory are freely available via the Internet:

<http://www.cl.cam.ac.uk/techreports/>

ISSN 1476-2986

Summary

Forensic investigators sometimes need to verify the integrity and processing history of digital photos and videos. The multitude of storage formats and devices they need to access also presents a challenge for evidence recovery. This thesis explores how visual data files can be recovered and analysed in scenarios where they have been stored in the JPEG or H.264 (MPEG-4 AVC) compression formats.

My techniques make use of low-level details of lossy compression algorithms in order to tell whether a file under consideration might have been tampered with. I also show that limitations of entropy coding sometimes allow us to recover intact files from storage devices, even in the absence of filesystem and container metadata.

I first show that it is possible to embed an imperceptible message within a uniform region of a JPEG image such that the message becomes clearly visible when the image is recompressed at a particular quality factor, providing a visual warning that recompression has taken place.

I then use a precise model of the computations involved in JPEG decompression to build a specialised compressor, designed to invert the computations of the decompressor. This recompressor recovers the compressed bitstreams that produce a given decompression result, and, as a side-effect, indicates any regions of the input which are inconsistent with JPEG decompression. I demonstrate the algorithm on a large database of images, and show that it can detect modifications to decompressed image regions.

Finally, I show how to rebuild fragmented compressed bitstreams, given a syntax description that includes information about syntax errors, and demonstrate its applicability to H.264/AVC Baseline profile video data in memory dumps with randomly shuffled blocks.

Acknowledgments

Firstly, I would like to thank my supervisor, Markus Kuhn, for his invaluable insights, advice and support.

Being a member of the Security Group has allowed me to learn about a huge variety of interesting and important topics, some of which have inspired my work. I am grateful to Markus Kuhn and Ross Anderson for creating this environment. I owe a debt of gratitude to my colleagues in the Security Group, especially Joseph Bonneau, Robert Watson, Saar Drimer, Mike Bond, Jonathan Anderson and Steven Murdoch, for their expertise and suggestions, and to my other friends at the Computer Laboratory, especially Ramsey Khalaf and Richard Russell.

I would like to thank Claire Summers and her colleagues at the London Metropolitan Police Service for motivating my work on video reconstruction, and providing information about real-world evidence reconstruction. I am grateful to the Computer Laboratory's technical staff, especially Pieter Brooks, who provided assistance with running experiments on a distributed computing cluster. I am also grateful to Trinity College and the Computer Laboratory for funding my work and attendance at conferences.

Finally, I am very grateful to my parents and brothers, who have been a constant source of support and encouragement.

Contents

1	Introduction	9
1.1	Outline	10
1.2	Notation	10
1.2.1	JPEG algorithm variables reference	12
2	Compression algorithms for photo and video data	13
2.1	Overview of data compression concepts	13
2.1.1	Bitstream syntax and entropy coding	15
2.2	Image compression	16
2.2.1	The JPEG still-image compression standard	17
2.2.2	The JPEG algorithm	18
2.3	Video compression	26
2.3.1	The H.264/AVC video compression standard	27
3	Copy-evidence in digital media	28
3.1	Prior work	29
3.1.1	Digital content protection schemes	29
3.1.2	Security printing	29
3.2	Digital copy-evidence	31
3.3	Quantisation in JPEG recompression	32
3.4	Marking method	33
3.4.1	Maximising distortion	33
3.4.2	Embedding	34

3.4.3	Clipping of IDCT output	35
3.5	Marking algorithm	35
3.5.1	Termination conditions and unmarkable blocks	36
3.5.2	Gamma-correct marking	37
3.5.3	Untargeted marks	38
3.5.4	Results	39
3.6	Analysis	41
3.6.1	Possible extensions to the algorithm	42
3.7	Conclusion	43
4	Exact JPEG recompression	44
4.1	Introduction	44
4.1.1	Exact recompression	45
4.1.2	Comparison with naïve recompression	46
4.1.3	Decompressor implementations	46
4.2	Applications	47
4.2.1	Avoiding quality loss	47
4.2.2	Compressor and parameter identification	47
4.2.3	Tampering detection	48
4.3	Prior work	48
4.3.1	Maintaining image quality during recompression	48
4.3.2	Acquisition forensics	49
4.3.3	Tampering detection	52
4.3.4	Residual information in JPEG artefacts	55
4.4	Exact recompression of JPEG images	55
4.4.1	Colour-space conversion	56
4.4.2	Chroma down-sampling	57
4.4.3	Discrete cosine transform	59
4.4.4	Determining possible quality factors	60
4.4.5	Quantisation and exhaustive search	61

4.4.6	YCbCr set refinement	63
4.5	Overall algorithm summary	63
4.6	Results	64
4.6.1	Detecting in-painting	67
4.7	Analysis	68
4.7.1	Possible extensions to the algorithm	69
4.8	Conclusion	70
5	Reconstruction of fragmented compressed data	71
5.1	Overview	71
5.1.1	Terminology	73
5.2	Background and prior work	74
5.2.1	Data acquisition, fragmentation and filesystems	74
5.2.2	Unfragmented file carving	76
5.2.3	Fragmented file carving	77
5.2.4	H.264/AVC error detection	80
5.3	The defragmentation problem	81
5.3.1	Syntax checkers	81
5.3.2	Decoding contexts	81
5.3.3	Finding valid bitstreams and defragmentation	83
5.3.4	False positives	83
5.4	Bitstream syntax description	83
5.4.1	The bitstream syntax flowgraph	85
5.4.2	Textual representation of bitstream syntax	87
5.5	H.264/AVC bitstream syntax checking	88
5.5.1	Assumptions about the video	88
5.5.2	Coding modes	91
5.5.3	NAL unit syntax	94
5.5.4	Error detection performance	97
5.6	Fragmented bitstream recovery algorithm	104

5.6.1	Algorithm notation and objects	106
5.6.2	Configuration bitstream parsing and data bitstream offset search	107
5.6.3	Data bitstream filtering	107
5.6.4	Data bitstream mapping (optional)	109
5.6.5	Data bitstream block search algorithm	111
5.7	Results	113
5.7.1	Input data	113
5.7.2	Data bitstreams	114
5.7.3	Proportion of data recovered successfully	116
5.8	Analysis	116
5.8.1	Possible extensions to the algorithm	116
5.9	Conclusion	117
6	Conclusions	121
A	JPEG encoder quality selection	124
A.1	IJG encoder	124
A.2	Adobe Photoshop CS2	124
B	H.264/AVC bitstream syntax	127

Chapter 1

Introduction

Compressed photo and video data files present both opportunities and challenges to forensic investigators dealing with digital evidence. Huge quantities of compressed data are generated every day by consumer digital cameras and commercial image/video recording systems. This motivates the development of algorithms which recover evidence from devices and detect tampering on visual data that has undergone lossy compression. The algorithms are of particular use to law enforcement agencies and journalists, who must routinely deal with compressed data with uncertain processing history.

A central challenge in digital forensics is the extraction of information from devices where details of storage formats or filesystem layouts is unavailable, due to a lack of documentation. Metadata might have been deleted deliberately, or might be invalid due to data corruption. The multitude of different devices storing video, some using proprietary container formats and filesystems, is a problem for forensics labs that receive evidence from many sources. Manual procedures for evidence recovery are time-consuming and require skilled investigators with knowledge of the characteristics of hardware, software, file formats and compression standards. Therefore, automatic, general-purpose algorithms that do not rely on detailed knowledge of the devices will be increasingly important as the volume of digital evidence to process becomes greater.

The widespread use of digital photo manipulation software provides an opportunity for forensic investigators. Alterations can affect hidden statistical correlations in photos and videos, which may expose an attempt to deceive the viewer. Investigators can exploit the disruption of the patterns introduced by compression algorithms early in a document's processing history as an indication that tampering has taken place.

1. Introduction

1.1 Outline

In this thesis, I show that it is possible to exploit the low-level details of compression schemes and their implementations to develop automatic tampering detection and data recovery algorithms that are applicable in scenarios involving compressed data.

Chapter 2 begins with a description of the JPEG compression scheme and the calculations performed by one decompressor implementation. Chapter 3 describes one approach to achieving copy-evidence properties in a JPEG image, taking advantage of the effects of a JPEG compression/decompression cycle. I show that it is possible to embed a low-resolution bi-level image within a homogeneous area of a cover image, which is imperceptible to viewers of the original document, but which becomes visible when the image is recompressed using particular quality settings.

Chapter 4 describes a specialised JPEG compressor which recovers compressed image data bitstreams given a decompression result as input. As a side-effect, the algorithm determines whether any regions of the decompression result were modified. It has applications in content protection system circumvention and tampering detection, and can be used to maintain image quality in processing pipelines that use compressed data.

Chapter 5 describes an automatic data recovery tool that locates and reconstructs fragmented compressed bitstreams, and demonstrates its applicability on memory dumps containing H.264/AVC Baseline profile video data. The tool uses a description of the compressed bitstream syntax, but does not rely on detailed knowledge of the video container or filesystem allocation unit ordering.

Finally, chapter 6 draws some conclusions and gives suggestions for future work.

1.2 Notation

This section describes the notational conventions I use throughout this thesis.

For a matrix \mathbf{a} (with h rows and w columns), the element in row i and column j is denoted by $a_{i,j} = (\mathbf{a})_{i,j}$ ($0 \leq i < h$, $0 \leq j < w$). I sometimes write $a[j, i]$ for the same value, where the indexing order is swapped.

The matrix transpose $\mathbf{b} = \mathbf{a}^\top$ has elements $b_{i,j} = a_{i,j}^\top = a_{j,i}$.

\mathbf{a}_j (or $\mathbf{a}[j]$) is the column vector $(a_{0,j}, \dots, a_{h-1,j})^\top$ and $(\mathbf{a}^\top)_j$ denotes the column vector $(a_{j,0}, \dots, a_{j,w-1})^\top$. The value at index i in \mathbf{a}_j is $a_j[i] = a_{i,j}$. I also use the notation $\mathbf{a}_j[s : e]$ to denote the vector $(a_{s,j}, \dots, a_{e-1,j})^\top$.

When indexing two-dimensional signals represented as vectors in raster-scan order, I use the

following notation:

$$\langle x, y \rangle_w = x + w \cdot y \quad (1.1)$$

$$\langle x, y \rangle_{w,h} = \langle \min(x, w-1), \min(y, h-1) \rangle_w \quad (1.2)$$

$$\langle i \rangle_w^{-1} = (i \bmod w, \lfloor i/w \rfloor) \quad (1.3)$$

I use the following functions, defined similarly over sets:

$$\max(x, y) = \begin{cases} x & x \geq y \\ y & x < y \end{cases} \quad (1.4)$$

$$\min(x, y) = \begin{cases} x & x \leq y \\ y & x > y \end{cases} \quad (1.5)$$

and $\text{sgn}(x) = x/|x|$ for non-zero x , and 0 otherwise.

Matrices containing sets of integers are written like $\bar{\mathbf{s}}$. I make use of integer intervals $\bar{x} = [x_{\perp}, x_{\top}]$, which contains integers from x_{\perp} to x_{\top} inclusive, and matrices containing intervals over the integers are denoted by $\bar{\mathbf{x}}$. $y \in \bar{x} \Leftrightarrow x_{\perp} \leq y \leq x_{\top} \wedge y \in \mathbb{Z}$. “Union” and intersection on such intervals are defined as

$$\begin{aligned} \bar{x} \cup \bar{y} &:= [\min(x_{\perp}, y_{\perp}), \max(x_{\top}, y_{\top})] \\ \bar{x} \cap \bar{y} &:= \begin{cases} \text{empty} & \text{if } x_{\perp} > y_{\top} \vee y_{\perp} > x_{\top}, \\ [\max(x_{\perp}, y_{\perp}), \min(x_{\top}, y_{\top})] & \text{otherwise.} \end{cases} \end{aligned}$$

$\lfloor x \rfloor$ denotes the largest integer less than or equal to x , and $\lceil x \rceil$ denotes the smallest integer greater than or equal to x (for real x). For scalar division I define

$$\begin{aligned} \text{divround}(x, q) &= \text{sgn}(x) \cdot \lfloor (|x| + \lfloor q/2 \rfloor) / q \rfloor, \\ \text{div}(x, q) &= \text{sgn}(x) \cdot \lfloor |x| / q \rfloor \quad \text{for non-zero } q. \end{aligned}$$

Multiplying a tuple by a scalar multiplies each element by the scalar: $\alpha \cdot (x_1, \dots, x_N) = (\alpha \cdot x_1, \dots, \alpha \cdot x_N)$. Addition is element-wise for two tuples of the same length N : $(x_1, \dots, x_N) + (y_1, \dots, y_N) = (x_1 + y_1, \dots, x_N + y_N)$.

1. Introduction

1.2.1 JPEG algorithm variables reference

Matrix	Rows \times Columns	Interpretation
\mathbf{u}	$3 \times w \cdot h$	$w \times h$ pixel image in the RGB colour space
\mathbf{v}	$3 \times w \cdot h$	\mathbf{u} in the YC_bC_r colour space
\mathbf{v}^-	$3 \times \lceil w/2 \rceil \cdot \lceil h/2 \rceil$	down-sampled \mathbf{v}
\mathbf{v}_0^T	$w \cdot h \times 1$	full-resolution luma
\mathbf{v}_1^{-T}	$\lceil w/2 \rceil \cdot \lceil h/2 \rceil \times 1$	down-sampled chroma
\mathbf{v}_2^{-T}	$\lceil w/2 \rceil \cdot \lceil h/2 \rceil \times 1$	down-sampled chroma
\mathbf{x}_b	8×8	b th MCU in one component
\mathbf{X}_b	8×8	\mathbf{x}_b in the DCT domain
\mathbf{Q}^Y	8×8	quantisation coefficients for luma
\mathbf{Q}^C	8×8	quantisation coefficients for chroma
$\hat{\mathbf{X}}_b$	8×8	DCT coefficients \mathbf{X}_b after quantisation
\mathbf{X}'_b	8×8	reconstructed DCT coefficients
\mathbf{x}'_b	8×8	b th reconstructed MCU in one component
\mathbf{v}'_1^{-T}	$\lceil w/2 \rceil \cdot \lceil h/2 \rceil \times 1$	reconstructed down-sampled chroma
\mathbf{v}'_2^{-T}	$\lceil w/2 \rceil \cdot \lceil h/2 \rceil \times 1$	reconstructed down-sampled chroma
\mathbf{v}'_0^T	$w \cdot h \times 1$	reconstructed full-resolution luma
\mathbf{v}'_1^T	$w \cdot h \times 1$	up-sampled chroma
\mathbf{v}'_2^T	$w \cdot h \times 1$	up-sampled chroma
\mathbf{v}'	$3 \times w \cdot h$	reconstructed image in the YC_bC_r colour space
\mathbf{u}'	$3 \times w \cdot h$	reconstructed image in the RGB colour space

Chapter 2

Compression algorithms for photo and video data

This chapter introduces visual data compression algorithms and describes the JPEG algorithm, used in chapters 3 and 4.

The development of efficient image and video compression algorithms for content distribution was originally driven by the telecommunications and entertainment industries, but a diverse range of consumer devices, including mobile telephones, cameras and mobile computers, now include software and hardware compressors for visual data. Since the majority of image and video files on electronic devices and Internet servers are stored in compressed form, forensic investigators must mostly deal with files that have previously been compressed.

The reconstruction algorithms in this thesis make use of the JPEG still image compression standard [38] and the H.264/AVC video compression standard [45], which are freely available. We generally rely on features of the relevant compression schemes that are likely to be shared by other standards.

2.1 Overview of data compression concepts

Practical compression system implementations (for standards such as MPEG-1/2/4, JPEG, PNG, ...) include two programs: an encoder and a decoder.

The *encoder* program, or compressor, takes uncompressed source data as input (for example, pixel values), removes redundant/irrelevant information, and returns a binary file called a *bitstream*, which represents the remaining data along with any requisite metadata for decompression.

The *decoder* program, or decompressor, takes a bitstream produced by an encoder as input and returns an uncompressed file in the same format as the original source; this file is either

2. Compression algorithms for photo and video data

identical to the source file, in the case of lossless compression, or is perceptually similar to it, in the case of lossy compression.

Because lossless compression systems must define a bijection between source and compressed data files, some files will in practice expand when they are encoded.

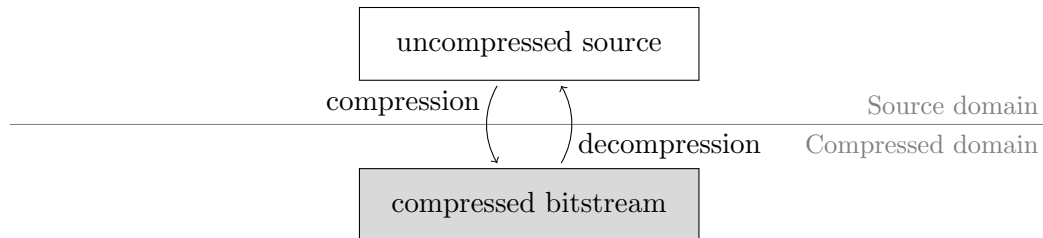


Figure 2.1: Lossless compression algorithms take source data and produce bitstreams which decompress to produce a file identical to the source data.

Lossy compression systems aim to remove both redundant and irrelevant data, normally making it impossible to reconstruct the exact file which was input. These compressors should keep perceptually important information and discard information which is not important to the observer of the decompression result. Audio/visual compression systems, for example, typically include a psychophysical model of the limitations of the human auditory/visual systems, so that information is discarded only when it cannot be heard or seen by the observer (due to variations in sensitivity to different inputs, masking and filtering inherent in human hearing/vision).

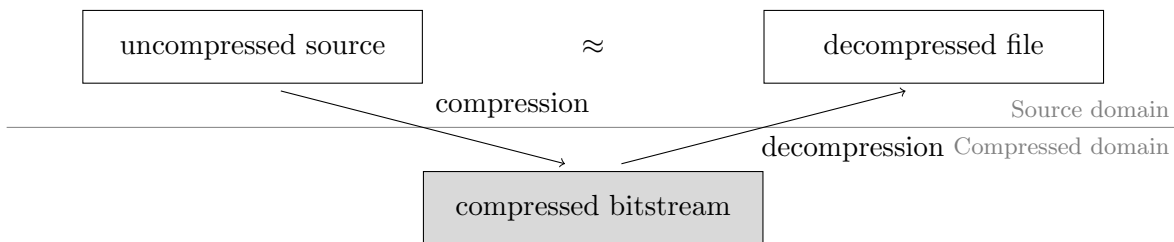


Figure 2.2: Lossy compression algorithms take source data and produce bitstreams which decompress to produce a file similar to the source data.

Designers of general-purpose compression algorithms optimise jointly for file size, computational complexity and, in the case of lossy algorithms, to minimise the distortion introduced by a compression/decompression cycle. More flexible compressor implementations present an interface where the user can specify a target bitrate, which can be calculated from the duration of the input (if known) and a target output file size.

Some lossy encoders allow the user to choose between constant or variable bitrate modes. Constant bitrate (CBR) encoding tries to keep a consistent rate throughout the document

(measured over a particular window size in the signal, such as per frame of a video), while variable bitrate (VBR) encoding can distribute bits in the output bitstream unevenly, allocating fewer bits to more predictable parts of the signal.

Two-pass compression algorithms are often used in conjunction with the VBR strategy. They first measure the relative complexity of different parts of the signal (for example, scenes in a video), then write the output bitstream during a second pass over the input, taking advantage of information about the entire signal. The overall aim is to achieve constant perceived quality.

Lossy compressors often have to choose between several options, each one making a different trade-off between bit cost and perceived distortion. These choices arise when coding values for quantised transform coefficients, motion vectors, and so on. Rate-distortion optimisation (RDO) is the action of choosing between several options, trying to minimise distortion whilst keeping within a bit-budget. To perform this minimisation, encoders try to avoid situations where it is possible to reallocate bits between independently coded features whilst reducing overall perceived distortion¹.

Useful compression schemes will map nearly all typical inputs onto smaller encoded bitstreams, whilst making good RDO decisions for a particular rate/distortion trade-off.

Salomon gives an overview of many lossy and lossless compression schemes [89].

2.1.1 Bitstream syntax and entropy coding

The overall structure of encoders varies significantly with the type of information processed. However, most encoders have a final lossless coding step, which maps the calculated, reduced redundancy data onto a binary stream for output. The data are normally integer values, each associated with a named syntax element, which denotes the meaning of the value (a sample from an image, a flag indicating presence of another value, etc.). A syntax element may have multiple, ordered values, which are associated with different decoding positions (transform coefficient indices, picture regions, frame numbers, etc.).

The standardisation document for the compression scheme describes a *bitstream syntax*, which is a graph specifying the order and coding mode of syntax element values which appear in valid bitstreams. Compliant encoders output bitstreams that a decoder can parse by referring to this syntax flowgraph.

There are two categories of coding modes. Symbol coding modes map syntax element values onto separate bitstrings, which are concatenated to produce the final bitstream. Stream coding modes map a sequence of syntax element values onto a single long bitstring, where each syntax element value may affect a non-integer number of bits. The overall process of turning the

¹In practice, this is usually achieved by selecting for each coding decision the option that has its local rate vs. distortion gradient closest to a known value λ . This parameter is chosen based on the desired bitrate or quality.

2. Compression algorithms for photo and video data

sequence of syntax element values into a bitstream based on their coding modes as specified in the bitstream syntax is called *entropy coding*.

If a symbol to be coded is associated with a random variable S_i with probability distribution $P(S_i)$, it should be coded so that the length of the codeword is as close as possible to the amount of information communicated by the observation of the symbol, $H(S_i) = -\log_2 P(S_i)$ bits. The probability distribution may be estimated based on prior knowledge of the source, shared by both the encoder and decoder, and can be updated at runtime after observing other syntax element values.

Huffman symbol coding maps each symbol onto an integer number of bits. It has two main limitations: firstly, the scheme is only optimal when each probability, $P(S_i) = 2^{-k}$ for some k , so that the rate of the code is equal to the entropy of the probability distribution. If any symbol has probability $P(S_i) > \frac{1}{2}$, variable-length coding must still output at least one bit, wasting between 0 and 1 bits per symbol. Secondly, Huffman codes cannot adapt elegantly to changes in symbol probabilities. Arithmetic coding remedies these problems, outputting a fractional number of bits per input symbol [71, Section 5.6: Disadvantages of the Huffman Code, page 101].

2.2 Image compression

In natural images, neighbouring pixels' intensities are normally highly correlated. Some dependency in audio/visual data is due to correlation, and correlation is more practical to tackle than dependency. Therefore, all algorithms for natural image compression work by removing redundancy due to correlation.

The most general source coding algorithms predict a value (such as a pixel intensity) based on its neighbourhood, and entropy-code the prediction error signal using probabilities which are based on the neighbourhood (see for example [10]). For this technique to work well in natural images, large neighbourhoods must be considered, using a lot of memory and requiring a large corpus of training images, as well as slowing down adaptation to changing image content.

Most compression algorithms for natural images instead use less expensive *transform coding* algorithms [32], where spatial domain information is linearly, reversibly transformed into a new representation that decorrelates pixel values. Ideally, the input to the final entropy coding step should be a sequence of independent random variables with known probability distributions, so that each output bit communicates close to one bit of information (on average).

2.2.1 The JPEG still-image compression standard

The lossy compression method described in the JPEG standard (ITU-T recommendations T.81 and T.83, ISO/IEC 10918-1/2 [38, 39]) has emerged as the most widely-used algorithm² for encoding continuous-tone still images for transmission and storage since its first publication in 1992. It affords compression ratios of 0.05–0.10 with almost no perceived loss in quality [89, Section 4.8 JPEG, page 337].

The first part of the JPEG standard (Digital compression and coding of continuous-tone still images: Requirements and guidelines, ITU-T recommendation T.81 (September 1992), ISO/IEC 10918-1:1994 [38]) specifies the compressed bitstream format normatively, and describes some elements of the compressor and decompressor informatively. Without additional metadata, the interchange format it specifies is known as JPEG Interchange Format (JIF). This format lacks information about the resolution (in dots per inch, for example), colour space and sampling pattern of the image. However, it includes fields for extension information (‘application markers’).

Digital cameras use the Exchangeable image file format [47] (Exif). It embeds useful metadata relevant to digital photographs, such as the location and date/time of capture, camera model and manufacturer, exposure duration and f-number, colour information and so on, within JIF’s extension fields. The older JPEG File Interchange Format [44] (JFIF) is sometimes used as an alternative.

The second part of the JPEG standard [39] (Digital compression and coding of continuous-tone still images: Compliance testing, ITU-T recommendation T.83 (November 1994), ISO/IEC 10918-2:1995) places restrictions on decompressor outputs. Because the first part of the standard does not give exact formulae for some calculations, implementations may use any algorithm which produces results within the specified tolerances.

The lossy, non-hierarchical compression algorithm described in the JPEG standard has several options for coding images: pixel values may be represented either to 8-bit (baseline) or 12-bit precision; the colour space used to represent pixel values may be chosen; the monochrome plane (rectangular array of integer samples) corresponding to each colour channel may be down-sampled horizontally, vertically or in both directions; two entropy coding schemes are specified (Huffman (variable-length) and arithmetic coding); and the order of coding may be sequential or progressive, where a reduced-quality version of the image is gradually refined during decoding. Though the colour space conversion and down-sampling steps are not described in the JPEG standard itself, all practical implementations must support these operations.

The most common choice of options encodes an 8 bits per sample red/green/blue (RGB) image using a luma/chroma (YC_bC_r) colour space with horizontally and vertically down-sampled

²The hierarchical and lossless coding techniques describe in the standard are less commonly used, and we do not consider them here.

2. Compression algorithms for photo and video data

chroma channels (also known as 4:2:0 down-sampling³) to a sequentially-ordered Huffman coded bitstream. Unless otherwise specified, I will assume these options are chosen when I refer to the JPEG algorithm.

2.2.2 The JPEG algorithm

High performance JPEG codecs use limited precision machine integer arithmetic to represent intermediate results in fixed-point, making a trade-off between accuracy and speed, while meeting the requirements of the compliance testing part of the standard [39].

The following description of the encoder uses formulae which are equivalent to the operations described in the standard, while the subsequent description includes the integer arithmetic (fixed-point) calculations performed by the Independent JPEG Group (IJG) decoder implementation (version 6b) [57].

Compression

1. An input bitmap in the RGB colour space is first converted to the $Y C_b C_r$ colour space.

In natural images, this reduces the inter-component correlations in pixel values, and allows the colour and brightness information to be processed independently.

We represent a $w \times h$ pixel uncompressed bitmap image with 3×8 -bit samples per pixel (red, green, blue) as a matrix \mathbf{u} with $w \cdot h$ columns and 3 rows. The tuple $(\mathbf{u}_i)^\top \in \{0, \dots, 255\}^3$ ($0 \leq i < w \cdot h$) contains the (red, green, blue) samples for the pixel at location $(x, y) = (i \bmod w, \lfloor i/w \rfloor) = \langle i \rangle_w^{-1}$.

A $Y C_b C_r$ representation \mathbf{v} of this RGB image \mathbf{u} is given by the per-pixel calculation

$$\mathbf{v}_i = \begin{pmatrix} 0.299 & 0.587 & 0.114 \\ -0.169 & -0.331 & 0.500 \\ 0.500 & -0.419 & -0.081 \end{pmatrix} \mathbf{u}_i + \begin{pmatrix} 0 \\ 128 \\ 128 \end{pmatrix}. \quad (2.1)$$

The transformed samples can be recovered in a decompressor by multiplication with the inverse matrix

$$\begin{pmatrix} 1.000 & 0.000 & 1.402 \\ 1.000 & -0.344 & -0.714 \\ 1.000 & 1.772 & 0.000 \end{pmatrix} \quad (2.2)$$

where all values are rounded to four significant figures.

³This notation for chroma down-sampling schemes is decoded as follows: $w:a:b$ indicates that in two rows of w luma samples, the first row contributes a chroma samples and the second row contributes b additional chroma samples. (w is known as the luma sampling reference, originally relative to a sampling rate of 3.375 MHz in broadcast television.)

Figure 2.3 shows the RGB axes from three different viewpoints in the tri-chromatic colour space, and the YC_bC_r axes which contain the RGB cube. We plot pixels from a 16×16 neighbourhood in the ‘Lena’ sample image as circles filled in with the respective pixel’s colour. The luma (Y) axis distribution has higher variance than the chroma axis distributions, indicating that the colour space transform has some decorrelating effect in this example.

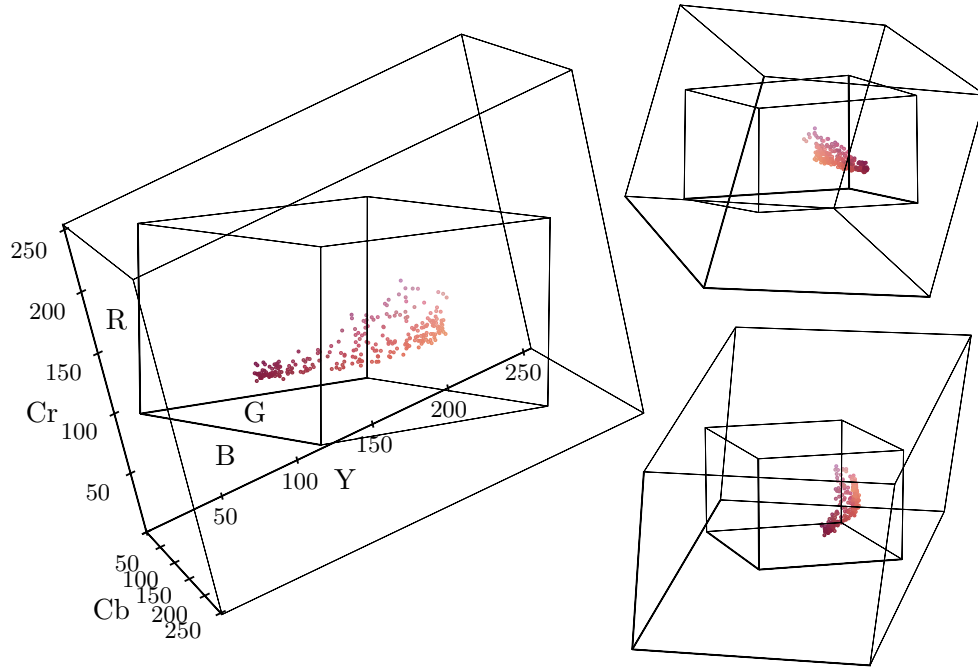


Figure 2.3: The RGB to YC_bC_r colour space conversion as a coordinate transform

If an encoder implementation uses integer arithmetic to perform the colour space conversion, information may be lost due to rounding.

2. The Y, C_b and C_r components resulting from colour space conversion are processed independently. The two chroma components are each down-sampled horizontally and vertically by a factor of two, while the luma component is left at its original resolution.

The human visual system (HVS) has better acuity for brightness than colour, because the central part of the retina (the fovea) has a lower density of short-wavelength adapted photoreceptors than medium- and long-wavelength adapted photoreceptors. The latter two types of receptor exhibit large amounts of overlap in spectral sensitivity (their peak responses lie only 30 nm apart) [17, Section 4.3.4, page 221]. The brain has more cells dedicated to addition of the medium/long wavelength receptors’ signals than to their subtraction. This makes the HVS more sensitive to errors in luma (the additive signal) than colour. The encoder can therefore store colour information with less precision and resolution than the luma channel without seriously affecting the perceived image quality.

2. Compression algorithms for photo and video data

The YC_bC_r image \mathbf{v} is padded by repetition so that its width and height are both multiples of two. The down-sampling operation averages non-overlapping squares of 2×2 pixels, giving \mathbf{v}^- .

The down-sampling operation (with input padding where necessary) can be implemented as

$$\mathbf{v}^-_i = \frac{1}{4} \sum_{\delta \in \{0,1\}^2} \mathbf{v}[\langle 2 \cdot \langle i \rangle_{\lceil w/2 \rceil}^{-1} + \delta \rangle_{w,h}], \quad (2.3)$$

for $0 \leq i < \lceil w/2 \rceil \cdot \lceil h/2 \rceil$.

If both chroma components are down-sampled horizontally and vertically by a factor of two, the total number of samples is halved.

3. The full-resolution luma component and down-sampled chroma components are each divided up into non-overlapping 8×8 sample blocks, known as minimum coded units (MCUs), which are processed independently.

After down-sampling of the chroma components, the YC_bC_r component tuple $(\mathbf{v}^T_0, \mathbf{v}^{-T}_1, \mathbf{v}^{-T}_2)$, with dimensions $((w, h), (\lceil w/2 \rceil, \lceil h/2 \rceil), (\lceil w/2 \rceil, \lceil h/2 \rceil))$, represents the image content. The following processing steps are applied to each component $\mathbf{c} \in \{\mathbf{v}^T_0, \mathbf{v}^{-T}_1, \mathbf{v}^{-T}_2\}$ separately; we denote the width and height of \mathbf{c} by n and m respectively.

The right and bottom edges of the component must be padded if its width or height are not multiples of 8. The standard does not specify what values should be used for padding data. In this example, we pad by repeating the right and bottom edge sample values. A decoder decompresses the padded component and crops it based on size metadata in the bitstream. The compressor can subtract 128 from each sample, which reduces the dynamic range requirements on the following transform step. (Mathematically, this is equivalent to subtracting 1024 from the lowest frequency component after the transform.) The b th MCU of \mathbf{c} , the 8×8 matrix \mathbf{x}_b , is given by

$$(\mathbf{x}_b)[j, i] = c[\langle 8 \cdot \langle b \rangle_{\lceil n/8 \rceil}^{-1} + (i, j) \rangle_{n,m}] - 128 \quad (2.4)$$

for $0 \leq i, j < 8$ and $0 \leq b < \lceil n/8 \rceil \cdot \lceil m/8 \rceil$.

An 8×8 forward discrete cosine transform (DCT)⁴ is applied to each MCU in each component. The 2-D DCT is a linear, separable transform which represents a block of sample values as the weights of sampled cosine functions at various frequencies. Figure 2.4 shows one of the transform's basis vectors along with the 1-D horizontally and vertically orientated cosine functions which are multiplied to give the 2-D function. The

⁴Specifically, the type two DCT is used, which interprets its input vector as being even around the point half-way between its first sample and the previous sample in the periodic extension.

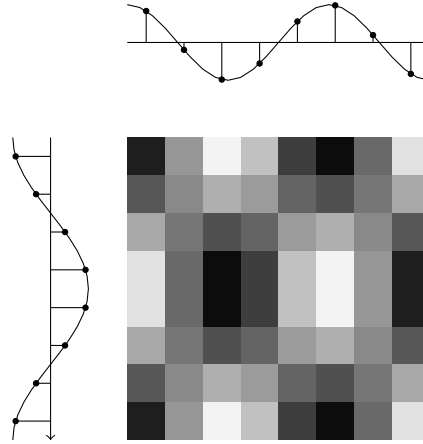


Figure 2.4: Cosines with 3/16 cycles per sample (horizontal) and 2/16 cycles per sample (vertical), and the 2-D DCT basis vector formed by their product.

representation of an MCU \mathbf{x}_b in the DCT basis is given by

$$(\mathbf{X}_b)_{u,v} = \frac{C(u)}{\sqrt{N/2}} \frac{C(v)}{\sqrt{N/2}} \sum_{i=0}^{N-1} \sum_{j=0}^{N-1} (\mathbf{x}_b)_{i,j} \cos\left(\frac{(2i+1)u\pi}{2N}\right) \cos\left(\frac{(2j+1)v\pi}{2N}\right), \quad (2.5)$$

where $0 \leq u, v < 8$ and

$$C(u) = \begin{cases} \frac{1}{\sqrt{2}} & u = 0 \\ 1 & u > 0. \end{cases}$$

An example decomposition of an 8×8 matrix of samples (from the ‘Lena’ sample image) into a weighted sum of the DCT basis vectors can be visualised as follows:

$$\begin{aligned} \blacksquare &= 1203 \cdot \blacksquare + 123 \cdot \blacksquare - 26 \cdot \blacksquare + 9 \cdot \blacksquare + 6 \cdot \blacksquare + 4 \cdot \blacksquare - 4 \cdot \blacksquare - 1 \cdot \blacksquare \\ &- 25 \cdot \blacksquare + 9 \cdot \blacksquare + 8 \cdot \blacksquare + 9 \cdot \blacksquare - 8 \cdot \blacksquare + 5 \cdot \blacksquare + 2 \cdot \blacksquare + 1 \cdot \blacksquare \\ &+ 18 \cdot \blacksquare - 10 \cdot \blacksquare - 1 \cdot \blacksquare - 3 \cdot \blacksquare + 0 \cdot \blacksquare + 5 \cdot \blacksquare + 0 \cdot \blacksquare + 2 \cdot \blacksquare \\ &- 12 \cdot \blacksquare + 8 \cdot \blacksquare + 7 \cdot \blacksquare - 4 \cdot \blacksquare + 3 \cdot \blacksquare - 6 \cdot \blacksquare - 1 \cdot \blacksquare + 3 \cdot \blacksquare \\ &+ 12 \cdot \blacksquare - 3 \cdot \blacksquare - 4 \cdot \blacksquare + 6 \cdot \blacksquare - 2 \cdot \blacksquare + 3 \cdot \blacksquare + 1 \cdot \blacksquare - 3 \cdot \blacksquare \\ &- 6 \cdot \blacksquare + 4 \cdot \blacksquare + 4 \cdot \blacksquare - 3 \cdot \blacksquare + 5 \cdot \blacksquare - 4 \cdot \blacksquare - 4 \cdot \blacksquare + 2 \cdot \blacksquare \\ &+ 0 \cdot \blacksquare - 1 \cdot \blacksquare - 4 \cdot \blacksquare + 4 \cdot \blacksquare - 4 \cdot \blacksquare - 1 \cdot \blacksquare + 0 \cdot \blacksquare + 0 \cdot \blacksquare \\ &- 1 \cdot \blacksquare + 3 \cdot \blacksquare + 1 \cdot \blacksquare - 3 \cdot \blacksquare + 6 \cdot \blacksquare + 1 \cdot \blacksquare - 2 \cdot \blacksquare + 2 \cdot \blacksquare \end{aligned} \quad (2.6)$$

The scalar coefficients are known as the *DCT coefficients* for the transformed block. In this example, the DCT coefficients are rounded to integers.

In an encoder implementation which uses integer arithmetic, some information may be lost due to rounding of DCT coefficients, intermediate results and basis function samples.

4. In photographic images, the DCT coefficients are much less correlated than the spatial-domain samples. The JPEG algorithm now discards information by uniformly quantising each DCT coefficient in each MCU. The quantisation factor depends on the coefficient’s

2. Compression algorithms for photo and video data

associated spatial frequency, the component plane being processed (luma/chroma) and, usually, a user-specified quality parameter. The quantisation factors are kept in two 8×8 *quantisation tables* (one for the luma component and one for the two chroma components), stored in the header of the bitstream.

The user of the encoder normally controls the choice of quantisation tables indirectly, via a scalar *quality factor* which multiplies the standardised, default quantisation tables. Other schemes are also possible; appendix A describes how quantisation factors are chosen in two popular encoder implementations (IJG [57] and Adobe Photoshop CS2 [37]).

As noted earlier, the HVS has higher acuity in brightness compared to colour vision. We are also more sensitive to errors in the amplitude of lower frequency signals. The default quantisation tables [38, Tables K.1, K.2] specify (a) more aggressive quantisation for DCT coefficients corresponding to higher spatial frequencies and (b) more aggressive quantisation for DCT coefficients in chroma blocks. Information deemed to be less perceptually important will be discarded.

The quantisation factor for a given spatial frequency, $(u, v) \in \{0, \dots, 7\}^2$ half-cycles per block, is drawn from the relevant quantisation table for the component being processed, \mathbf{Q}^Y for luma blocks and \mathbf{Q}^C for chroma blocks.

Each DCT coefficient $(\mathbf{X}_b)_{u,v}$ in each block in each component is quantised using the appropriate entry from the quantisation table, $Q_{u,v}$, by the following calculation:

$$(\hat{\mathbf{X}}_b)_{u,v} = \text{divround}((\mathbf{X}_b)_{u,v}, Q_{u,v}) = \text{sgn}((\mathbf{X}_b)_{u,v}) \cdot \left\lfloor \frac{|(\mathbf{X}_b)_{u,v}| + \lfloor Q_{u,v}/2 \rfloor}{Q_{u,v}} \right\rfloor. \quad (2.7)$$

5. All further coding is lossless, using a Huffman code table shared between the encoder and decoder. The standard specifies general purpose tables, but also specifies a syntax which allows encoders to include their own tables in the bitstream.

The majority of the data in the JPEG bitstream for a typical compressed image will consist of Huffman codewords representing quantised DCT coefficients, $(\hat{\mathbf{X}}_b)_{u,v}$. To code blocks of quantised DCT coefficients compactly, the entropy coding step (1) re-orders quantised DCT coefficients in a zig-zag pattern (figure 2.6), (2) encodes (run, level) pairs, indicating a run of zeros followed by the value level, (3) uses a short codeword for the ‘end of block’ (EOB) symbol, which indicates that all further coefficients in the re-ordered sequence are zero and (4) encodes the top-left $(0, 0)$ cycles per block coefficient (the DC coefficient) as a difference from the equivalent value in the previous block, as they will normally be correlated in nearby blocks.

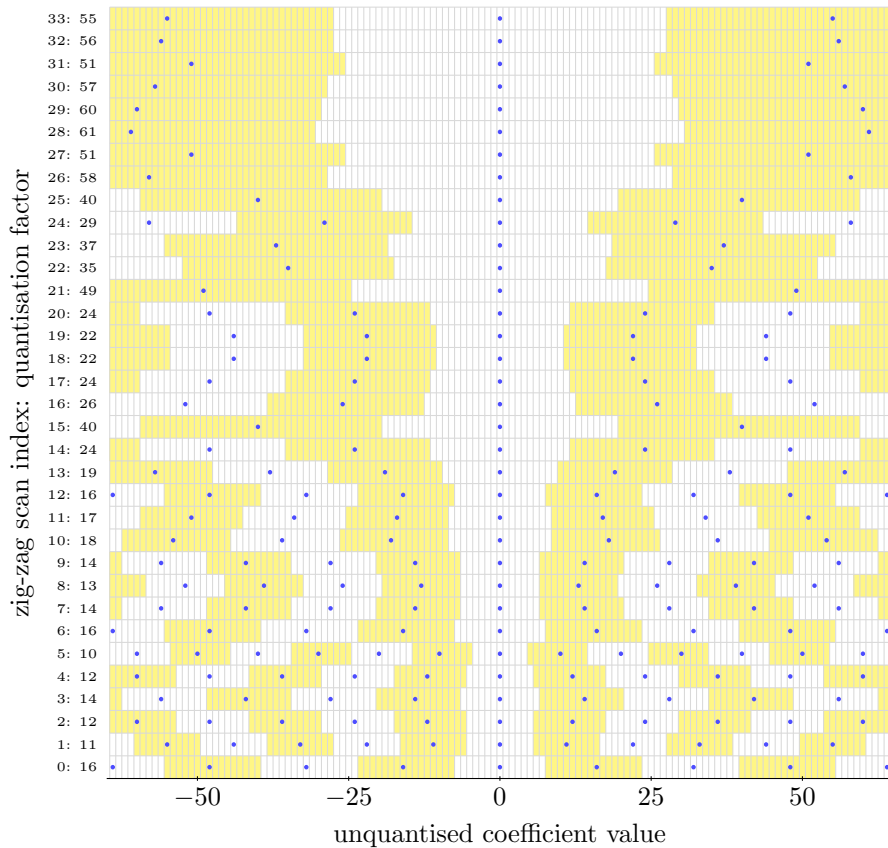


Figure 2.5: Each row of this chart is associated with a particular DCT coefficient position in zig-zag scan order (see figure 2.6). The alternately shaded rectangles in each row cover groups of DCT coefficient values that are mapped onto the same quantised coefficient; the corresponding dequantised coefficient value is indicated by a circle at the centre of the group. The quantisation table is [38, Table K.1, page 143].

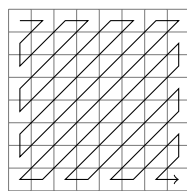


Figure 2.6: The encoder re-orders quantised DCT coefficients so that later coefficients in the bitstream correspond to higher spatial frequencies.

Decompression

1. The IJG decoder is structured to use memory sparingly, so that it can run on embedded devices which have little storage available. The decoder performs lossless decoding of Huffman codewords in the stream as they are required, sequentially loading each MCU row into a buffer for processing. Each MCU in each row contains 64 quantised DCT coefficients.
2. Each quantised DCT coefficient in each MCU is dequantised. This operation maps the coefficient onto an integer multiple of the relevant quantisation factor. The quantisa-

2. Compression algorithms for photo and video data

tion tables, \mathbf{Q}^Y for luma blocks and \mathbf{Q}^C for chroma blocks, are encoded in the input bitstream's header.

Each quantised DCT coefficient $(\hat{\mathbf{X}}_b)_{u,v}$ in each MCU is dequantised as

$$(\mathbf{X}'_b)_{u,v} = (\hat{\mathbf{X}}_b)_{u,v} \cdot Q_{u,v}. \quad (2.8)$$

Figure 2.5 shows what ranges of coefficients are mapped to the same value after a quantisation/dequantisation cycle for several block indices in zig-zag scan order, and the associated values for the dequantised DCT coefficient.

- At this stage, the decoder has reconstructed an estimate \mathbf{X}'_b of the block which was present after the DCT in the encoder, \mathbf{X}_b . The next stage is to perform an inverse DCT on each block, which transforms the frequency representation of the block back into the spatial domain. The calculations involved in the IJG codec's default inverse DCT algorithm, defined in `jidctint.c` (implementing the Loeffler/Ligtenberg/Moschytz fast IDCT [67]), are equivalent to the following calculation, performed on each block \mathbf{X}'_b :

$$\mathbf{x}'_b = \max \left(0, \min \left(255, \left\lfloor \frac{1}{2^{18}} \left(\left\lfloor \frac{1}{2^{11}} (\mathbf{T}\mathbf{X}'_b + 2^{10}) \right\rfloor \mathbf{T}^T + 2^{17} \right) \right\rfloor \right) \right) \quad (2.9)$$

with element-wise rounding, scalar multiplication and application of min and max, and the transform matrix \mathbf{T} is

$$\begin{pmatrix} 8192 & 11363 & 10703 & 9633 & 8192 & 6437 & 4433 & 2260 \\ 8192 & 9633 & 4433 & -2259 & -8192 & -11362 & -10704 & -6436 \\ 8192 & 6437 & -4433 & -11362 & -8192 & 2261 & 10704 & 9633 \\ 8192 & 2260 & -10703 & -6436 & 8192 & 9633 & -4433 & -11363 \\ 8192 & -2260 & -10703 & 6436 & 8192 & -9633 & -4433 & 11363 \\ 8192 & -6437 & -4433 & 11362 & -8192 & -2261 & 10704 & -9633 \\ 8192 & -9633 & 4433 & 2259 & -8192 & 11362 & -10704 & 6436 \\ 8192 & -11363 & 10703 & -9633 & 8192 & -6437 & 4433 & -2260 \end{pmatrix}. \quad (2.10)$$

Note that the final step of the inverse DCT clips the resulting values to lie in the range $\{0, \dots, 255\}$, which ensures that they fit in an 8-bit unsigned integer representation.

The inverse DCT outputs are mapped back into scan order, resulting in three scan-order components.

Each block of reconstructed sample values belongs to one of three components $\mathbf{c}' \in \{\mathbf{v}'^T_0, \mathbf{v}'^T_1, \mathbf{v}'^T_2\}$. The particular component which contains a given block is dictated by its position in the bitstream.

The dimensions of the image in pixels (w, h) are encoded in the file's header. The luma component (which is not down-sampled) has $8 \cdot \lceil w/8 \rceil$ samples horizontally and $8 \cdot \lceil h/8 \rceil$ samples vertically; the down-sampled chroma components have $16 \cdot \lceil \lceil w/2 \rceil / 8 \rceil = 16 \cdot \lceil w/16 \rceil$ samples horizontally and $16 \cdot \lceil h/16 \rceil$ samples vertically.

We map the blocks \mathbf{x}'_b of a component \mathbf{c}' with dimensions (n, m) back to scan order:

$$c'_i = c'[\langle x, y \rangle_n] = (\mathbf{x}'[\langle \lfloor x/8 \rfloor, \lfloor y/8 \rfloor \rangle_{n/8}])_{y \bmod 8, x \bmod 8} \quad (2.11)$$

4. Each down-sampled component is up-sampled using a 2-D four-tap separable smoothing filter.

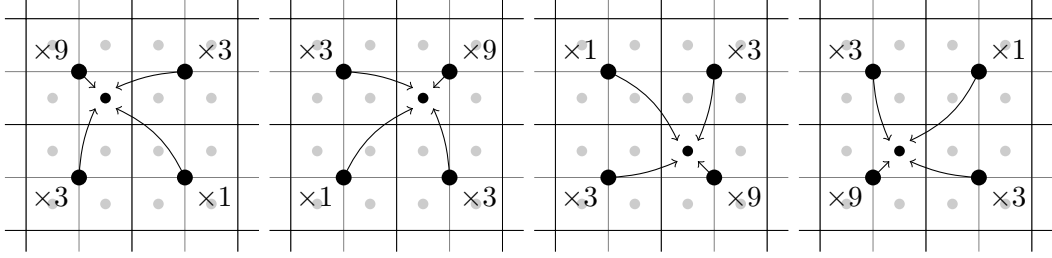


Figure 2.7: The chroma up-sampling filter in the IJG decompressor weights contributions from neighbouring samples by $\frac{1}{16}$ (1, 3, 3, 9) in order of increasing proximity.

The IJG decoder uses fixed-point arithmetic to calculate the outputs of the filtering operation (for down-sampled component indices $c \in \{1, 2\}$):

$$\begin{aligned} (\mathbf{v}^T_c)[\langle x, y \rangle_{2n}] = & \left\lfloor \frac{1}{16} (\alpha \cdot v'^-[\langle i-1, j-1 \rangle_n, c] + \right. \\ & \beta \cdot v'^-[\langle i, j-1 \rangle_n, c] + \\ & \gamma \cdot v'^-[\langle i-1, j \rangle_n, c] + \\ & \left. \delta \cdot v'^-[\langle i, j \rangle_n, c] + 8) \right\rfloor, \end{aligned} \quad (2.12)$$

with weights

$$(\alpha, \beta, \gamma, \delta) = \begin{cases} (1, 3, 3, 9) & \text{if } x = 2i, y = 2j, \\ (3, 1, 9, 3) & \text{if } x = 2i-1, y = 2j, \\ (3, 9, 1, 3) & \text{if } x = 2i, y = 2j-1, \\ (9, 3, 3, 1) & \text{if } x = 2i-1, y = 2j-1. \end{cases} \quad (2.13)$$

Each input sample is located at the centre of 2×2 output samples. Each output sample is a function of the four closest inputs (with padding by repetition at the boundaries of the image).

5. The decoder converts the $YCbCr$ image \mathbf{v}' to the RGB colour space and outputs it as a bitmap.

The first step of the colour space conversion calculates the chroma contributions in fixed-point arithmetic:

$$\mathbf{w}' = \begin{pmatrix} 0 & 0 & [1.40200 \times 2^{16} + 0.5] \\ 0 & -[0.34414 \times 2^{16} + 0.5] & -[0.71414 \times 2^{16} + 0.5] \\ 0 & [1.77200 \times 2^{16} + 0.5] & 0 \end{pmatrix} \mathbf{v}'. \quad (2.14)$$

2. Compression algorithms for photo and video data

To calculate the RGB representation \mathbf{u}' of the YC_bC_r image \mathbf{v}' we then undo the fixed-point arithmetic scaling and add the luma component. Finally, we clip the outputs so that they are in the range $\{0, \dots, 255\}$.

$$\mathbf{u}'_i[j] = \min(255, \max(0, \text{divround}(\mathbf{w}'_i[j], 2^{16}) + \mathbf{v}'_i[0])). \quad (2.15)$$

2.3 Video compression

This section introduces video compression, some relevant terminology and the H.264/AVC standard.

Video compression algorithms operate on sequences of images. The input image sequence can typically be partitioned into scenes that exhibit a high degree of temporal redundancy between their constituent pictures. Most video compression techniques use (1) a compression algorithm optimised for still images, which is applied to those pictures that have mostly new (unpredictable) content, to produce *key frames*, (2) a way to produce a prediction based on previously decoded pictures which takes into account motion, and (3) an additional image compression algorithm optimised to operate on the residual data resulting from the subtraction of a prediction from a decoded key frame, producing a *predicted frame*.

Entropy coding produces a sequence of bitstreams, storing data from key and residual frames along with signalling metadata. Beyond the most basic requirements imposed by prediction, the choice of whether to encode a particular picture as key or predicted data is left up to the encoder; making this choice to satisfying bandwidth requirements is known as *rate control*.

Each picture is partitioned into one or more regions called *slices*⁵, and each slice is further subdivided into a sequence of equally sized units called *macroblocks*. Macroblocks are square, non-overlapping regions in the slice, and may be split up further into sub-macroblocks or macroblock partitions. Each macroblock is indexed by a macroblock address, uniquely identifying it within the picture. Macroblock addresses increase in raster-scan order throughout each picture, starting from zero.

Video compression standards normally specify how to generate a sequence of bitstreams, one per slice (for example), that must then be assembled along with some other structured signalling data to produce a playable video file, according to some separately-standardised container format.

Chapter 5 processes H.264/AVC Baseline streams where each picture has a single slice containing a grid of 16×16 pixel macroblocks.

⁵The H.264/AVC standard allows encoders to use arbitrarily shaped slices, while some older codecs mandate that slices form contiguous runs in raster-scan order.

2.3.1 The H.264/AVC video compression standard

The H.264/AVC standard (Advanced video coding for generic audiovisual services, ITU-T recommendation H.264, ISO/IEC 14496-10 Advanced Video Coding [45]) is a widely-used lossy compression scheme for digital video, first standardised in 2003 by the Joint Video Team (JVT), a collective partnership formed from members of the ITU-T Video Coding Experts Group (VCEG) and the ISO/IEC Moving Pictures Experts Group (MPEG). The ISO and ITU-T standards have identical content.

A large and increasing number of devices include H.264/AVC encoding/decoding capability, as the standard can be used to communicate high quality video at relatively low bitrates (compared with older video compression standards such as H.263 and MPEG-2). The 3GPP standard suggests that mobile telephones should be compatible with the H.264/AVC Baseline profile [18]. Many closed-circuit television recorders and consumer video cameras also store video in the H.264/AVC Baseline profile.

Chapter 3

Copy-evidence in digital media

This chapter presents a new type of content marking algorithm which adds a high-frequency pattern to JPEG images that is imperceptible to the unaided eye, but turns into a clearly readable, large-letter warning if the image is recompressed with some different quality factor.

Our technique aims to achieve a goal similar to copy-evident security-printing techniques for paper documents, namely to have an easily recognisable message appear in lower-quality copies, while leaving the appearance of the original unharmed. We exploit non-linearities in the JPEG process, including the clipping of the result of the inverse discrete cosine transform.

The demonstration images in this chapter should ideally be viewed on a digital display without scaling, as they rely on carefully adjusted patterns which can be altered by filtering and other processing steps. To view a web-based demonstration of the effect, see [58].

The work in this chapter was published in [59]: Andrew B. Lewis, Markus G. Kuhn: Towards copy-evident JPEG images. *Digitale Multimedia-Forensik*, 39. Jahrestagung der Gesellschaft für Informatik 2009, Lübeck, Germany, GI-Edition: in *Lecture Notes in Informatics*, Volume P154, pages 1582–1591.

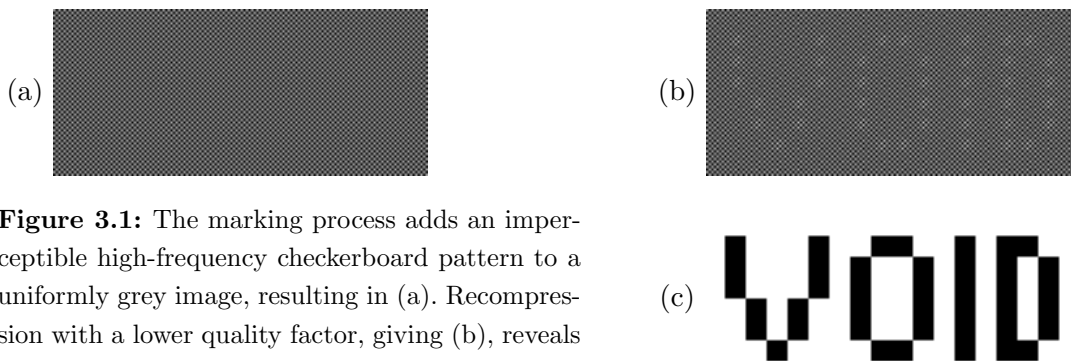


Figure 3.1: The marking process adds an imperceptible high-frequency checkerboard pattern to a uniformly grey image, resulting in (a). Recompression with a lower quality factor, giving (b), reveals the embedded bi-level message (c).

Richard Clayton originally suggested the project on copy-evidence, motivated by the idea of trying to warn website users when they receive degraded versions of images from their Internet service provider. I came up with the idea of using the interaction between dequantisation and post-IDCT clipping to differentiate separate image blocks, though Markus and I discussed some other possible techniques. He helped me to improve a first draft of the paper, and drew my attention to the issue of gamma correction.

3.1 Prior work

This section describes prior work on digital content protection and security printing techniques that achieve physical copy-protection properties using an approach analogous to ours. Section 4.3 describes prior work on forensic analysis of JPEG images, and requantisation/re-compression.

3.1.1 Digital content protection schemes

Content producers sometimes wish to control the distribution of their digital media. This is difficult because the right to view a file generally allows viewers to make and transmit binary-identical copies of its contents, in the absence of specialist hardware or mandatory access control systems. One alternative option is to identify the origin of copies, by embedding unique tracing information.

Watermarking schemes embed an invisible digital signal which allows the content producer to trace which ‘genuine’ version of a file was copied and distributed (see for example [14, 78, 80]). Attacks which try to remove the watermark while minimising distortion to the content have also been studied ([79, 82]).

When the distribution channel cooperates with content producers, perceptual hashing can be used to detect and discard copied material, even if it has undergone minor modifications. The distributor produces for each incoming document a content-dependent summary string, called a perceptual hash; new files are compared against this summary to see whether they may be unauthorised copies [34].

This chapter discusses a new approach to content protection, which embeds an invisible signal in a high-quality document that turns into a visible warning message after recompression.

3.1.2 Security printing

Some security documents (for example, banknotes, tickets, academic transcripts and cheques) are printed with a carefully adjusted *copy-evident* background pattern that looks uniform to the unaided eye, but will show a clearly visible large-letter warning, like “COPY” or “VOID”,

3. Copy-evidence in digital media

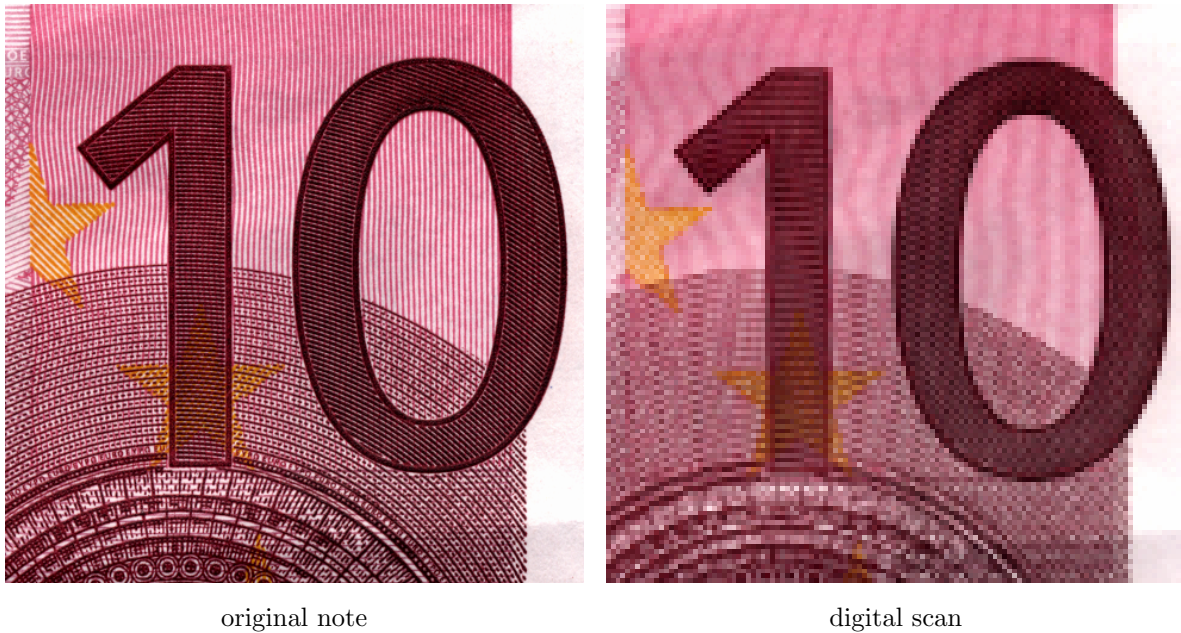


Figure 3.2: The top-right corner of the EUR 10 note is printed with a scan-trap, which causes aliasing when captured at low resolutions with a digital scanner (right).

after having been photocopied (Figure 3.3). This differs from some other security-printing techniques, which rely on tools to decode the hidden message.

Screen-trap and scan-trap printing techniques use periodic screens of arbitrarily shaped image elements (such as dots and lines) as a carrier, into which an invisible message is modulated [99]. Screen traps cause interference with colour separation screens in the printing process, and scan traps cause aliasing when sampled by a digital scanner. Various types of modulation may be used: the phase, angle, size, frequency, shape or colour of screen elements may be altered to encode the cover and covert message in the security printed image.

One such technique is screen-angle modulation (SAM) [92, 93]. The screen elements for this technique are very fine lines, whose orientation is locally modulated with a covert image. The chosen image becomes visible after copying. It is also possible to hide a covert image within a cover image, rather than in a uniform region, by modulating the width of the screen elements with the cover image.

Further information on such security-printing techniques is available in [99, 100]. In general, they cause nearly invisible high-frequency differences in the image signal to turn into clearly visible low-frequency components.

3.2 Digital copy-evidence

Digital files in memory can be copied exactly (and without any degradation), unless the user is prevented from reading the files by hardware or operating system access control mechanisms. However, it is quite common for visual data to be recompressed before redistribution, in order to reduce file sizes. For example, movies distributed on Blu-ray discs may be recompressed to lower bitrates, before being placed on a server for distribution. Some web proxies can also recompress images and videos, to save bandwidth. Recompression introduces distortion in the new version of the file, as the compression algorithm must throw away information.

By adding a suitably crafted pattern to digital images, videos or sound files before distribution, that is imperceptible in the original output of the marking process but likely to become visible (or audible) after application of standard lossy processing techniques (such as requantisation or resampling), we may be able to achieve properties analogous to those of security-printed documents. This would be useful for (1) warning users that they are viewing a degraded version of a document and (2) deliberately introducing objectionable distortions, spoiling recompressed versions. For example, the first case is relevant to digital photographers who would like to warn viewers when an Internet service provider has recompressed their images to a lower quality factor to make the HTTP connection appear faster.

Commonly used encoding and processing algorithms have been designed specifically to minimise perceptible distortion, yet marking algorithms need to maximise distortion in derivative copies. One possible approach is to add signals to the marked copy that are carefully balanced to cancel out each other's distortions, hoping that any further processing will destroy that balance. This might involve generating a compressed representation that, even though it decompresses correctly, could never have been generated by a normal compression step. It might also involve exploiting non-linearities (quantisation, clipping, gamma correction) or artefacts (aliasing, blocking) that compression algorithms sometimes introduce.

Ideally, we would even like to have control over the conditions under which the embedded mark becomes visible. In some applications we prefer a *targeted mark*, which only becomes

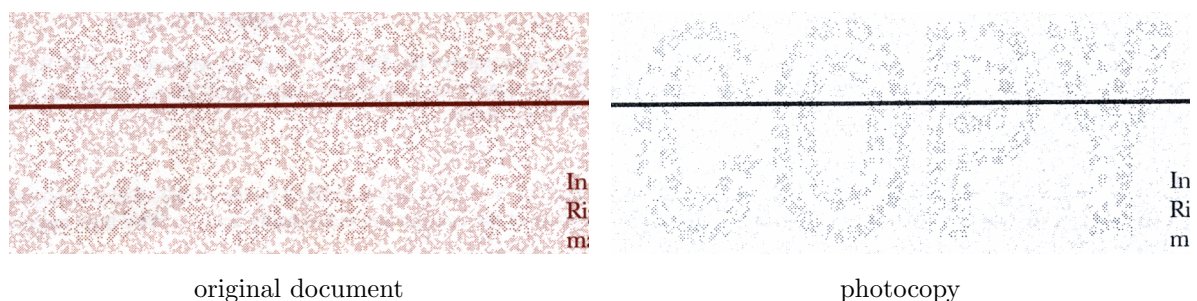


Figure 3.3: The background pattern of this academic transcript was printed using two different dot sizes, adjusted to result in the same halftone (left). The photocopier fails to reproduce the smaller dots, leaving the regions printed with larger dots to form a visible warning (right).

3. Copy-evidence in digital media

visible when one particular a priori known processing step is applied. For example, imagine a video that shows a warning if it has been uploaded to a particular website where all material is recompressed with fixed settings. In other applications, we might prefer an *untargeted mark*, which becomes visible with high probability as soon as any of a number of possible processing parameters are applied.

This chapter describes the result of our exploration of this area, namely the generation of a JPEG image of uniform colour, which on recompression with a particular quantisation table will result in a message appearing.

3.3 Quantisation in JPEG recompression

To produce suitable marks for JPEG images, we need to take into account the processing steps which produce JPEG bitstreams and decompress them, described in section 2.2.2. This section summarises the most relevant features of the compression algorithm.

Recall that the compressor calculates the discrete cosine transform of all non-overlapping 8×8 blocks in the image's luma channel and two down-sampled chroma channels, to represent each block as a sum of scaled, sampled two-dimensional cosines. For each spatial frequency in a block, the associated coefficient $(\mathbf{X}_b)_{u,v}$ is then linearly quantised by a factor $Q_{u,v}$ provided in a quantisation table, which determines with what precision the amplitude of that frequency component is represented. Information is intentionally discarded during chroma down-sampling (if enabled) and quantisation of DCT coefficients. Subsequent steps code the latter without further loss of information. Decompression inverts each step in turn, performing dequantisation, inverse DCT, chroma up-sampling (if required) and conversion back to the RGB colour space.

Appendix A describes how the quantisation table \mathbf{Q} is derived from a scalar *quality factor* (from 1–100) in the IJG encoder [57]. \mathbf{Q} is encoded in the header of the JPEG file so that the decompressor has it available for dequantisation. For any block index b , let $X_{u,v} = (\mathbf{X}_b)_{u,v}$ with $(u,v) \in \{0, \dots, 7\}^2$. The frequency domain coefficient is quantised by a factor $Q_{u,v}$ to give

$$\hat{X}_{u,v} = \text{divround}(X_{u,v}, Q_{u,v}) \quad (3.1)$$

The corresponding dequantisation operation in the decompressor multiplies the quantised coefficient by the quantisation factor (read from a table in the JPEG header):

$$X'_{u,v} = Q_{u,v} \cdot \hat{X}_{u,v} \quad (3.2)$$

Blocks with $\hat{X}_{u,v} = 0$ for high values of u and v (the perceptually less important higher frequencies) are coded very compactly in the final lossless stage. Therefore, in practice, most quantisation tables have high values $Q_{u,v}$ for high values of u and v . For example, the IJG codec

implementation’s default quantisation table for luma (quality factor 75, the same table as that recommended by the JPEG standard for providing a ‘nearly indistinguishable’ reconstruction of the original [38, Annex K.1]) is

$$\mathbf{Q} = \begin{pmatrix} 8 & 6 & 5 & 8 & 12 & 20 & 26 & 31 \\ 6 & 6 & 7 & 10 & 13 & 29 & 30 & 28 \\ 7 & 7 & 8 & 12 & 20 & 29 & 35 & 28 \\ 7 & 9 & 11 & 15 & 26 & 44 & 40 & 31 \\ 9 & 11 & 19 & 28 & 34 & 55 & 52 & 39 \\ 12 & 18 & 28 & 32 & 41 & 52 & 57 & 46 \\ 25 & 32 & 39 & 44 & 52 & 61 & 60 & 51 \\ 36 & 46 & 48 & 49 & 56 & 50 & 52 & 50 \end{pmatrix}. \quad (3.3)$$

3.4 Marking method

We now describe our method for creating a JPEG file with an embedded targeted mark, which will become visible after recompression with a known quantisation table \mathbf{Q}' . We embed a single pixel (one bit, foreground or background) of the marking message in each 8×8 luma DCT block (Figure 3.1). We replace each such block with a visually equivalent block that contains an added high-frequency checkerboard dither pattern. We choose the amplitude of that dither pattern such that half its pixel values end up close to a clipping limit (0 or 255). The exact amplitude chosen differs depending on whether the block represents a foreground or background pixel of the marking message. We choose this pair of amplitudes such that their values are (a) as close together as possible, (b) rounded in opposite directions after requantisation with \mathbf{Q}' , and (c) such that up to half of the pixels in a requantised foreground block will exceed the clipping limits after the inverse DCT in the decoder (Figure 3.4). As a result, the clipping operation in the decoder will affect the average pixel value in foreground blocks, but not in background blocks, leading to a visible difference.

3.4.1 Maximising distortion

In a JPEG encoder, each quantisation decision boundary

$$B_{u,v}(n) = \frac{1}{2}(n \cdot Q_{u,v} + (n - \text{sgn}(n)) \cdot Q_{u,v}) = Q_{u,v} \cdot (n - \text{sgn}(n)/2) \quad (3.4)$$

lies centred between two adjacent multiples of the quantisation factor $Q_{u,v}$, where $n \in \mathbb{Z} \setminus \{0\}$. The pair of consecutive integers $|X_{u,v}^\top(n) - X_{u,v}^\perp(n)| = 1$ on either side of this boundary map

3. Copy-evidence in digital media

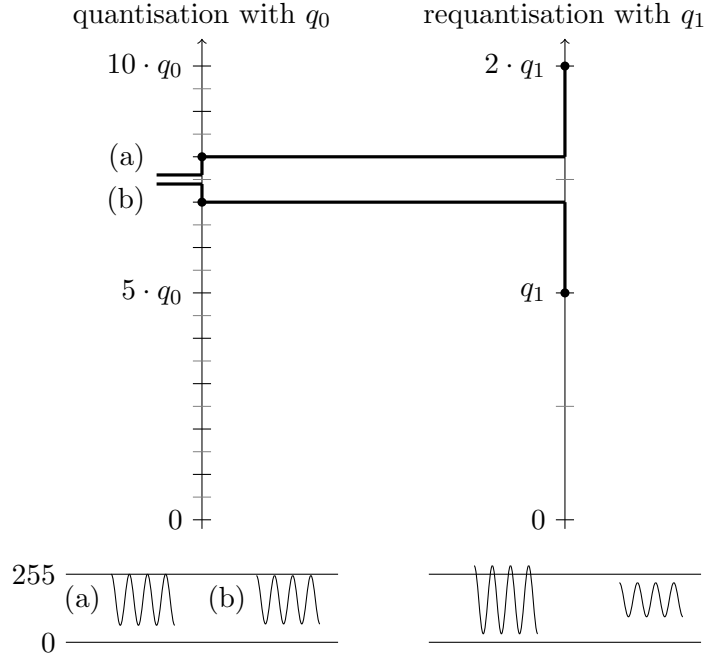


Figure 3.4: The quantisation of two values (a) and (b) for a $7/2$ cycles per block frequency component, first with quantisation factor q_0 , then at a lower quality with quantisation factor q_1 . The results of the inverse transform when the block is combined with a DC component equivalent to 192 are shown one dimensionally. Note that the higher amplitude signal (a) will be clipped after recompression, which reduces its mean.


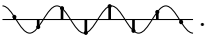
to adjacent integers n and $n - \text{sgn}(n)$, respectively, when quantised:

$$\begin{aligned}
 X_{u,v}^{\top}(n) &= n \cdot Q_{u,v} - \text{sgn}(n) \cdot \lfloor Q_{u,v}/2 \rfloor \\
 &= B_{u,v}(n) + (Q_{u,v} \bmod 2) \cdot \text{sgn}(n)/2, \\
 X_{u,v}^{\perp}(n) &= n \cdot Q_{u,v} - \text{sgn}(n) \cdot (\lfloor Q_{u,v}/2 \rfloor + 1) \\
 &= X_{u,v}^{\top}(n) - \text{sgn}(n).
 \end{aligned} \tag{3.5}$$

A DCT coefficient taking on one of these values will incur the maximum quantisation error when compressed. For a particular DCT coefficient position (u, v) , if we compress two blocks, one using $X_{u,v}^{\top}(n)$ and the other using $X_{u,v}^{\perp}(n)$, these will each experience maximum quantisation error, but in opposite directions, despite the fact that the uncompressed appearance of the two blocks is very similar. Figure 3.4 shows this effect where the first compression uses a low quantisation factor $Q_{u,v} = q_0$ and the second uses a high quantisation factor $Q'_{u,v} = q_1$ (harsher quantisation).

3.4.2 Embedding

To embed a binary message (such as a bitmap showing the text “COPY”) in the cover image, we map each pixel in the message to an 8×8 block in the cover, and set the amplitude of

a particular DCT coefficient position (u, v) to $X_{u,v}^\top(n)$ in foreground blocks and $X_{u,v}^\perp(n)$ in background blocks when quantised in the marked original with q_0 . To make this effect as noticeable as possible, we choose the coefficient (u, v) so that the associated recompression quantisation factor $q_1 = Q'_{u,v}$ is large. $X_{7,7}$ is the highest spatial frequency component and normally uses a large quantisation factor. This coefficient's frequency component corresponds in the spatial domain to a windowed checkerboard pattern ; the associated 1-D sampled cosine basis vector is .

A 2-D checkerboard pattern will be perceived with a brightness approximately equal to its mean value (subject to gamma correction), and two checkerboard patterns with the same mean but different amplitudes will be almost indistinguishable.

3.4.3 Clipping of IDCT output

However, we wish to introduce contrast between blocks in a perceptually more important low frequency. The results of the inverse DCT are clipped so that they lie in the range $\{0, \dots, 255\}$. If we arrange, by suitable choice of n , for some of the spatial domain image samples in foreground message blocks to exceed 255 after recompression with \mathbf{Q}' , these values will be clipped, while the lower values in the checkerboard pattern will not be clipped. Similarly, sample values less than 0 will be clipped after recompression. The perceived brightness of the foreground block will, therefore, be reduced (or increased) compared to a block corresponding to a background pixel in the message, where no clipping will occur: the balance of high and low samples in the checkerboard pattern will be destroyed in the recompression step. Figure 3.5 demonstrates this effect.

This results in a low-frequency contrast between foreground and background blocks, leading to a visible message in the recompressed version. In the marked original, we set $q_0 = Q_{7,7}$ as small as possible while still providing a slight difference in the amplitude of the checkerboard pattern between foreground blocks and background blocks in the spatial domain, and make sure that the amplitudes are on either side of a quantisation boundary (using the amplitudes $X_{u,v}^\top(n)$ and $X_{u,v}^\perp(n)$, from (3.5)). Writing the bitstream directly, rather than using a JPEG compressor, allows for exact control over coefficient values and the quantisation table required.

3.5 Marking algorithm

Some combinations of block values and target quantisation tables lead to unmarkable blocks, for example, if addition of a checkerboard pattern of amplitude $X_{7,7}^\top(n)$ to the original block causes it to clip already (i.e. the smallest value for $|X_{7,7}|$ that would just cause clipping lies between a multiple of the requantisation factor and the next higher quantisation decision boundary), then this will cause unbalanced distortion in the marked original.

3. Copy-evidence in digital media

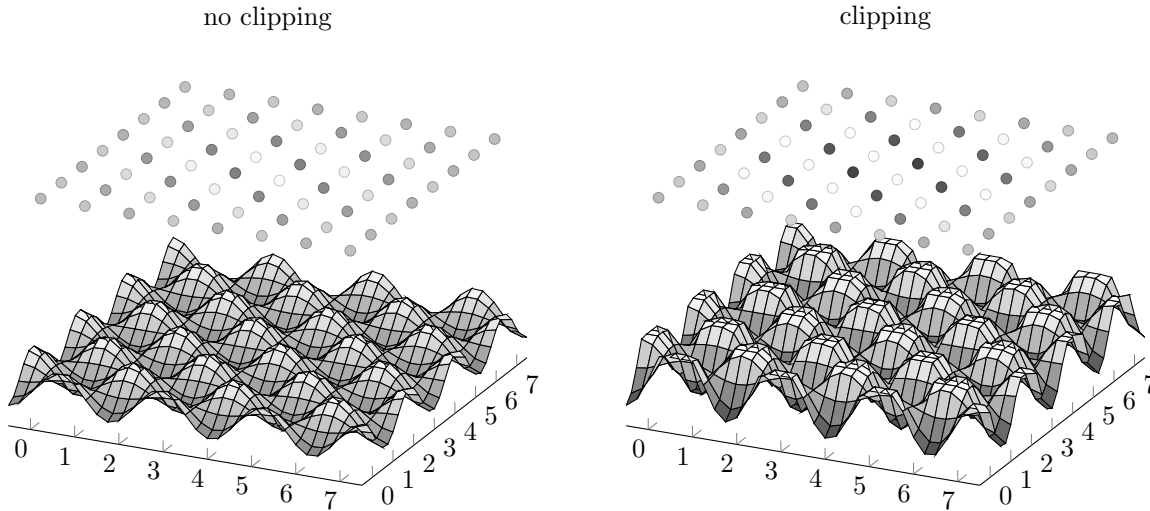


Figure 3.5: The results of the inverse DCT are clipped to the range $\{0, \dots, 255\}$. The left plot shows a high-frequency DCT basis function at a particular amplitude and DC offset, where no clipping takes place. The right plot shows the same function but with a higher amplitude. The function is clipped, lowering the perceived average intensity of the block in the spatial domain.

Because the $X_{7,7}$ component corresponds to a windowed checkerboard pattern (sampling the cosine basis function introduces a low beat frequency), the block will not appear as a uniform checkerboard pattern after recompression.

Our marking process is shown in Algorithm 1. Given an 8×8 block of DCT coefficients \mathbf{B} from the original image, the binary value of the message m and the target quantisation table \mathbf{Q}' , $\text{MARKBLOCK}(\mathbf{B}, m, \mathbf{Q}')$ searches through the possible amplitudes x for the checkerboard pattern and returns either FAIL (for unmarkable blocks), or a replacement image block with an added checkerboard pattern at the amplitude necessary to cause clipping after recompression with \mathbf{Q}' . One value for the pattern’s amplitude is tested on each iteration, with the current higher amplitude candidate marked block stored in $\mathbf{H}[x]$ (returned when $m = 1$), and the previous iteration’s marked block stored in $\mathbf{H}[x - 1]$ (returned when $m = 0$).

If it terminates successfully, the algorithm provides a block of DCT coefficients as output. This block should be written directly to a JPEG bitstream, to avoid the rounding which might be caused by JPEG compression.

3.5.1 Termination conditions and unmarkable blocks

As the algorithm searches over increasing checkerboard pattern amplitudes, three error conditions can arise, indicating that a block is unmarkable. The algorithm returns the successfully marked block in all other cases. The algorithm returns FAIL_1 if the added checkerboard pattern causes clipping even before compression, FAIL_2 if addition of the pattern causes clipping

Algorithm 1 Marking algorithm for JPEG image blocks


DCT(\mathbf{b}) returns the discrete cosine transform of block \mathbf{b} .

IDCT(\mathbf{B}) returns the inverse discrete cosine transform of block \mathbf{B} without clipping.

CLIPS(\mathbf{b}) returns true if any sample in \mathbf{b} exceeds 255 or is less than 0.

QUANTISE(\mathbf{B}, \mathbf{Q}) quantises \mathbf{B} using table \mathbf{Q} according to Equation (3.1).

DEQUANTISE(\mathbf{B}, \mathbf{Q}) dequantises \mathbf{B} using table \mathbf{Q} according to Equation (3.2).

CHECKERBOARD(x) returns an 8×8 checkerboard pattern  with elements $+x$ and $-x$.

$\mathbf{H}[x]$ stores the candidate DCT coefficient block, with spatial domain representation $\mathbf{h}[x]$.

$\hat{\mathbf{H}}[x]$ and $\hat{\mathbf{h}}[x]$ are those same blocks after requantisation with \mathbf{Q}' .

function MARKBLOCK($\mathbf{B} \in \mathbb{Z}^{8 \times 8}$, $m \in \{0, 1\}$, $\mathbf{Q}' \in \mathbb{N}^{8 \times 8}$)

for $x \leftarrow 1$ to 128 **do**

\triangleright For each amplitude value x

$\mathbf{h}[x] \leftarrow \text{IDCT}(\mathbf{B}) + \text{CHECKERBOARD}(x)$

if CLIPS($\mathbf{h}[x]$) **then**

return FAIL₁

\triangleright The checkerboard signal is out of range

$\mathbf{H}[x] \leftarrow \text{DCT}(\mathbf{h}[x])$

if CLIPS(IDCT($\mathbf{H}[x]$)) **then**

return FAIL₂

\triangleright The original marked block must not clip

$\hat{\mathbf{H}}[x] \leftarrow \text{DEQUANTISE}(\text{QUANTISE}(\mathbf{H}[x], \mathbf{Q}'), \mathbf{Q}')$

$\hat{\mathbf{h}}[x] \leftarrow \text{IDCT}(\hat{\mathbf{H}}[x])$

if CLIPS($\hat{\mathbf{h}}[x]$) and $x > 1$ **then**

if $\hat{H}[x]_{7,7} \neq \hat{H}[x-1]_{7,7}$ **then**

if $m = 1$ **then return** $\mathbf{H}[x]$ **else return** $\mathbf{H}[x-1]$

else

return FAIL₃ \triangleright Clipping occurs on recompression, but $\mathbf{H}[x]$ and $\mathbf{H}[x-1]$
 are not either side of the quantisation boundary of the
 highest frequency coefficient: $\nexists n : X_{7,7}^\top(n) = H[x]_{7,7}$

before recompression in $\mathbf{h} = \text{IDCT}(\mathbf{H})$ (where no quantization has taken place) and FAIL₃ if clipping occurs after recompression but the highest frequency coefficient (which contributes the windowed checkerboard pattern) has not changed.

The algorithm must terminate after any of these error conditions, because successful termination at a given amplitude requires that no clipping took place at the previous (lower) amplitude.

3.5.2 Gamma-correct marking

To minimise the perceptual impact of marking, we should add checkerboard patterns which do not alter the perceived brightness of input blocks. However, *pixel values* from $\{0, \dots, 255\}$ are

3. Copy-evidence in digital media

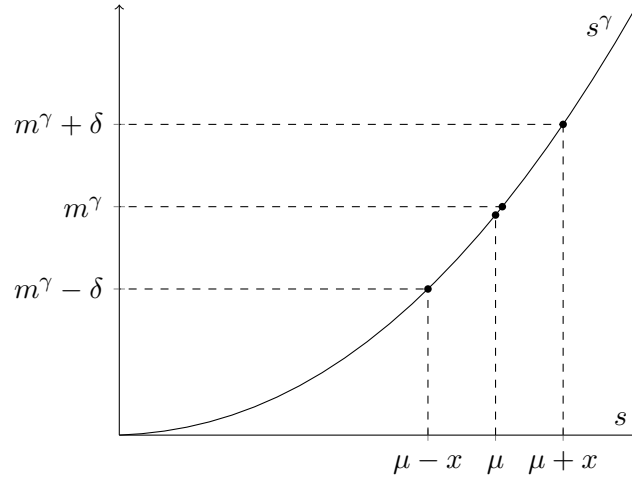


Figure 3.6: The mean value of the added checkerboard pattern μ should be chosen based on its amplitude x so that the perceived brightness of the marked block is the same as that of the original block, m^γ , taking into account gamma correction.

not proportional to actual display *brightness* (photons per second), but instead are related by a power law (gamma correction): a pixel value of s results in a pixel brightness proportional to s^γ , where the constant γ is the exponent for the display device (typically $\gamma \approx 2.2$).

To find the checkerboard pattern's mean pixel value μ for a given amplitude x (in the image sample domain) such that its brightness matches that of the original block m^γ , we solve Equation (3.8) to find the brightness amplitude δ given x and m , then substitute this back into Equation (3.7) to find μ [56, pp. 57–60]:

$$\mu \pm x = (m^\gamma \pm \delta)^{\frac{1}{\gamma}} \quad (3.6)$$

$$\mu = \frac{1}{2} \left((m^\gamma + \delta)^{\frac{1}{\gamma}} + (m^\gamma - \delta)^{\frac{1}{\gamma}} \right) \quad (3.7)$$

$$x = \frac{1}{2} \left((m^\gamma + \delta)^{\frac{1}{\gamma}} - (m^\gamma - \delta)^{\frac{1}{\gamma}} \right) \quad (3.8)$$

Figure 3.6 illustrates the relationship between these variables.

If this is implemented in a function `GAMMACORRECT(m, x)`, which returns μ , it can be used to alter the additive checkerboard pattern in Algorithm 1, making the replacement blocks perceptually similar to the original blocks.

3.5.3 Untargeted marks

This marking algorithm produces a targeted mark, which requires that the recompression quantisation factor is known. When a range of quantisation factors might be used, and the image is sufficiently large, we can embed several targeted marks so that a message appears under recompression with any of the factors.

If it is acceptable for the hidden message to appear at one of several non-overlapping regions in the image, the algorithm can be applied as described to each region separately, marking each one with a different target quantisation factor.

Otherwise, multiple targeted mark blocks can be interleaved. We partition the marking region into equally-sized, non-overlapping rectangles, each containing n DCT blocks. In the targeted mark, a single DCT block contributed one bi-level pixel of the message, while in this scheme each partition contributes one pixel. If we must target k different quality factors, each partition should contain k blocks.

If there are fewer than k blocks in each partition, marking may still be possible. Some quality factors share the same quantisation factors for the highest frequency coefficient¹. Also, blocks sometimes requantise correctly under multiple distinct quantisation factors $\{q_1, \dots, q_M\}$. This occurs when (1) the marking algorithm chooses a quantisation decision boundary b that is applicable for all the quantisation factors, that is, for each $q \in \{q_1, \dots, q_M\}$, there exists some k such that $B_{7,7}(k) = q \cdot (k - \text{sgn}(k)/2) = b$, and (2) the candidate block's DC component is such that clipping occurs in marked foreground blocks at all those quantisation factors.

In the IJG implementation, the quantisation boundaries which are available for marking at the highest number of distinct quantisation factors (and quality factors) are 495 and 693, which both have eight possibilities. Respectively, these are quality factors [99, 97, 95, 91, 89, 85, 45, 25], with associated quantisation factors [2, 6, 10, 18, 22, 30, 110, 198], and [99, 97, 93, 91, 89, 79, 32, 25], with associated quantisation factors [2, 6, 14, 18, 22, 42, 154, 198].

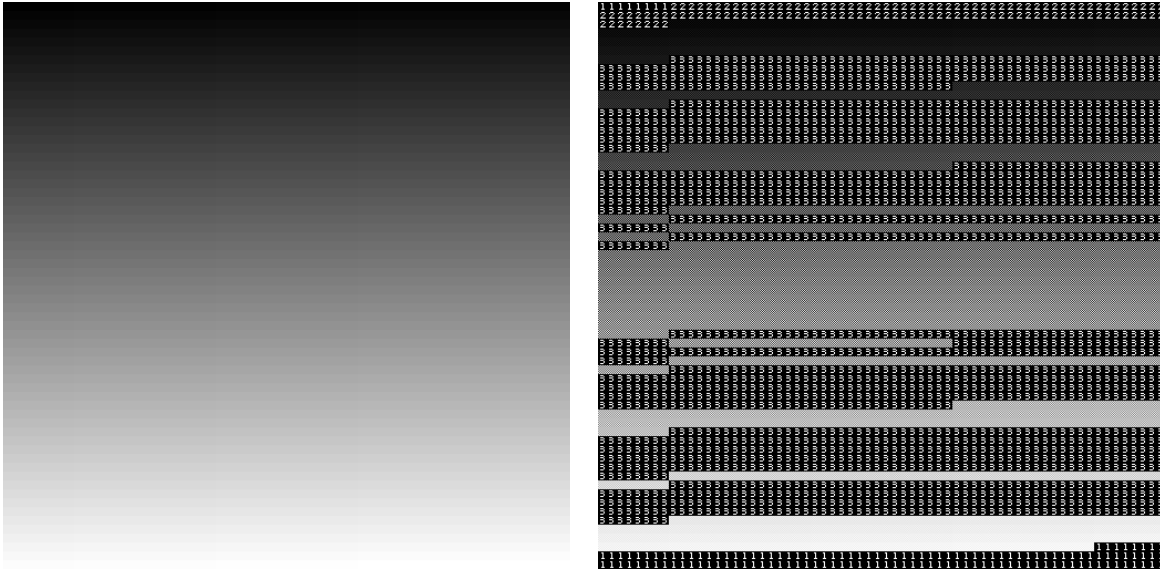
If the untargeted mark is likely to cause multiple blocks in a partition to clip (rather than just one block), the marker can achieve a uniform appearance by placing blocks which clip at the same time as far away from each other as possible, for example, using an ordered dithering pattern [3].

3.5.4 Results

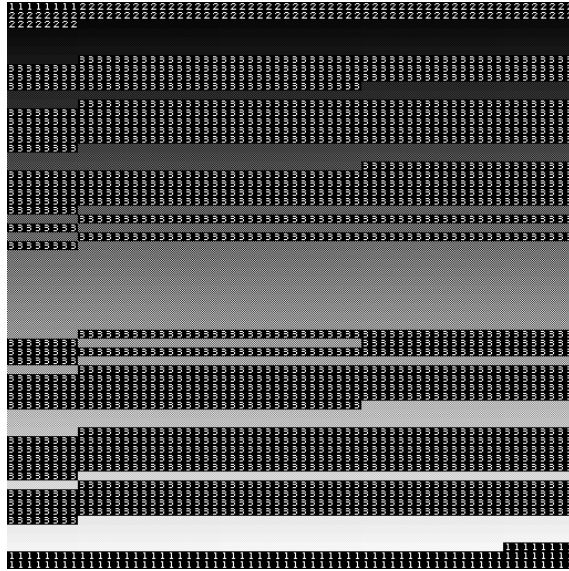
To test the marking on all possible uniform blocks, we marked a 512×512 pixel test image consisting of a grid of 64×64 non-overlapping 8×8 pixel blocks with a black to white gradient in raster-scan order. The test image contains two horizontally adjacent blocks at each DCT domain brightness value, to allow comparison of the cases $m = 0$ and $m = 1$ (Figure 3.7 (a)): the pixel at (x, y) is within a block $\mathbf{X}_{\langle i, j \rangle_{64}}$, where $(i, j) = (\lfloor x/8 \rfloor, \lfloor y/8 \rfloor)$, which has one non-zero DCT coefficient taking the value $(\mathbf{X}[\langle i, j \rangle_{64}])_{0,0} = \lfloor i/2 \rfloor + 32 \cdot v - 1024$. Figure 3.7 shows the results of applying $\text{MARKBLOCK}(\mathbf{X}[\langle i, j \rangle_{64}], i \bmod 2, \mathbf{Q}')$, where \mathbf{Q}' is the quantisation table for IJG quality factor 50, to each block in this test image (b) before and (c) after recompression. Unmarkable blocks have been replaced with a digit indicating the type of failure (as described in subsection 3.5.1).

¹Quality factors 1–19 in the IJG implementation share a quantisation factor of 255

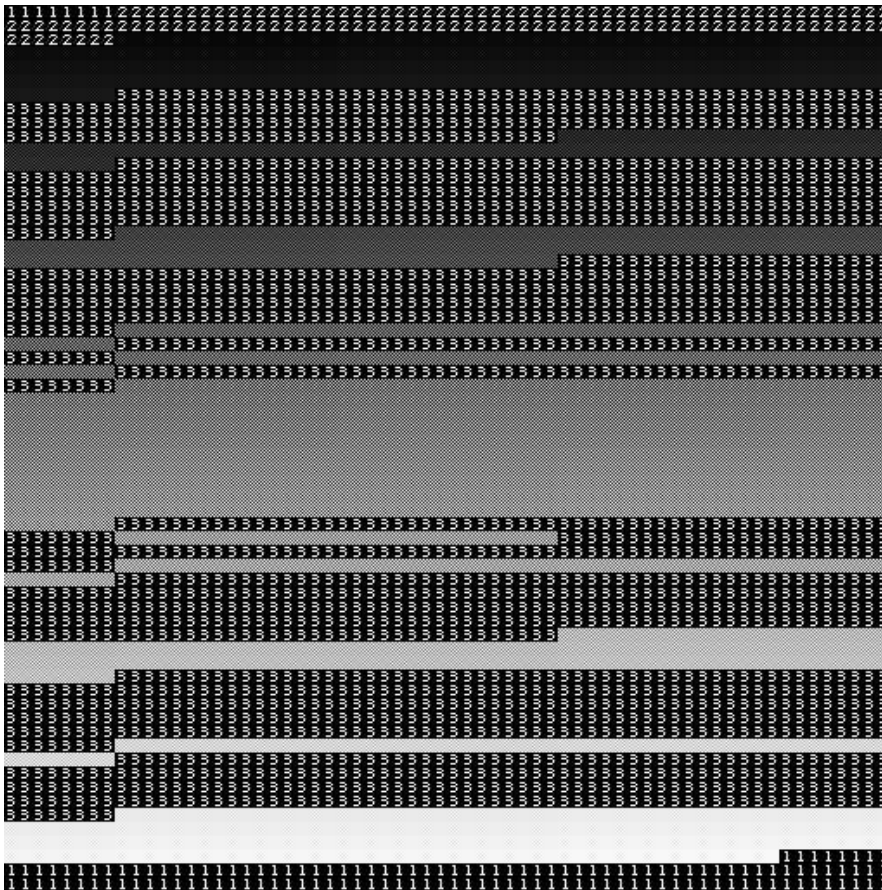
3. Copy-evidence in digital media



(a) original



(b) marked



(c) recompressed at quality factor 50

Figure 3.7: Marking and recompression of an image with each DCT domain brightness value (a) and a repeating message (0, 1). Unmarked blocks in the marked image (b) are replaced with a digit corresponding to the type of error in Algorithm 1. (c) shows the result of recompression.

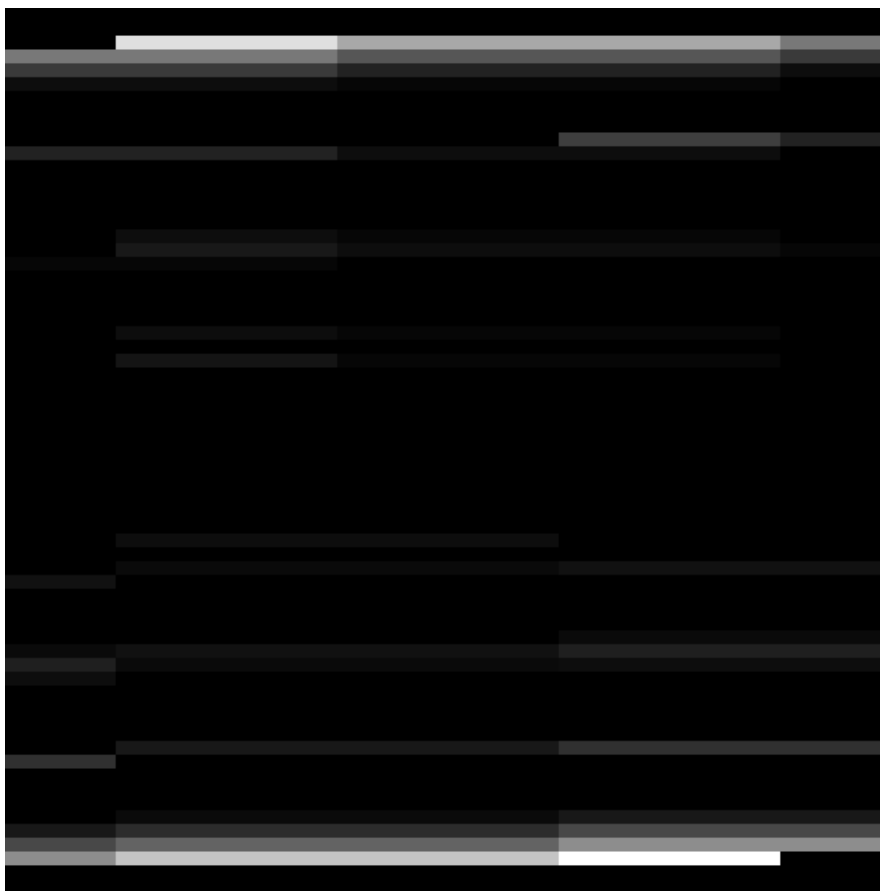


Figure 3.8: The relative contrast difference achieved by each pair of horizontally adjacent blocks in figure 3.7, where black denotes no contrast and white denotes the maximum contrast of any block pair

Figure 3.8 gives a crude guide to the mark's visibility after recompression. Each horizontally adjacent pair of blocks in figure 3.7 (with message $(0, 1)$) maps onto a pair of co-located blocks in figure 3.8. For each pair of blocks, we calculate the difference between their average intensities, and use this as an estimate of the perceived contrast between foreground and background blocks after recompression. Black denotes that the blocks have the same mean values (no contrast), while white blocks have the highest contrast achieved between any block pair.

3.6 Analysis

Based on figure 3.7, it is clear that marking is not possible at a significant proportion of brightness values in the gradient. However, markable brightness values are distributed over the range, so a similar brightness may be markable. This is useful if an alteration to the original block's content is acceptable. The most clear contrast is achieved at markable brightness values near black and white, as shown in figure 3.8.

3. Copy-evidence in digital media

Figures 3.7 and 3.8 show that our algorithm would be unsuitable for marking full-colour photographic images, because it requires brightness level adjustments that distort the original marked image, even in relatively uniform regions.

Although the visibility of the mark in a high-quality original image is independent of the target recompression quality factor, as the amplitudes of foreground and background message checkerboard patterns can always be close, the message's visibility in recompressed copies is dependent on the target quality factor: lower-quality copies exhibit a higher maximum attainable brightness difference between foreground and background message blocks after clipping.

If the marking technique is used by content distributors, the requirement of knowing the target recompression quality factor may be too stringent. Furthermore, multiplexing several targeted marks is impractical in small images. Recompression to a quality factor that is slightly different to the target adversely affects the mark's visibility. Unpredictable recompression quality factors are therefore a simple countermeasure.

The mark is sensitive to filtering and resampling operations, such as the scaling operations performed by digital monitors at non-native resolutions, and browser image resizing. The message tends to remain invisible in the original image, although aliasing can cause Moiré patterns in marked regions.

If a display device rounds sample values (to display 8 bits per sample data on a 6 bits per sample monitor, for example), some spatial domain amplitudes can create a barely visible discrepancy in the original image. In this case, it may be possible to select a different pair of amplitudes which the display rounds in the same way. In the absence of temporal dithering, this has the advantage of making the high-quality original's foreground and background message blocks identical.

Subsequent low-pass filtering of recompressed copies must remove the high-frequency checkerboard pattern, leaving the contrast between foreground and background message blocks intact.

3.6.1 Possible extensions to the algorithm

Our algorithm is able to embed a visible message because DCT blocks are processed independently in the JPEG compression/decompression algorithms. For other codecs, where the lossy processing of a given region may be affected by the rest of the image, techniques may still exist that maximise distortion due to recompression, even if it is not possible to display a message.

Using the same technique on video content is likely to be impossible because compressors' rate control algorithms are not standardised, and their state normally depends on prior input. It is therefore hard to predict what quantisation factors will be chosen by adaptive rate control during the course of recompression.

As an initial exploration of the feasibility of digital copy-evidence, our mark is practically useful for producing warnings that image recompression has taken place, without relying on special tools. If it is possible to develop more powerful, resilient copy-evident marking algorithms, they may make use of the same characteristics of compressors, especially non-linearities. However, compressors and compression schemes are designed to minimise distortion, so copy-evident marks working against this goal will always be difficult to develop.

3.7 Conclusion

Our marking algorithm shows that it is possible to produce a copy-evident multimedia file, in which a human-readable message becomes visible after recompressing a marked image, by taking advantage of non-linear processing in the JPEG algorithm.

The challenge remains to extend our approach to mark non-uniform still images, where the distortion added during embedding must be minimised, and video data, where rate control and adaptive quantisation make the copied document's properties less predictable. The result would be a digital video that would be severely degraded by recompression to a lower quality, making the algorithm useful for digital content protection.

Chapter 4

Exact JPEG recompression

This chapter describes a new type of compressor designed to recover the bitstreams associated with a given decompression result. As a side-effect, our algorithm also finds the compression parameters and outputs whether any regions of the input image cannot be the result of decompression, which may be useful as an indication of tampering.

4.1 Introduction

Lossy perceptual coding algorithms (JPEG, MPEG, etc.) were designed to compress raw audio-visual data captured by sensors. Ideally, such data should only ever go through a single lossy compression/decompression cycle. In practice, however, an image is often compressed already at the beginning of its editing history, such as in a digital camera, and repeatedly compressed later, after decompression and editing. Only very limited manipulation is practical without first decompressing (for example, cropping and copying along certain boundaries, rotation by 90° , mirroring, scaling by certain factors [88]).

This chapter describes a variant of the JPEG baseline image compression algorithm, designed to compress images that were generated by a JPEG decompressor. The algorithm inverts the computational steps of one particular JPEG decompressor implementation (Independent JPEG Group, IJG), and uses interval arithmetic and an iterative process to infer the possible values of intermediate results during the decompression, which are not directly evident from the decompressor output due to rounding.

The work in this chapter was originally published in [60]: Andrew B. Lewis, Markus G. Kuhn: Exact JPEG recompression. IS&T/SPIE Electronic Imaging, 17–21 January 2010, San Jose, California, USA.

Markus Kuhn originally suggested the project on exact JPEG recompression. We came up with the idea of using interval arithmetic when he suggested a way to invert an operation

which involved information loss. I applied this idea to each stage of JPEG decompression, and developed the algorithms for iterative recovery of down-sampled image components, colour space conversion, discrete cosine transform and quantisation table reconstruction. Markus helped me to improve the writing in a first draft of the paper, and was especially helpful with developing a notation to describe the procedure precisely.

4.1.1 Exact recompression

A decompressor maps compressed bitstreams onto uncompressed data, or a special value ERROR in the case of a bitstream syntax error. Decompressors associated with useful lossy compression schemes output a relatively small subset of all possible uncompressed files, in normal usage.

An *exact recompressor* maps an uncompressed input document I_1 onto a set of bitstreams, such that the decompressor maps any of these bitstreams onto $I_2 = I_1$ (figure 4.1). The set of output bitstreams may be empty, in which case the input I_1 was not produced by a process equivalent to the decompressor.

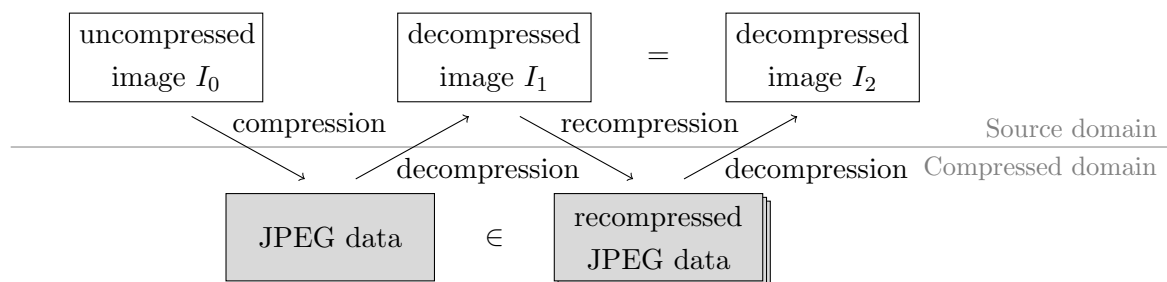


Figure 4.1: Exact recompressors map a decompression result I_1 onto a set of bitstreams, such that the decompressor maps any of these bitstreams back onto I_1 .

Exact recompressors are *complete* if they generate the set of all equivalent input bitstreams, and *stable* if localised edits on the data after decompression only lead to localised further loss of information during recompression.

It is theoretically possible to write an exact, complete recompressor for any decompressor by searching over all bitstreams and outputting only those which produce the input image on decompression. In practice, this search is intractable for non-trivial bitstream lengths. We propose the alternative strategy of partitioning the computations performed by the decompressor into a series of independent stages which can be inverted individually, followed by a search that, for efficiency, relies on the fact that localised modifications to the bitstream only affect a small region of the decompressed output.

4. Exact JPEG recompression

4.1.2 Comparison with naïve recompression

Naïve recompression is the application of standard lossy compression algorithms to decompressed data, which in practice rarely achieves exact or stable recompression, even with identical quantisation and down-sampling parameters [75]. This is due to rounding and clipping of intermediate results, and the fact that some compressors do not apply the inverse functions of the corresponding decompression steps.

Normal compressors are often employed in situations where the user would prefer the bitstream to be as close as possible to the original bitstream, or different only in those areas which have been modified since decompression. We call the use of a normal compressor for this task ‘naïve recompression’ because no special tools are involved.

When previously compressed files undergo multiple compression cycles (that is, they are compressed and decompressed repeatedly with the same parameters), the decompressor must eventually output a file which is the same as one of its previous outputs. At this point, the outputs repeat. More precisely, let \mathbf{s}_k be the decompression result after k naïve recompression cycles; then we find that for some threshold t and any $0 \leq i, j < t$ where $i \neq j$, $\mathbf{s}_i \neq \mathbf{s}_j$, and $\mathbf{s}_{t+k} = \mathbf{s}_{t-n+k}$ for some $n > 0$ and all $k \geq 0$.

For example, recompressing the ‘Lena’ sample image using the IJG codec, we find that the 12th decompression result is identical to the 11th decompression result at quality factor 75 ($t = 12$, $n = 1$). When chroma smoothing in the decompressor is deactivated, the 10th decompression result is identical to the 9th ($t = 10$, $n = 1$). At quality factor 95, the first repetition occurs in the 36th decompression result, which is identical to the 35th ($t = 36$, $n = 1$).

If we perform the same experiment, but using exact recompression instead of naïve recompression on all but the first cycle (where the compressor may handle never-before-compressed data, \mathbf{s}_0), we find that $\mathbf{s}_i = \mathbf{s}_j$ for all $i, j > 0$.

4.1.3 Decompressor implementations

It is common for a compression standard to allow a range of decompressor implementations, rather than specifying exactly what output a particular bitstream should produce on decompression. Since exact recompressors invert the calculations involved in decompression, in this case each one is associated with a particular decompressor program.

This chapter describes the implementation of an exact, complete, stable recompressor for the DCT-based JPEG baseline algorithm (see chapter 2), as implemented in the widely-used open-source Independent JPEG Group (IJG) decompressor, version 6b [57]. It reads an RGB image and either returns one or more JPEG bitstreams that on IJG decompression will result in the input image, or it identifies regions in the input that could not have been output by the IJG decompressor. The recompression is exact because our algorithm, when provided with

a decompressed image, returns a (sometimes singleton) set of bitstreams, including one with the original JPEG data (figure 4.1).

4.2 Applications

There are three main situations where exact recompression is useful: avoiding quality loss, recovering compression parameters and detecting tampering after decompression.

4.2.1 Avoiding quality loss

Firstly, editors that read and write compressed data can make use of exact recompression. Plugins already exist for some image editors that keep track of which blocks have not been modified since a JPEG image was opened, so that these blocks can be copied directly in compressed form when the image is saved [83], avoiding unnecessary further information loss. The complexity of integrating this into the application could be avoided with an exact, stable recompressor, which can be applied without auxiliary information.

Secondly, some copy-protection mechanisms keep the compressed bitstream confidential, via encryption, giving end-users plaintext access only to the output of the decompressor. They rely on the fact that captured plaintexts will have to be recompressed, degrading their quality. Their reliance on the unavailability of exact recompression motivates its study, to understand both its practicality and how best to modify decompressors to prevent it, without reducing signal quality.

A practical example of one such content-protection scheme, X-pire [101], uses a web-browser plugin to view encrypted images, with cryptographic keys read from a separate web server. After a certain calendar date, specified by the image's uploader, the image can no longer be decrypted. If the plugin displays unmodified decompressor output, an exact recompressor could recover the underlying compressed bitstream, allowing further unrestricted distribution without quality degradation due to recompression.

4.2.2 Compressor and parameter identification

If a forensic investigator has matching exact recompressors available for many decompressor implementations, they can see which exact recompressors fail on a given document. This result allows them to claim that either the associated decompressors were not used, or the document was modified after decompression.

In addition to determining which decompressor produced an image, our tool can provide clues to investigators by recovering compression parameters, which may match those used by particular devices or software.

4. Exact JPEG recompression

4.2.3 Tampering detection

Exact recompression can also be used as a forensic technique, to provide information about the processing history of a document. If we have an exact recompressor for a decompressor that processes spatially/temporally separate parts of the document independently, it is possible to localise regions that are inconsistent with decompression. This may be a sign that tampering has taken place.

4.3 Prior work

Naïve recompression of images usually causes degradation in quality, due to the accumulation of rounding errors and smoothing. The fact that repeated recompression can cause information loss is well-known, and has been tackled in several different ways in the past. Decompressors also introduce particular patterns to their output, which can be useful for forensic investigators. This section reviews prior work in recompression and forensic analysis of images which contain previously compressed data.

4.3.1 Maintaining image quality during recompression

If a user wants to recompress an image in order to save on storage space, while minimising additional distortion, they may find that distortion is not monotonically increasing with lower quality factors. Bauschke et al. [2] suggest an algorithm which finds a new, lower recompression quality factor, designed to minimise the perceptual impact of distortions due to requantisation. Our exact recompressor could provide precise information about the distribution of DCT coefficient values to this algorithm, giving a tool which could recompress images from bitmap format to a lower quality factor while minimising perceived distortion. Furthermore, for some data, exact recompression can lead to a more compact representation, as it will search for those quantisation parameters that lead to the smallest output without altering content.

Even when identical compression parameters are used during naïve recompression, rounding and truncation generally lead to further information loss. Schlauweg et al. [91] note that fluctuations in transform coefficient values can cause problems for authentication based on cryptographic watermarks, where a signature authenticating a document is embedded within the content itself. In one application of watermarking, the signature should be destroyed only when meaningful modifications take place, but not under small alterations. They show an attack on a scheme [65] that relies on two ‘invariant properties’ in JPEG images; in fact, these properties, which are based on relative values of pairs of DCT coefficients, can change during naïve recompression. They propose using error-correcting codes to make the watermark more resilient to bit errors. Exact recompression could be used to recover the DCT coeffi-

cients exactly when checking for the watermark in a bitmap image, while avoiding additional fluctuations in DCT coefficient values.

4.3.2 Acquisition forensics

Digital image acquisition devices and processing tools normally introduce characteristic statistical patterns to the files they produce. The processing history of an image is lost when metadata are discarded or the image is saved in a format which doesn't keep track of editing steps. Digital image forensics techniques try to deduce the processing history on the basis of any statistical patterns still present in the document. One approach makes use of the patterns introduced by the JPEG algorithm.

Acquisition forensics techniques try to recover information about the device used to capture or generate an image based on its statistical properties. Several techniques analyse digital photographs, trying to determine the device used to capture the image. Some try to find out which form of interpolation was used to generate a full-colour image based on the image captured under the Bayer array filter over the camera's sensor. Disruptions to the correlations introduced by interpolation might indicate tampering (see [86, 26] for example). The interpolation algorithm might be characteristic of a particular camera or manufacturer. Another interpolation characterisation algorithm [85] uses an expectation/maximisation algorithm to find an interpolation kernel iteratively; this technique was later improved by Kirchner [51].

Lukáš et al. [69] proposed an alternative approach to camera identification, which was later improved by Chen et al. [9]. It identifies the camera sensor which captured a particular image, using around a hundred images from each candidate camera. To calculate a characteristic noise signal for each camera, they use a wavelet-based denoising filter to estimate sensor noise in each test image. These are averaged and correlated with the noise signal of the image under investigation. The camera with the most similar noise signal is considered to be most likely to have captured the image. Goljan et al. [31] used this technique on a large set of images, to evaluate its performance in real-world scenarios.

Several acquisition forensics techniques are designed to detect whether images contain data output by JPEG decompressors, or characterise exactly which compression parameters were used.

Some simple techniques for analysing JPEG bitstreams simply extract the quantisation tables and match these with those used by a particular device or software tool (see [53, 20, 21, 33], for example).

More advanced algorithms analyse the data produced on decompression, rather than relying on the availability of JPEG bitstreams.

Fan and de Queiroz [19] describe a method for detecting the discontinuities in pixel values which appear at block boundaries in JPEG-compressed images, and use this to propose an

4. Exact JPEG recompression

efficient JPEG detector. They also describe the maximum possible range of rounding errors on DCT coefficient values, by assuming that pixel values can experience a maximum error $-0.5 \leq e < 0.5$ and substituting this into the formula for the DCT. These assumptions are not suitable for an exact recompressor, because IJG DCT implementation does not use arbitrary precision real values for its intermediate results and basis function samples.

JPEG compression history (Neelamani et al. [75])

Neelamani et al. [75] describe methods that estimate the compressed representation colour space G^* , down-sampling scheme S^* and quantisation tables Q^* (where the asterisk denotes that these are the actual values) associated with a particular JPEG decompression result. They call these values the ‘compression history’ of the image. They solve a maximum a posteriori estimation problem

$$(\hat{G}, \hat{S}, \hat{Q}) = \arg \max_{G, S, Q} P(\Omega_{G, S} | G, S, Q) P(G) P(S) P(Q),$$

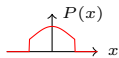
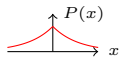
to find the compression history which maximises the probability of observing the DCT coefficient values, $P(\Omega_{G, S})$. Treating the DCT coefficient values as independent, this can be evaluated as

$$(\hat{G}, \hat{S}, \hat{Q}) = \arg \max_{G, S, Q} \prod_{\tilde{X}_{G, S} \in \Omega_{G, S}} P(\tilde{X}_{G, S} | G, S, Q) P(G) P(S) P(Q).$$

The authors need estimates $\tilde{X}_{G, S}$ of the original DCT coefficients X_q in order to calculate these probabilities. It is possible to search over G and S because they may take on only a small set of values.

The original JPEG image’s DCT coefficients X_q were transformed back to the spatial domain, then the colour planes were up-sampled (if appropriate), and the $YCbCr$ image was transformed back to RGB space. The compression history estimation algorithm takes the RGB image as input, performs colour space conversion and chroma down-sampling operations, and applies the DCT to get $\tilde{X}_{G, S}$, estimating X_q .

The difference between these estimates and the original values is modelled with a single round-off term: $\tilde{X} = X_q + \Gamma$. It is common to model the rounding errors Γ with a truncated Gaussian

distribution  and the DCT coefficient values with a Laplace distribution .

The Laplace distribution’s scale parameter λ is determined from the observed data. The probability of a DCT coefficient taking a particular value, given that it is quantised with factor $q \in \mathbb{Z}$, is

$$P(X_q = t | q) = \sum_{k \in \mathbb{Z}} \delta(t - kq) \cdot \int_{(k-0.5)q}^{(k+0.5)q} \frac{\lambda}{2} \exp(-\lambda \cdot |\tau|) d\tau$$

Rounding errors are assumed to be independent, so the authors convolve this distribution with the error term's distribution and normalise:

$$P(\tilde{X} = t) \propto \int P(X_q = \tau | q)P(\Gamma = t - \tau) d\tau.$$

If we assume a uniform prior $P(q)$ for quantisation factors, we can now find the most likely value for a particular quantisation factor $q = \hat{Q}_{i,j}$ by maximising $P(\tilde{X} | q)$. This is repeated for each quantisation factor $\hat{Q}_{i,j}$ for $(i, j) \in \{0, \dots, 7\}^2$:

$$\hat{q} = \arg \max_{q \in \mathbb{Z}} \left(\prod_{\tilde{X} \in \Omega} P(\tilde{X} | q) \right)$$

This finds the maximum a posteriori estimate of the quantisation tables.

Finding the compression parameters of the image in this manner allows for the use of arbitrary colour spaces, down-sampling schemes and quantisation tables. It is also not implementation-specific; the algorithm relies on features inherent in every JPEG decompressor.

However, the performance of the algorithm may vary depending on which decompressor is used. The authors found that quantisation table estimates contained some errors during testing. In particular, their algorithm uses Tikhonov-regularised deconvolution filter [97] to down-sample the colour planes, introducing noise which can lead to incorrect DCT coefficient estimates. Their technique is statistical rather than exact; it calculates the most probable compression settings based on noisy estimates of DCT coefficients, instead of calculating the range of possible values for each DCT coefficient based on all the data available. Exact recompression is specific to a given decompressor implementation, but does not suffer from these other shortcomings.

Using histograms of DCT coefficients for quantisation table estimation

Various other algorithms [23, 19, 70] also use the forward DCT and histograms of its coefficients to estimate the quantisation factors used. As this does not, in practice, exactly invert the corresponding inverse DCT implementation, the resulting small perturbations blur the peaks in the DCT coefficient histograms, which hinders the estimation of quantisation factors and warrants probabilistic techniques. In contrast, exact recompressors must invert the implementation of both the inverse DCT and the chroma-interpolation operations. At any stage where we lack the information needed to unambiguously identify a single input integer, we output the smallest interval guaranteed to contain the corresponding original value.

Non-prime quantisation factors also cause a problem for quantisation table estimation. Because dequantisation can produce values which are any integer multiple of the quantisation factor, observing a DCT coefficient value eliminates only those quantisation factors which are not among its divisors; furthermore, a DCT coefficient equal to zero does not communicate

4. Exact JPEG recompression

any information about the quantisation tables. The latter case is common at higher spatial frequencies, which are heavily quantised.

4.3.3 Tampering detection

If some regions of an image lack the statistical properties introduced by a JPEG compression cycle, while other areas appear to contain decompressor output, this may indicate that parts of the image were modified after being output by a decompressor. Our exact recompressor localises any areas inconsistent with decompression.

Exact recompression can also be used to hinder forensic analysis. Naïve recompression leaves traces in its output, such as the JPEG double-compression artefacts described by Popescu and Farid [85], whereas exact recompression adds no further information.

Double-compression detection

Several approaches have been proposed that determine whether images have previously been compressed more than once using JPEG. They may also determine the quality factors (or, more generally, the quantisation tables) associated with the primary (earlier) and secondary (later) compression cycles.

Popescu and Farid first presented a method for detecting double-compression with different quality factors [85], using the fact that the histogram of DCT coefficient values for a given spatial frequency can become periodic after double-compression.

Another technique for detecting double JPEG compression is presented by Fu et al. [24]. They found that the logarithms of DCT coefficient values in singly-compressed images were distributed uniformly, which implies that the first digits of the DCT coefficients would follow Benford's law [4], so that the digit '1' should appear about 30% of the time on average compared with the approximately 11% probability that would be expected if the first digits had a uniform distribution. Doubly-compressed images did not show the same distribution. Li et al. [61] reproduce these results, analysing the first-digit distribution of all non-DC coefficients, but using linear discriminant analysis to classify whether images underwent one or two compression cycles. They then perform a similar analysis on a subset of the DCT coefficients, to help improve the detector performance when pairs of quality factors have quantisation factors where one is an integer multiple of the other. They show that, despite the fact that the generalised Benford's law does not hold so strongly on coefficients associated with higher spatial frequencies and higher quantisation factors, it is still possible to detect recompression with pairs of quality factors up to about 95 when individual frequencies are considered, rather than the global histogram.

Double-compression detection can be important for steganalysis, as some steganalysis tools

rely on detecting whether an image has been doubly- or singly compressed (see Pevný et al. [81]).

When images are composed of some areas which exhibit double-compression artefacts, and other areas which only show the artefacts expected after a single compression cycle, this may be a useful indication that the image contains content from two sources. Several algorithms therefore try to find regions which are double-compressed adjacent to other singly-compressed areas.

Lin et al. [66] use machine learning to classify regions of blocks as being singly- or doubly-compressed, using Popescu’s method ([85]) to derive a feature vector for each block.

Farid notes that ‘Estimating the quantisation from only the underlying DCT coefficients is both computationally non-trivial, and prone to some estimation error’ [22]. He presents an algorithm to detect the quality factors used in a doubly-compressed image. He finds the minima in the sum of squared differences of image pixel values as pairs of trial quality factors vary. The two lowest values occur at the primary and secondary quality factors in a double-compressed image. By measuring the squared differences between pixel values rather than DCT coefficient values, he avoids false detection of integer divisors of the quantisation factors; the pixel values experience contribution from all non-zero DCT coefficients, and it is unlikely that all spatial frequencies in the luma/chroma channels will be quantised by pairs of factors that are integer multiples of one another.

Krawetz presented the same basic technique [55], calculating the difference of pixel values between a trial compression and the original image at several candidate quality factors. (There are more examples on the author’s website [54].)

Most of these algorithms rely on the use of quality factors to determine the quantisation tables (see appendix A), so that there are only one hundred possibilities for each of the luma and chroma quantisation tables. In exact JPEG recompression, we also assume that the quantisation tables were chosen based on a quality factor, but the algorithm can still output a description of the set of all possible quantisation tables otherwise.

Detecting tampering on decompressed images

Since double-compression detection techniques rely on the image under investigation containing a DCT block grid starting at its upper-left pixel, cropping the images by up to seven pixels horizontally and vertically can be a defence against these algorithms. Li et al. [63] present a method without this weakness, using a sliding 8×8 pixel window over the image, calculating the ratio of the highest frequency components’ magnitudes to that of the DC component at each position. The ratio is minimised at the edges of DCT blocks. After some post-processing, it is possible to locate discrepancies in the block grid by manual inspection. (Li et al. [62] also present the same idea with a slightly modified measurement in the sliding window, which

4. Exact JPEG recompression

makes a prediction of the highest frequency components, and calculates the deviation between the predicted and actual values.)

Li et al. [64] describe an algorithm that generates an image representing the grid of DCT blocks present in an uncompressed image, indicating for a given region the offset of decompressed data modulo eight horizontally and vertically. They use the periodicity of the block grid and median filtering to suppress image content with high spatial frequency components. By manual inspection of the generated image, they show that it is possible to see regions which have block grids that are inconsistent with the grid established by the rest of the image. It is unlikely that a forger will paste content into a position matching the background image's grid, because (1) there are 63 positions in each 8×8 block which do not match and only one which does and (2) even if they want to hide the tampering, it is normally important for image content to match, so they may not have flexibility in positioning the new block.

Qu et al. [87] address the problem of detecting double-compression when the block grids of the two compression cycles do not match. They evaluate the DCT of each block for each possible shifting, and calculate an independence measurement on the resulting coefficients. They combine the values to produce a map, where peaks in the map coincide with shifts that maximise the independence measurement. In doubly-compressed images with different block grids, the map will not be symmetric, and they use machine learning to identify this case.

Ye et al. [102] propose an algorithm which estimates the quantisation tables using the filtered second-order differences in the DCT coefficient histograms, then apply this to calculate each DCT coefficient's remainder during requantisation, averaged over a specified region. This relies on the fact that block edges in decompressed data which are not positioned to coincide with the background's block boundaries will produce non-zero high frequency components in the DCT. They call this value the 'blocking artefact'. They propose segmenting the image into separate regions and detecting discrepancies between their blocking artefact values.

Poilpré et al. [84] investigate how Bayer array interpolation and JPEG blocking artefacts are represented in the Fourier transform of the probability map introduced by Popescu and Farid ([85]), and look at the effects of tampering in the frequency domain.

Further recompression at low quality factors adds a new block grid to the image, and is likely to suppress the sharp edges within DCT blocks, which these algorithms rely on.

Stamm et al. [94] suggest a way to remove the artefacts of a JPEG compression cycle from the histogram of DCT coefficients. They add noise to DCT coefficients so that the modified DCT coefficient histogram matches a maximum likelihood estimate of the original histogram before quantisation. For the histograms associated with high spatial frequencies, which are typically sparse or contain no non-zero entries, they simply use the fact that the recipient's JPEG decompressor will clip inverse DCT outputs to the range $\{0, \dots, 255\}$, which is expected to introduce non-zero DCT coefficients at high spatial frequencies. In conjunction with a method for suppressing blocking artefacts, they suggest using the algorithm to hide tampering. We

propose exact JPEG compression as an alternative approach to hiding localised tampering, by finding modified regions (using exact JPEG recompression), then compressing only these areas, and copying the encoded blocks of the other, exactly recompressed areas.

4.3.4 Residual information in JPEG artefacts

The JPEG algorithm processes 8×8 blocks independently. At higher quantisation factors (lower qualities), the compressor is generally not able to represent fine detail in part of a block without also introducing distortion elsewhere in the block. Ho and Chang [35] show that when some pixels in the decompression result are replaced with new data (to hide the original pixel values below during redaction, for example), some residual information about the replaced pixels can remain elsewhere in the block. When there are only a few possibilities for the replaced pixels, it is possible to search for the most probable choice given the visible artefacts in the rest of the block. The authors suggest the quantisation table estimation algorithms described in [19, 85]. Our algorithm could be used to find the set of all possible quantisation tables given the decompression result. Furthermore, by representing the replaced region's pixels with the interval containing all possible pixel values, our algorithm could be used to calculate whether any of the candidates for the replaced region in the compressed domain are impossible.

4.4 Exact recompression of JPEG images

The input to the recompressor is an uncompressed RGB image. Our recompressor implementation inverts each stage in turn, refining sets of intermediate values in an iterative process, until it reaches a fixed point. At any stage during execution, the sets are guaranteed to contain the intermediate values that actually occurred during the preceding decompression. If a set becomes empty (for example, due to intersection with a disjoint set), this indicates that the input image was not produced by the exact recompressor's corresponding decompressor implementation, or that the image was modified after decompression. Figure 4.2 gives an overview of information flow in the recompressor.

We use the notational conventions established in chapters 1 and 2.

The input RGB image has width w and height h divisible by sixteen:¹

$$\mathbf{u}^T[\langle x, y \rangle_w] \in \{0, \dots, 255\}^3 \quad \text{with } 0 \leq x < w = 16 \cdot w_b \text{ and } 0 \leq y < h = 16 \cdot h_b. \quad (4.1)$$

¹The information loss caused by post-decompression cropping across a block boundary can be modelled using intervals, but our implementation does not support this.

4. Exact JPEG recompression

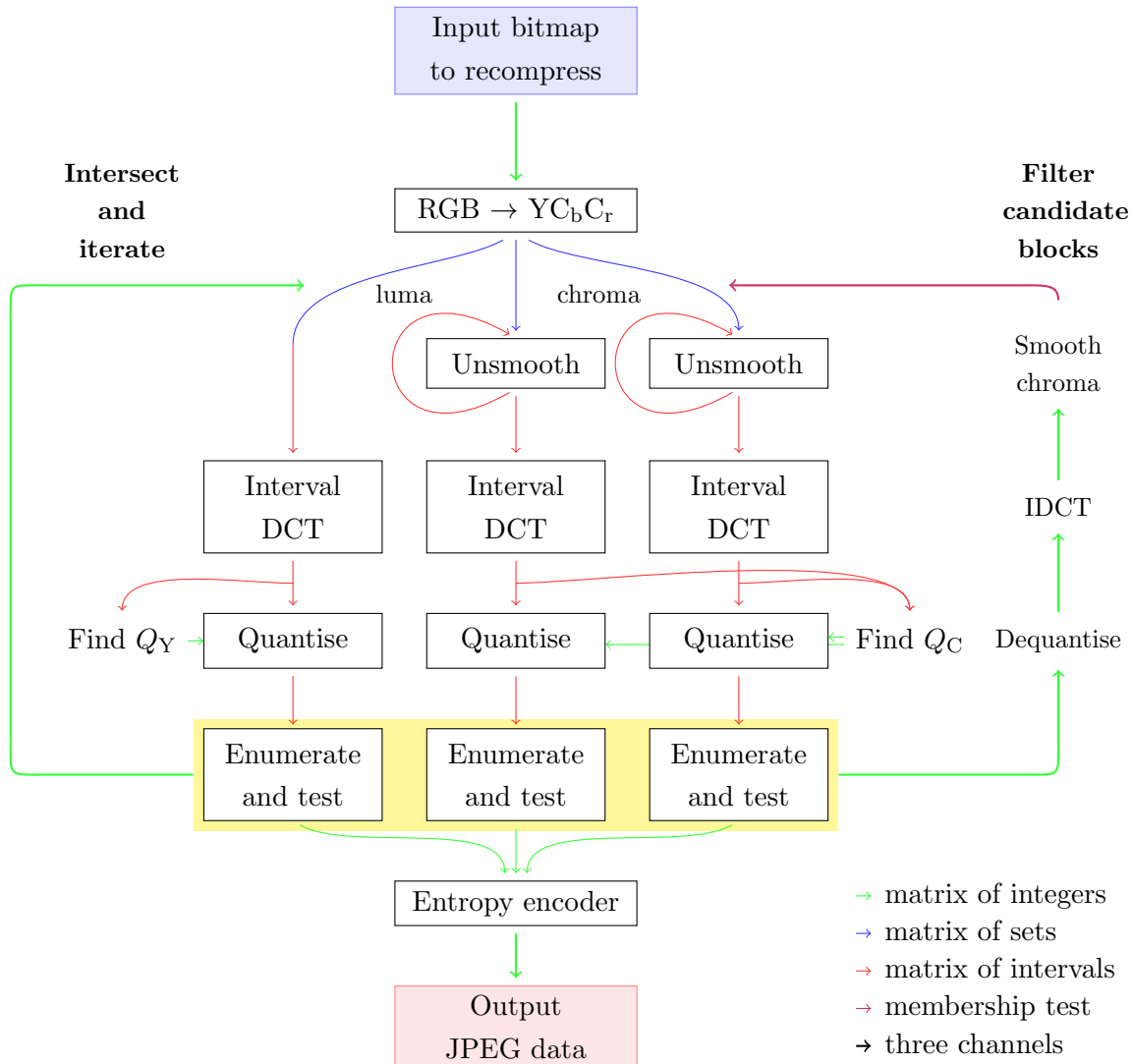


Figure 4.2: Information flows in the exact JPEG recompression algorithm

4.4.1 Colour-space conversion

The final step in decompression applies the per-pixel colour-space transformation, converting each 3×8 -bit luma and chroma ($YCbCr$) value into a 3×8 -bit RGB value, according to equations (2.14) and (2.15).

We model this colour space conversion by the function $C(\mathbf{v}^T[i])$, which maps $YCbCr$ triples onto RGB triples. Our exact recompressor implements C^{-1} , which maps each RGB triple to the set of all $YCbCr$ values in the domain of C that map to this RGB colour. C^{-1} therefore associates with each RGB colour a set of possible $YCbCr$ colours. We apply C^{-1} to each input

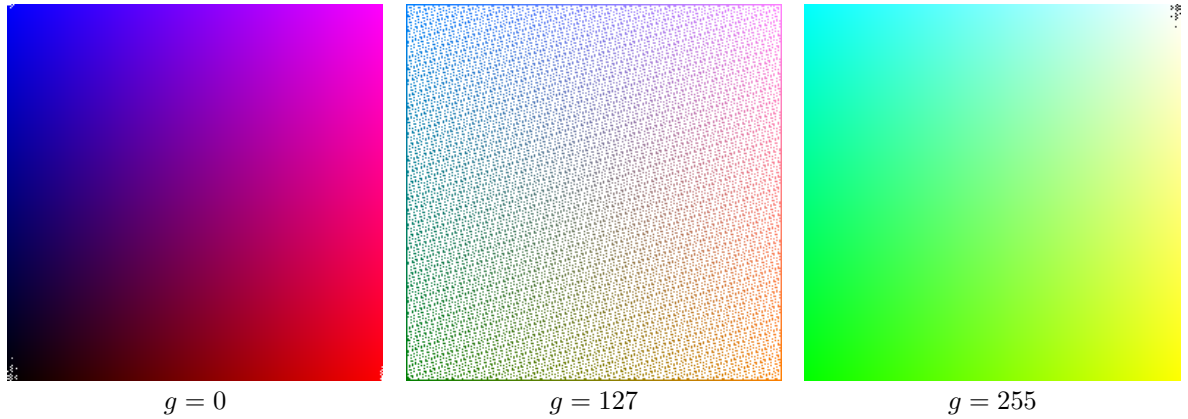


Figure 4.3: Three slices through the RGB cube, with the ‘green’ axis normal to the slices. Pixel values output by the IJG decompressor are shown in their associated colours, while other values are plotted in white ($g < 255$) or black ($g = 255$). Other slices with $0 < g < 255$ are similar to that shown for $g = 127$.

RGB pixel $\mathbf{u}^T[\langle x, y \rangle_w]$, resulting in a set $\mathbf{v}^T[\langle x, y \rangle_w]$ for each pixel:

$$\begin{aligned} \mathbf{v}^T[\langle x, y \rangle_w] &= C^{-1}(\mathbf{u}^T[\langle x, y \rangle_w]) \\ C^{-1} &: \{0, \dots, 255\}^3 \rightarrow \mathcal{P}(\{0, \dots, 255\}^3) \text{ and} \\ C^{-1} &: (r, g, b) \mapsto \{(y, cb, cr) \in \{0, \dots, 255\}^3 : C(y, cb, cr) = (r, g, b)\}. \end{aligned}$$

In our implementation, the inversion of C is tabulated in a 2^{24} -entry look-up table, mapping RGB values to sets of YC_bC_r values.

The RGB triple $(0, 255, 0)$ is associated with 29714 possible YC_bC_r values, the largest set in the domain of C^{-1} . Around 74.6 percent of all RGB triples are associated with an empty set, as the decompressor can never output them². Figure 4.3 shows three slices through the RGB cube, with colour values never produced by the JPEG algorithm filled in white (for $g < 255$) or black (for $g = 255$). The boundary surfaces of the RGB cube are more populated because their points have more nearest neighbours in YC_bC_r space.

4.4.2 Chroma down-sampling

In the default down-sampling mode, both chroma channels are stored at half the horizontal and vertical resolution of the luma channel. The decompressor’s up-sampling operation, implemented using fixed-point integer arithmetic, is described in equation (2.12). The division by sixteen and subsequent rounding causes information loss, but we mitigate this by exploiting the redundancy introduced when the up-sampling process quadruples the number

²Ker observed this sparsity in the context of steganalysis [50].

4. Exact JPEG recompression

of pixels. We iteratively recover as much information as possible about the down-sampled chroma planes, using interval arithmetic to keep track of uncertainty.

We know a set of possible YC_bC_r values for each pixel of each up-sampled component $c \in \{1, 2\}$, given by $\ddot{v}[\langle x, y \rangle_w, c]$. We represent our knowledge of down-sampled values $v^-[\langle i, j \rangle_{w/2}, c]$ in the form of matrices containing intervals.

Now considering a single component c , we write these intervals as $\bar{w}_{i,j}$ and the up-sampled component pixel value possibilities as $v_{x,y} \in \ddot{v}[\langle x, y \rangle_w, c]$, for notational convenience. The intervals are initialised to $[0, 255]$ and then refined repeatedly using the known sets of possible values in the up-sampled plane, $\ddot{v}[\langle x, y \rangle_w, c]$, and our current estimates for the down-sampled plane, $\bar{w}_{i,j}$, by rearranging (2.12).

To evaluate formulae with intervals as variables, we use

$$[q_\perp, q_\top] + [r_\perp, r_\top] = [q_\perp + r_\perp, q_\top + r_\top] \quad (4.2a)$$

$$[q_\perp, q_\top] \times \alpha = [q_\perp \times \alpha, q_\top \times \alpha] \quad (4.2b)$$

and to rearrange these formulae, we use

$$[p_\perp, p_\top] = [q_\perp, q_\top] + \alpha \implies [q_\perp, q_\top] = [p_\perp - \alpha, p_\top - \alpha] \quad (4.3a)$$

$$[p_\perp, p_\top] = [q_\perp, q_\top] \times \alpha \implies [q_\perp, q_\top] = \left[\left\lfloor \frac{p_\perp}{\alpha} \right\rfloor, \left\lfloor \frac{p_\top}{\alpha} \right\rfloor \right] \quad (4.3b)$$

$$[p_\perp, p_\top] = \left[[q_\perp, q_\top] \times \frac{1}{\alpha} \right] \implies [q_\perp, q_\top] = [p_\perp \times \alpha, p_\top \times \alpha + (\alpha - 1)]. \quad (4.3c)$$

Note that in (4.3b), if p_\perp or p_\top is not divisible by α , we set the desired interval \bar{q} to the smallest interval that on multiplication by α will contain all the multiples of α in \bar{p} .

Rearranging equation (2.12) gives the interval for a down-sampled value $v^-[\langle i, j \rangle_{w/2}, c]$ in terms of the other down-sampled values in the formula and an up-sampled output value $v[\langle x, y \rangle_w, c]$. Applying the rules in (4.3) to solve (2.12) for a down-sampled value $w_{i,j}$, in relation to an up-sampled value $v_{x,y}$, with $x = 2i$, $y = 2j$, we have

$$\bar{w}_{i,j} = \left[\left[\frac{1}{\delta} (v_{x,y} \times 16 - (8 + \alpha \cdot \bar{w}_{i-1,j-1} + \beta \cdot \bar{w}_{i,j-1} + \gamma \cdot \bar{w}_{i-1,j})) \right], \right. \\ \left. \left[\frac{1}{\delta} (v_{x,y} \times 16 + 15 - (\alpha \cdot \bar{w}_{i-1,j-1} + \beta \cdot \bar{w}_{i,j-1} + \gamma \cdot \bar{w}_{i-1,j})) \right] \right], \quad (4.4)$$

where $v_{x,y}$ is an integer and the $\bar{w}_{i',j'}$ variables are intervals. Where $\ddot{v}[\langle x, y \rangle_w, c]$ contains several possible values $v_{x,y}$, we have to evaluate the right-hand side of (4.4) for each in turn, and assign the union of the resulting intervals to $\bar{w}_{i,j}$. Each sample in each down-sampled colour plane is the subject of 16 equations, of which (4.4) is one example, because each down-sampled value $w_{i',j'}$ influenced the surrounding 16 pixels when the decoder up-sampled them. The overdetermined system of equations is solved iteratively using Algorithm 2. We change the scan order in each iteration of the algorithm to accelerate convergence.

Algorithm 2 Down-sample one component, $\bar{v}[\langle x, y \rangle_w, c]$

 $k \leftarrow 0$ $\bar{w}_{i,j}^0 \leftarrow [0, 255]$ at all positions $-1 \leq i \leq \frac{w}{2}, -1 \leq j \leq \frac{h}{2}$ **repeat** $k \leftarrow k + 1$ change scan order of (x, y) ($\begin{smallmatrix} \rightarrow \\ \vdots \\ \rightarrow \end{smallmatrix}$, $\begin{smallmatrix} \leftarrow \\ \vdots \\ \leftarrow \end{smallmatrix}$, $\begin{smallmatrix} \rightarrow \\ \vdots \\ \leftarrow \end{smallmatrix}$, $\begin{smallmatrix} \leftarrow \\ \vdots \\ \rightarrow \end{smallmatrix}$)**for** each sample position (x, y) in the up-sampled plane **do**set (i, j) based on (x, y) using Equation (2.13)**for** $(i', j') \in \{(i-1, j-1), (i, j-1), (i-1, j), (i, j)\}$ **do** $\bar{w}_{i',j'}^k \leftarrow \bar{w}_{i',j'}^{k-1} \cap \bigcup_{s \in \bar{v}[\langle x, y \rangle_w, c]} \bar{a}$ where \bar{a} is the smallest possible interval that satisfies equation (2.12) with \bar{a} for $w_{i',j'}$, s for $v_{x,y}$ and the estimates \bar{w}^{k-1} for the other w values.**until** $\bar{w}^k = \bar{w}^{k-1}$ **return** \bar{w}^k

Since the two chroma channels were up-sampled independently, we also down-sample them independently in Algorithm 2. As the next step (inverting the IDCT) also relies on interval arithmetic, we convert the sets of possible luma values (at the original resolution) to an interval representation: $\bar{v}[\langle x, y \rangle_w, 0] = [\min(\bar{v}[\langle x, y \rangle_w, 0]), \max(\bar{v}[\langle x, y \rangle_w, 0])]$.

The denote the intervals resulting from down-sampling as $\bar{v}^-[\langle i, j \rangle_{w/2}, c]$ (for $c \in 1, 2$) and the luma intervals are $\bar{v}[\langle x, y \rangle_w, 0]$.

4.4.3 Discrete cosine transform

The IJG decompressor implements the inverse DCT using the calculation described in equation (2.9).

To invert the IDCT, we need to solve $\text{IDCT}(\mathbf{X}) = \mathbf{x}$ for \mathbf{X} , knowing only that the 8×8 matrix result \mathbf{x} lies within a given interval matrix $\bar{\mathbf{x}}$. This will result in a frequency-domain interval matrix $\bar{\mathbf{X}}$. We can later refine the result to

$$\bar{\mathbf{X}}' = \{\mathbf{X} \in \bar{\mathbf{X}} : \text{IDCT}(\mathbf{X}) \in \bar{\mathbf{x}} \wedge \mathbf{X} \text{ matches quantisation constraints}\}. \quad (4.5)$$

Subsection 4.4.5 describes the quantisation constraints. The interval matrices $\bar{\mathbf{x}}$ stem from the previously down-sampled chroma ($\bar{v}^-[\langle i, j \rangle_{w/2}, 1]$, $\bar{v}^-[\langle i, j \rangle_{w/2}, 2]$) and luma ($\bar{v}[\langle x, y \rangle_w, 0]$) planes, tiled into non-overlapping 8×8 blocks, giving $\bar{\mathbf{x}}_b^c$ as the 8×8 matrix for block b in component c .

To invert (2.9), we apply the rules in (4.3), in conjunction with an additional rearrangement rule for matrix pre-multiplication: if $\mathbf{TX} = \bar{\mathbf{Y}}$, given an interval matrix $\bar{\mathbf{Y}}$ and a non-singular

4. Exact JPEG recompression

fixed matrix \mathbf{T} , we can efficiently find an interval matrix $\bar{\mathbf{X}}$ guaranteed to contain \mathbf{X} as

$$\begin{aligned} X_{i,j \perp} &= \left[\sum_k T_{i,k}^{-1} \cdot \begin{cases} Y_{k,j \perp}, & \text{if } T_{i,k}^{-1} \geq 0 \\ Y_{k,j \top}, & \text{if } T_{i,k}^{-1} < 0 \end{cases} \right] \\ X_{i,j \top} &= \left[\sum_k T_{i,k}^{-1} \cdot \begin{cases} Y_{k,j \top}, & \text{if } T_{i,k}^{-1} \geq 0 \\ Y_{k,j \perp}, & \text{if } T_{i,k}^{-1} < 0 \end{cases} \right], \end{aligned} \quad (4.6)$$

and similarly for matrix post-multiplication $\mathbf{X}\mathbf{T} = \bar{\mathbf{Y}}$. Because the elements of the matrix \mathbf{T}^{-1} are fractions of very large integers, the multiplications in (4.6) require arbitrary-precision arithmetic over rational numbers. We also use the rules

$$\begin{aligned} \max(\bar{x}, a) = \bar{y} &\implies [x_{\perp}, x_{\top}] = \begin{cases} [-\infty, y_{\top}], & \text{if } y_{\perp} \leq a \\ [y_{\perp}, y_{\top}], & \text{otherwise} \end{cases} \\ \min(\bar{x}, a) = \bar{y} &\implies [x_{\perp}, x_{\top}] = \begin{cases} [y_{\perp}, \infty], & \text{if } y_{\top} \geq a \\ [y_{\perp}, y_{\top}], & \text{otherwise.} \end{cases} \end{aligned} \quad (4.7)$$

Inverting the inverse DCT finds an interval containing each DCT coefficient in each block. We denote the 8×8 matrix of intervals for block b in component c by $(\bar{\mathbf{X}}_b^c)$.

4.4.4 Determining possible quality factors

The JPEG bitstream header contains 8×8 quantisation tables for luma and chroma. Each matrix element specifies a divisor (quantisation factor) for uniform quantisation of the corresponding coefficient in every transformed 8×8 block.

The recompressor DCT described outputs intervals for (dequantised) DCT coefficients, where each interval contains the result of a dequantisation operation. For each coefficient position $(i, j) \in \{0, \dots, 7\}^2$, we initially assume that any quantisation factor between 1 and 255 is possible (baseline JPEG uses 8-bit precision for these values), then eliminate any factor which is inconsistent with the interval we obtain for the coefficient in any block. The set of possible quantisation factors for the DCT coefficient position (i, j) in component $0 \leq c < 3$ is given by

$$\begin{aligned} \ddot{P}_{i,j}^c &= \{q \in \{1, \dots, 255\} : \nexists b. (\bar{\mathbf{X}}_b^c)_{i,j} = [X_{\perp}, X_{\top}] \wedge \text{div}(X_{\perp}, q) = \text{div}(X_{\top}, q) \wedge \\ &\quad ((X_{\perp} < 0 \wedge q \nmid X_{\top}) \vee (X_{\perp} \geq 0 \wedge q \nmid X_{\perp}))\}, \end{aligned} \quad (4.8)$$

where the predicates ensure that all blocks' DCT coefficient intervals contain at least one possible dequantisation result. In our implementation, the set of possible quantisation factors is stored efficiently in two 8×8 tables of 256-bit masks, which describe the set of quantisation factors possible at each position in each quantisation table.

In the IJG compression utility, the quantisation tables are selected based on a quality factor $f \in \{1, \dots, 100\}$ which selects what scaling factor will be applied to the matrices suggested

by Annex K of the JPEG standard [38] (see appendix A). Therefore, when the user specifies a quality factor, only 100 quantisation table pairs are possible. Given the possible quantisation factors at each coefficient position, the set of possible quality factors is given by

$$Q = \left\{ f \in \{1, \dots, 100\} : \forall (i, j) \in \{0, \dots, 7\}^2. (\mathbf{Q}_f^0)_{i,j} \in \ddot{P}_{i,j}^0 \wedge (\mathbf{Q}_f^1)_{i,j} \in \ddot{P}_{i,j}^1 \wedge (\mathbf{Q}_f^2)_{i,j} \in \ddot{P}_{i,j}^2 \right\}, \quad (4.9)$$

where \mathbf{Q}_f^0 and $\mathbf{Q}_f^1 = \mathbf{Q}_f^2$ are the luma and chroma quantisation tables associated with quality factor f .

4.4.5 Quantisation and exhaustive search

If an image was compressed with quality factor f , the set of possible quality factors in (4.9) will include f and also higher quality factors whose sets of possible dequantised values are a superset of those associated with quality factor f .³

In addition, our uncertainty in the DCT coefficient values may allow quality factors lower than f which also give quantisation bins that lie within all DCT coefficient intervals, but where the refinement (4.5) yields an empty set for one or more blocks. In this case, we remove f from the set of possible quality factors and try the next higher candidate for f .

For each block number b in component c , the quantised intervals with quality factor f are given by

$$\begin{aligned} (\hat{\mathbf{X}}_b^c)_{i,j} &= [\hat{X}_\perp, \hat{X}_\top] \\ \hat{X}_\perp &= \begin{cases} \text{div} \left(X_\perp, (\mathbf{Q}_f^c)_{i,j} \right) & X_\perp < 0 \vee (\mathbf{Q}_f^c)_{i,j} \mid X_\perp \\ \text{div} \left(X_\perp, (\mathbf{Q}_f^c)_{i,j} \right) + 1 & \text{otherwise} \end{cases} \\ \hat{X}_\top &= \begin{cases} \text{div} \left(X_\perp, (\mathbf{Q}_f^c)_{i,j} \right) + 1 & X_\top < 0 \vee (\mathbf{Q}_f^c)_{i,j} \mid X_\top \\ \text{div} \left(X_\perp, (\mathbf{Q}_f^c)_{i,j} \right) & \text{otherwise.} \end{cases} \end{aligned} \quad (4.10)$$

with $[X_\perp, X_\top] = (\bar{\mathbf{X}}_b^c)_{i,j}$.

The number of possibilities for a particular quantised block b in component c is given by

$$\prod_{(i,j) \in \{0, \dots, 7\}^2} \left| (\hat{\mathbf{X}}_b^c)_{i,j} \right| \quad (4.11)$$

where $|\bar{X}|$ denotes the number of integers in the interval \bar{X} .

³For example, quality factor 100 implies no quantisation, which means all values $s \in \{-1024, \dots, 1023\}$ are possible for each DCT coefficient.

4. Exact JPEG recompression

IDCT refinement

Based on running our recompressor on many images with different quality factors, we found that the number of possibilities for most blocks allows for an exhaustive search over quantised DCT coefficient blocks when the quality factor is less than about 90. For higher quality factors, the intervals output by the inverted IDCT are normally sufficiently large to make a search infeasible. In our implementation, we set the limit on the maximum allowable number of possibilities to $l = 2^{20}$ block values⁴.

If the number of possibilities for a block in (4.11) is less than the threshold l , for each possible value of the block we dequantise the quantised coefficients, perform an IDCT according to (2.9), and check whether outputs lie within the intervals $\bar{\mathbf{x}}_b^c$ for block index b in component c . We approximate the set of blocks that meet this condition by an 8×8 interval matrix. If exactly one value for the block meets the condition, the block is marked ‘exact’. If more than one value meets the condition, the block is marked ‘ambiguous’ and passes to the next stage of the search.

If the number of possibilities for a block is greater than l , we mark the block as infeasible to search.

$$\left(\hat{\mathbf{X}}_b^{lc}\right)_{i,j} \subseteq \left(\hat{\mathbf{X}}_b^c\right)_{i,j} \quad (4.12)$$

Impossible blocks

If the IDCT refinement stage finds that none of the possibilities for a block are consistent with the unquantised intervals $\bar{\mathbf{x}}_b^c$, the block is marked ‘impossible’. This indicates that the block was not output by the IJG decompressor, so we assume that the chosen quality factor was incorrect, and return to the quantisation stage with the next quality factor in (4.9).

Full decompression refinement of ‘ambiguous’ blocks

Blocks which were marked as ‘ambiguous’ and are co-located with exact blocks in the other colour channels are decompressed to the RGB representation and checked against the uncompressed input data. We tighten the intervals to bound those values which decompress to the original input data. If exactly one value remains, the block is marked as ‘exact’.

$$\left(\hat{\mathbf{X}}_b^{lc}\right)_{i,j} \subseteq \left(\hat{\mathbf{X}}_b^c\right)_{i,j} \quad (4.13)$$

After this step, remaining ambiguous blocks represent multiple possible bitstreams which decompress to the same image.

⁴This gives a worst case search that calculates a comparable number of inverse DCTs as are required to decompress one second of 720p60 high definition video in a block/DCT-based video codec such as MPEG-2.

4.4.6 YC_bC_r set refinement

The colour-space conversion is the first source of uncertainty in the exact recompressor, as we derive sets of YC_bC_r values for each pixel in the original image. By propagating back the spatial domain values from the IDCT refinement and up-sampling the chroma using (2.12), we find which YC_bC_r triples are not consistent with the refined values, remove these from the sets $\ddot{v}[\langle x, y \rangle_w, c]$ and run another iteration of the recompressor beginning with chroma down-sampling. We repeat the entire process until no further refinement of the YC_bC_r triples is possible.

4.5 Overall algorithm summary

Figure 4.2 shows information flows in our exact JPEG recompression algorithm. The sequence of operations when operating on exactly recompressible input is as follows:

1. RGB to YC_bC_r colour space conversion, giving sets of possible YC_bC_r values
2. Down-sample chroma planes in interval representation
3. Invert the IDCT on each block of intervals
4. Determine possible quantisation settings by a process of elimination
5. Quantise DCT coefficient intervals
6. For each block possibility, dequantise and perform a trial DCT
 - Eliminate possibilities where the result does not lie in the intervals established before the inverse IDCT
 - ‘Exact’ blocks have exactly one possibility
 - ‘Ambiguous’ blocks have several possibilities
 - Blocks with too many possibilities are infeasible to search
 - No blocks are marked ‘impossible’ as the input is exactly recompressible
7. For each block marked ‘ambiguous’, decompress each possibility as an independent block. Eliminate possibilities that do not match the co-located uncompressed input after decompression, and mark the block as exact if one possibility remains.
8. For each block marked ‘ambiguous’ or ‘exact’, decompress each possibility, and filter the original YC_bC_r up-sampled chroma/luma planes based on the results
9. If this filtering updated any of the YC_bC_r sets determined in step 1, repeat the process from step 2

4. Exact JPEG recompression

10. Otherwise, output as follows:

- All blocks marked ‘exact’: the unique bitstream (consisting of quantisation tables and quantised DCT coefficients for each block)
- All blocks marked ‘exact’ or ‘ambiguous’: output a description of all possible bitstreams and one example
- One or more blocks were infeasible to search: naïvely recompress those blocks, and output other blocks as above

4.6 Results

We tested our recompressor on 1338 images from the uncompressed image database UCID [90]. The original images have 512×384 RGB pixels. Using the IJG utilities `cjpeg` and `djpeg` for compression and decompression, we performed one compression cycle on each image using each of the quality factors $f \in \{40, 60, 70, 75, 80, 82, 84, 86, 88, 90\}$, giving 13380 test images.

As the test images are the result of a decompression operation using the IJG decompressor, no blocks were classified as ‘impossible’ by our recompressor, meaning that all blocks in the images are either exactly recompressed, ambiguous (meaning that multiple JPEG bitstreams produce the input on decompression) or infeasible to search.

Figure 4.4 shows the recompression performance on a representative subset of these quality factors. The histograms show the binned proportion of infeasible blocks in each image for quality factors $g \in \{40, 60, 75, 88, 90\}$. For a given image, a proportion of zero indicates that the entire image was recompressed perfectly, and one indicates that no blocks were recompressible.

We ran our recompressor on each image, calculating the proportion of blocks in the image that were infeasible to search. Figure 4.4 shows that these blocks are rare at lower quality factors, whereas at quality factors higher than 85, the number of infeasible blocks sharply increases. At quality factor 90, more than a quarter of all blocks were infeasible to search (see table 4.6).

The number of infeasible blocks is generally correlated with the number of saturated values input to the interval DCT (that is, the number of spatial domain YC_bC_r samples equal to 0 or 255), which must be mapped to large intervals, as the last operation of the IDCT is to clip its output. The comb plots show the average number of saturated pixels among those images in each bin of the histograms. Figure 4.5 shows the same experiment but where the input images were first desaturated. Recompression performance increased substantially, but quality factors of around ninety or greater precluded whole-image recompression in almost all cases⁵.

⁵If we consider the general problem of range limiting and saturation in exact recompression, it is worth noting that formats exist that store black and white values using non-extreme values, in order to allow space

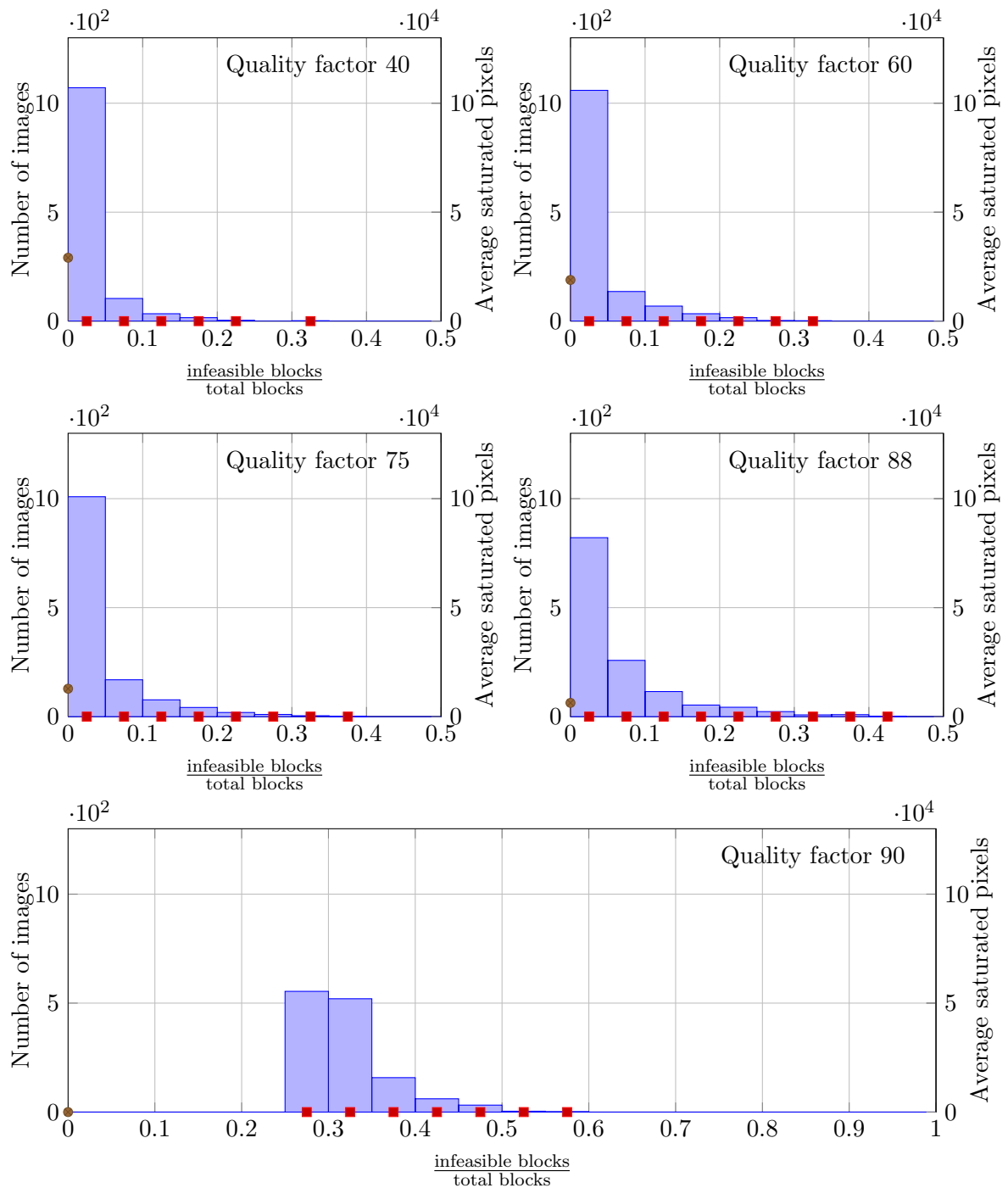


Figure 4.4: Each histogram summarises the performance of the exact recompressor at one particular quality factor on a dataset of 1338 images. For each image, we applied the exact recompressor and noted the proportion of blocks in the image that were infeasible to search. The histograms show the number of images with each binned proportion \square , the number of images that were completely recompressed \bullet and the average number of saturated RGB pixels in the images that populate each bin \blacksquare .

4. Exact JPEG recompression

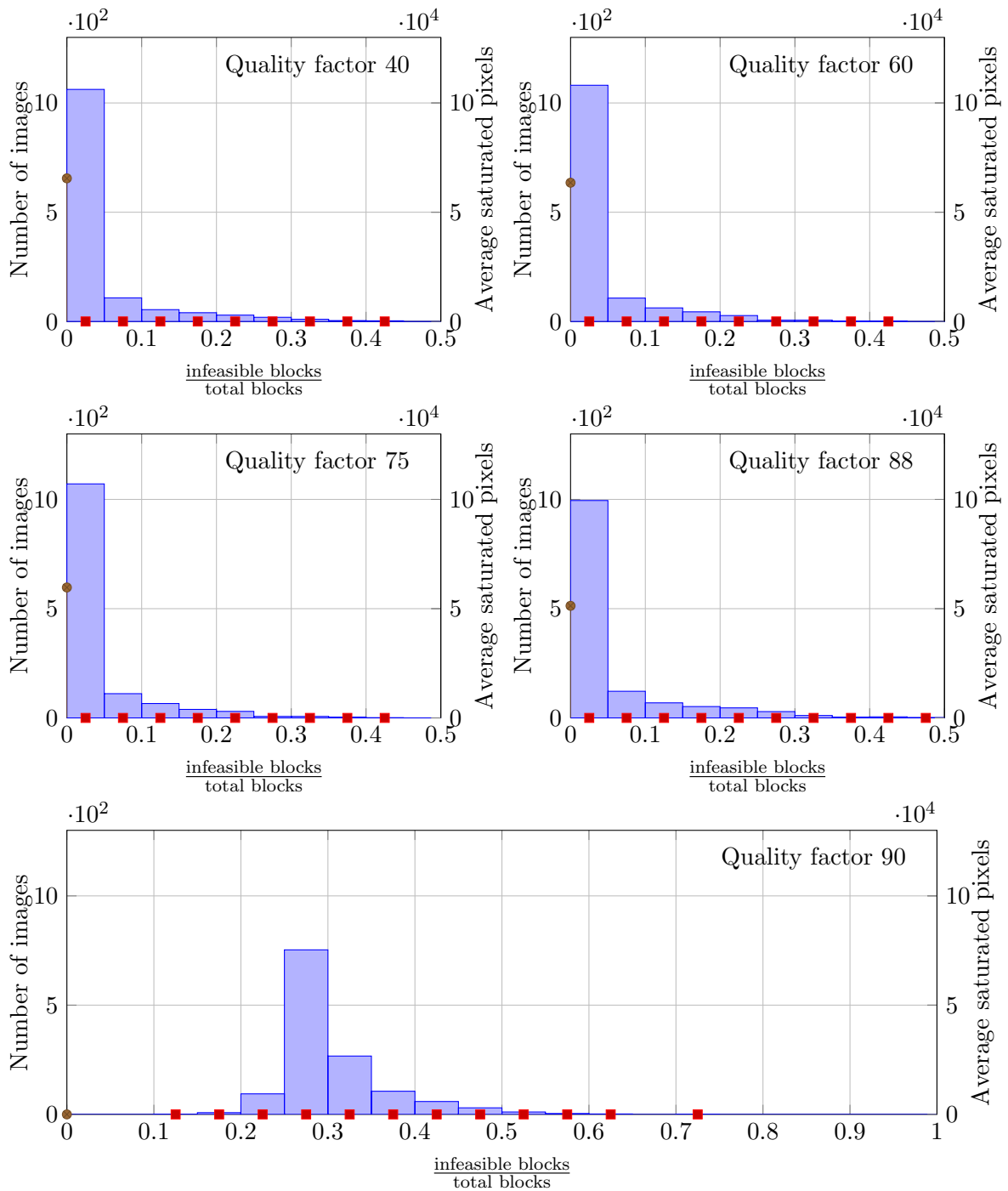


Figure 4.5: The same experiment as shown in figure 4.4, but where each test image was first pre-processed to remove very dark and very light pixels before recompression.

Images that were previously compressed at high quality factors are difficult to recompress because the quantisation step does not reduce the number of possibilities sufficiently to allow a search. At lower quality factors (i.e., higher quantisation factors) only a small number of possibilities normally remain inside the intervals resulting from IDCT reversal.

Exact recompression is computationally expensive. Higher quality factors and saturated pixels tend to lead to longer runtimes, because each block has more possibilities which must be filtered. On our test machines, which have 2 GHz CPUs, the easiest images took around thirty seconds to recompress, while the most difficult images took up to thirty minutes.

Our exact recompressor is able to match or outperform naïve recompression in all cases, as infeasible blocks can be replaced with naïvely recompressed blocks, and other blocks are either ambiguous or exact, so result in an identical image block to the co-located input block on decompression.

Quality factor	Blocks recompressed exactly	Ambiguous blocks
40	98.0	0.1%
60	97.0	0.1%
70	96.6	0.1%
75	96.2	0.1%
80	95.5	3.5%
82	95.2	4.6%
84	94.8	6.8%
86	94.1	6.6%
88	94.2	6.5%
90	67.9	3.4%

Figure 4.6: Exact recompression recovers more than 94% of image blocks in our test data set, up to quality factor 88. At higher quality factors, the search to refine the DCT results is often infeasible for many blocks, but 68% of blocks still recompressed exactly.

4.6.1 Detecting in-painting

Our exact recompressor finds any regions of the image that are not consistent with JPEG decompression. This subsection shows how to use exact recompression to attack an image-based CAPTCHA (‘completely automated public Turing test designed to tell computers and humans apart’) that uses in-painting to generate new image content automatically.

In [103], Zhu et al. describe a CAPTCHA based on the difficulty of automatic object recognition from photographs. Their algorithm generates challenges by cropping a small region from for overshoot/undershoot after processing. This includes ITU-R BT.601 for encoding analog signals in digital video [46] which has been referenced in some MPEG standards.

4. Exact JPEG recompression

a randomly-chosen image containing an object of interest, filling in the cropped region using an in-painting algorithm (described in [95]), then generating seven candidates with similar content to the cropped region. The seven candidates and the original cropped image region are shuffled and presented to the user, who must choose which of the eight possibilities is the correct replacement for the in-painted region, and indicate where it belongs in the image.

Their algorithm relies on the difficulty of determining which area has been filled in automatically. Given the outline of the replaced area, selecting the correct candidate and moving it into place is quite easy.

Figure 4.7 shows the result of applying our exact recompressor to a typical challenge image. The algorithm fails to recompress the image, and outputs a bitmap showing the region which is inconsistent with JPEG decomposition.

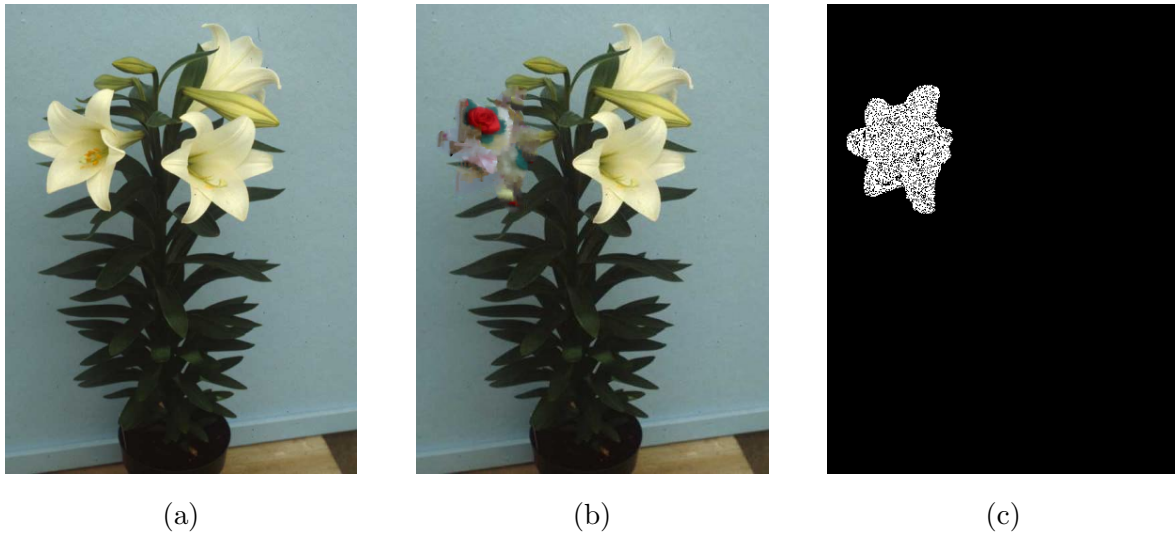


Figure 4.7: (a) shows an original JPEG decomposition result, used as a source image for the CAPTCHA. Cropping and in-painting a region of the image results in (b). Our exact recompressor successfully isolates the in-painted area (c).

As a counter-attack, the CAPTCHA could use uncompressed source material for challenge images, or apply a final processing step which disrupts the patterns introduced by JPEG decomposition (such as down-sampling or blurring).

4.7 Analysis

Our results show that it is possible to recover partial or complete JPEG bitstreams that encoded a given IJG decomposition result when the compression quality factor is less than about 90. Preprocessing the test images to remove very dark and light pixels allowed a higher proportion of DCT blocks to be recovered.

The algorithm relies on a search to filter candidate quantised DCT coefficient blocks for each block in the image. In our implementation, the size of the per-block search is limited by a threshold, which we chose so that recompression terminated after around thirty minutes on all images in our dataset. The algorithm fails on blocks that are skipped due to this threshold. In the IJG compressor, quantisation factors decrease monotonically with increasing quality factor. This led to a higher proportion of failed blocks in high quality images.

Images compressed at higher quality factors required more computation time, and had a higher proportion of skipped blocks. The primary reason is the increased search size caused by lower quantisation factors, especially those applied to lower spatial frequencies. Very dark and light pixels also degraded performance.

Our algorithm successfully located modified regions of decompressor output that were inconsistent with computations performed during decompression. Based on our experiments, inverting colour space conversion was already sufficient to locate tampered regions. In practice, it is unlikely that naïve tampering on a decompression result would avoid the three-quarters of RGB cube values that the IJG decompressor never outputs. Our algorithm can detect inconsistencies in earlier stages of the decompression algorithm as well.

Exact recompression is necessarily limited to detecting tampering on uncompressed output, when the original source was generated by a known decompressor implementation. This makes it less useful for forensics work, because images under investigation are often in compressed format. However, when used in conjunction with double compression detection algorithms, exact recompression is a useful forensics tool.

4.7.1 Possible extensions to the algorithm

The performance of our algorithm in terms of time cost and the proportion of blocks marked infeasible to search could be improved by implementing logic for deciding how many candidates to test for a given DCT block before skipping it. Processing blocks with fewer possibilities first should improve the overall computation time by reducing the search space on later iterations of the algorithm. Furthermore, obtaining a partial solution quickly might be acceptable in image editing software, avoiding quality degradation due to recompression of unmodified regions.

Performing exact recompression on a series of test images produced with quantisation tables that varied gradually, rather in the steps caused by the quality factor/quantisation table mapping, could help to determine which spatial frequencies' quantisation factors caused the change in performance between quality factors 88 and 90. The desired approximate computation time (or infeasible block proportion) could be added as an option to the tool, to guide the algorithm's choice of search threshold for each block.

Developing exact recompressors for other JPEG decompressor implementations would give a set of programs useful for decoder identification. If the computations performed by different

4. Exact JPEG recompression

decompressors produce different results, those exact recompressors that successfully recover the bitstream for a given image indicate the set of decompressors that could possibly have produced the image.

We have investigated how saturation in the luma channel affects the performance of exact recompression. Saturated pixels in the chroma channels will also affect performance, though the quantisation factors applied to the colour channels are higher so the improvement is likely to be smaller than that observed on luma data.

Exact recompression might be feasible for other lossy formats. In particular, exact recompressors for video formats would be useful to attack DRM schemes that rely on the quality reduction caused by naïve recompression to reduce the value of unauthorised copies. Such a recompressor would be more difficult to implement because video decompressors must generally store more state than image decompressors. Tracking possible states might be too computationally expensive. Information loss during motion compensation might also make exact recompression impossible. However, video keyframes are usually processed similarly to JPEG images, which might make recompression to recover parts of the bitstream feasible.

Where more than one bitstream produced the same output ('ambiguous' blocks), it is possible to produce the smallest possible bitstream yielding the input image on decompression, by selecting the possibility that has the shortest coded representation in JPEG's entropy coding scheme.

4.8 Conclusion

Exact recompression is useful as an approach to minimising information loss in processing pipelines handling compressed data. We have also adapted the algorithm to recover information of value to forensic investigators.

Our implementation successfully recovers 96% of DCT blocks at the default IJG quality factor, while images compressed at high quality factors, and images with saturated pixels, lower the performance of our algorithm. At quality factor 90 we are still able to recover 68% of blocks exactly.

Chapter 5

Reconstruction of fragmented compressed data

The latest generation of video cameras use the H.264/AVC compression format to store video data efficiently. Because the files are usually larger than a single block of storage, they may be split up into many fragments when they are written to disk or memory. Fragmentation can occur when no sufficiently long runs of contiguous blocks are available, and also in flash memory devices which try to avoid wearing out individual blocks by distributing writes.

Fragmentation is a problem for forensic investigators whenever block allocation information is inconvenient to access or completely absent. Files might be deleted but intact in deallocated space, or fragmented in flash memories with inaccessible wear-levelling metadata. Compressed bitstreams are particularly difficult to defragment based on content alone because they are produced by algorithms which try to remove redundancy.

In this chapter, I present a general-purpose algorithm for location and defragmentation of compressed bitstreams with arbitrarily permuted blocks, without relying on detailed information about multimedia containers or filesystem layout. The algorithm uses an efficient syntax-checking parser as part of a specialised search algorithm, taking advantage of remaining redundancy in compressed bitstreams due to restrictions on syntax.

I demonstrate the algorithm on Baseline profile H.264/AVC bitstreams, and show that it can locate and defragment video files from a variety of sources.

5.1 Overview

Forensic investigators often need to recover files from raw memory dumps without relying on filesystem data structures, especially when they are searching hard disks and mobile device memories for deleted material. Deleted files remain intact in unallocated space, until they

5. Reconstruction of fragmented compressed data

are overwritten by new data. The process of recovering files from raw memory dumps ('disk images' or 'storage images') without filesystem metadata is sometimes called 'carving', because the investigator needs to find each file's bytes among data which may at first seem homogeneous.

The task is made more difficult when files are split up into two or more physically non-contiguous pieces due to the storage device (or filesystem) allocation algorithm. Such files are described as fragmented. If a byte address n in an image contains byte m in a file, and the image address $n - 1$ does not contain file byte $m - 1$, we say that there is a discontinuity between bytes $n - 1$ and n in the image ($m, n \in \{1, 2, 3, \dots\}$).

Blocks are the smallest data allocation units on a device (or filesystem) under consideration. They are equally sized, non-overlapping, uniformly spaced sequences of bytes. Depending on how an image was acquired, its block size may either depend on the filesystem allocation strategy, or on the low-level hardware data layout. For example, a hard disk might have 512 byte long track sectors, while its filesystem might use four kilobyte blocks. Capturing an image using the operating system's filesystem interface would yield an image with a block size of four kilobytes, while using the low-level hardware interface of the disk might produce an image with 512 byte blocks.

Discontinuities can only occur at the uniformly spaced block boundaries in the image: for a block size of b bytes, block boundaries are just before the byte addresses $b \cdot n$ ($b, n > 0$). Contiguous sequences of bytes between any two adjacent block boundaries are also contiguous in files, while sequences of bytes which lie across one or more block boundaries might not be. The interface provided by the storage device handles the mapping from logical (file) addresses onto physical (image) addresses. Logically contiguous reads/writes may be physically non-contiguous if the read/written memory address range contains a block boundary.

Fragmentation is also common in images captured from mobile devices and solid-state disks, which use non-volatile flash memory, where the metadata on block ordering may be inaccessible or absent. The types of files that are usually of interest to forensic investigators (email records, images, logs, sound files, and videos) are usually found fragmented in hard disk images, because they are written by programs that append data to growing files, and can be quite large. Recovery tools must rely on redundant ordering information in the files' contents to piece them back together. Compressed files present a particular challenge because, at first glance, they look like random noise.

In this chapter we present an algorithm which locates and defragments compressed bitstreams automatically, and demonstrate its application in recovery of H.264/AVC video bitstreams [45]. As a source of redundancy, the tool relies on syntax errors in the bitstream format. These indicate when a compressed bitstream is internally incorrectly ordered. Our tool is the first such utility that recovers files when blocks in the image are permuted arbitrarily, without relying on probabilistic techniques.

The defragmentation tool takes as input a bitstream syntax description, which may be written for any format, and an image which could contain fragmented bitstreams conforming to the description. It generates an efficient syntax-checking parser based on the user-specified bitstream syntax description. We also use the syntax description to generate all valid bitstrings (up to a given syntax element), locate positions in the image that match any of these bitstrings, then by a process of elimination we construct a map of valid bitstream extents in the image. Finally, we apply a specialised depth-first search to find out which disk block permutations within each extent lead to complete, error-free bitstreams. The tool returns the locations of any conforming bitstreams and the associated permutation on the image blocks, which allows them to be decoded correctly according to the generated parser. It can also output a file containing the bitstreams, which may be playable in standard viewers, depending on the compression format.

Section 5.2 describes prior work on automatic file carving and syntax error detection in H.264/AVC Baseline profile bitstreams. Section 5.3 gives a description of the automatic defragmentation problem. Sections 5.4 and 5.5 present our language for providing bitstream syntax descriptions, and include part of the description file for H.264/AVC Baseline video bitstreams. Section 5.6 describes the main search algorithm, which uses the bitstream syntax description. Sections 5.7 and 5.9 evaluate the performance of our algorithm and summarise our conclusions.

This chapter contains as-yet unpublished material. I presented some of the work at the International Communications Data and Digital Forensics (ICDDF) conference, 28th–30th March 2011, Heathrow, UK. My presentation was by invitation of the London Metropolitan Police Service digital forensics laboratory.

5.1.1 Terminology

In this chapter, I use the following terminology:

Images are binary files (sequences of bytes) captured as raw memory dumps from storage devices such as Flash memories, solid-state disks or hard disks.

Bitstreams are sequences of bytes embedded within an image that may contain useful information. To parse a bitstream, it may be necessary to decode other bitstreams first, in order to build up a decoding context.

Metadata structures are serialised binary data (bitstrings) within the image that store auxiliary information. They are used by filesystems or devices to index and locate files within the storage medium, check/maintain data integrity, and so on.

Extents specify subsequences of bits within an image, based on an offset and bit-length.

5. Reconstruction of fragmented compressed data

Fragmented images can contain bitstreams that might be split up into pieces. We consider one particular mode of fragmentation, where blocks (filesystem/device allocation units) may have been shuffled.

File carving algorithms try to locate bitstreams matching given criteria in an image, without relying on filesystem metadata.

5.2 Background and prior work

Automatic file carving algorithms take a disk image as input and return a list of extents within this image that appear to have data of a sought file type. They are used to extract (possibly deleted) files stored in a computer or mobile device memory, accessed through a low-level hardware interface. The files may be useful evidence in forensic investigations or espionage. Such algorithms can also recover unintentionally deleted files, or files in storage with corrupted filesystem metadata. Software filesystem interfaces generally fail in these circumstances, so carving algorithms operate on the underlying raw data, possibly making assumptions about the filesystem.

This section first reviews the current literature on automatic file carving in unfragmented and fragmented filesystems. A common feature of these methods is the use of an algorithm that evaluates the likelihood that a given byte sequence is part of a particular type of file. Similarly, our defragmenter relies on a syntax checker to determine whether a given bitstream is error-free. Therefore, subsection 5.2.4 covers prior work on error detection in H.264/AVC bitstreams, as this is the data format used in our practical demonstration of the algorithm.

Work in this area is mainly motivated by law enforcement forensic science laboratories and some commercial/private interest in data recovery. The annual Digital Forensics Research Workshop (DFRWS [8]) has driven some of the work in file carving, partly through its forensics challenges, which encourage competitors to recover as much information as possible from a provided disk image containing many types of data. Their website contains several interesting reports from participants (for example, [5]).

5.2.1 Data acquisition, fragmentation and filesystems

The first step in recovering data from a device is to capture a disk image (‘imaging’ the device). For flash memory in mobile telephones there are three main approaches [6]:

1. using software tools written by a telephone manufacturer (intended for maintenance engineers to diagnose problems with devices) or hackers. These tools are sometimes called ‘flashers’ and rely on a physical interface on the device, such as a USB port;

2. opening the device and using JTAG, or similar internal in-system diagnostic ports of the memory chip to access it directly; or
3. desoldering the memory chip and accessing it through its bus interface using custom hardware.

Forensic investigators prefer to avoid turning the device on, as this can trigger garbage collection or wear-levelling operations, which might destroy useful data.

Software tools such as `dd` on Unix can image undamaged flash memory cards and USB storage devices, and the same approach applies for hard disks.

It is usually necessary to deal with fragmentation when recovering deleted files, and files stored in wear-levelled flash memories.

Flash memory fragmentation due to wear-levelling

Memory blocks are sometimes referred to as clusters. Flash memory blocks are sometimes called erase units, because each write operation involves loading a block into fast memory, updating any modified bytes, and writing back the entire block. Each erase operation may deteriorate a block's performance (that is, increase its probability of errors). Erase units typically wear out after 10^4 – 10^6 writes [25].

In devices where an erase unit may be written many times, such as in a general-purpose filesystem on a personal computer, the flash memory controller may use 'wear-levelling' algorithms that maintain a mapping from logical block indices (referenced by the filesystem) to physical blocks indices. They can alter the physical block address on each write to a logical block, simultaneously updating the mapping. The algorithm which distributes write operations is often proprietary and hard to reverse engineer, so in this chapter's simulations we assume that blocks are randomly permuted¹, which can give any block ordering that a more advanced wear-levelling algorithm might produce.

Flash memory erase units are typically 4, 16 or 128 kilobytes long, and each has an associated 'spare area', which stores error correction information, wear-levelling metadata and information about whether the block exhibits a high error rate and should not be used [25]. Based on our discussions with the London Metropolitan Police forensics department, images captured from flash memories often appear to be fragmented in $8 \times 512 = 4096$ byte blocks.

Wear-levelling may be performed either by the software device driver or a hardware controller. In the former case, an image acquired directly from the hardware may exhibit fragmentation.

One possible approach to defragmentation is to use any remaining metadata to reconstruct information about the files (see for example [68]). However, this technique relies on detailed

¹If further assumptions can be made about the wear-levelling algorithm, they can be used as a heuristic to make the defragmentation algorithm faster.

5. Reconstruction of fragmented compressed data

knowledge of the device's metadata format, and is impossible if wear-levelling information is stored in unaddressable memory, has not been documented by the vendor, or files have been deleted, wiping metadata.

Recovery of deleted files

When there is not enough free space to store files contiguously, filesystems allocate two or more separate extents of contiguous free blocks. For example, Microsoft's FAT32 filesystem has four kilobyte blocks, and each file index entry is associated with a linked list of pointers to blocks containing its data.

When files are deleted, their blocks are marked as unallocated, and metadata describing the blocks allocated to the file may be deleted, but the file's content is normally left intact. (For example, UNIX/Linux filesystems, such as ext3, delete pointers to inodes from a directory when a file is deleted [7, File recovery, Page 446].)

Modern filesystems do not heavily fragment most files, based on a survey of hundreds of second-hand hard disks [27]. However, files of forensic interest are often fragmented because they are frequently appended to, and may be many blocks long [28]. Compressed video bitstreams are very susceptible to fragmentation because they can be quite large and are often written sequentially, and concurrently with other files.

File carving software which processes unallocated data to find deleted files must therefore frequently deal with fragmentation.

5.2.2 Unfragmented file carving

Current automatic file carving tools generally rely on locating particular known header/footer byte sequences (markers) to identify ranges of bytes which may contain the sought file type. For example, JPEG compressors produce bitstreams that start with the hexadecimal byte sequence `FF DE FF` (then either `E0` or `E1`), and end with `FF D9` [28].

Certain data structures are also amenable to file carving. Some file formats have fields containing pointers (integer offsets) to positions within the file at which known byte sequences can be found. For example, the ISO base media file format [42] uses a sequence of 'boxes', each of which is represented in the bitstream by a length tag and an ASCII-encoded four character text string specifying the box's type; if a box is l bytes long, the parser can expect to see another box after skipping l bytes (with its own length tag and four character text description). The text descriptions come from a known set of possible types. PDF files also have these type of structures, which makes them easier to carve [12].

Several software tools are available for automated carving in the absence of fragmentation.

Foremost [52] recovers deleted files by detecting header and footer byte sequences. It was the basis for Scalpel [36], a newer and faster program. Both programs return bitstreams contained between a file type’s header/footer markers. They are open-source.

The Netherlands Forensic Institute’s Defraser (Digital Evidence Fragment Search and Rescue) tool [30] is designed for compressed image/video file carving and supports a wide variety of compressed formats and containers, but does not recover fragmented files. According to its website, it “is a forensic analysis application that can be used to detect full and partial multimedia files in datastreams. It is typically used to find (and restore) complete or partial video files in datastreams (for instance, unallocated disk space)”. It uses ‘detectors’ to discriminate between valid and invalid candidate bitstreams. The developers are currently implementing support for H.264/AVC video. The tool is open-source, and has a plugin interface so that users can write new detectors.

Van der Knijff described a procedure for recovering an MPEG-4 [41] video from an unfragmented flash memory dump [98]. He carves a file to find the video’s key frames, and decodes the final bitstream with `ffmpeg`, outputting frames as JPEG files.

Several commercial utilities recover partially corrupted image files from memory cards and filesystems (for example, [15, 16]). Open-source utilities are also available (for example, [1]).

5.2.3 Fragmented file carving

Recovering data in fragmented files is a more difficult problem, because the tool must identify each discontinuity, and join logically adjacent sections of the file. Pal and Memon survey several techniques [76].

A common approach is to find candidates for the header and footer of the file based on searching for particular byte sequences, then do a search of potential fragmentation positions using a modified decoder to detect whether jumping at a given offset produces a valid bitstream. The approach normally assumes that the level of fragmentation is low: 1–4 fragments per file is typical. The techniques were often used manually by forensic investigators, until user-assisted and automatic tools became available [12].

Defragmentation algorithms

Some papers formulate defragmentation as a path-finding problem. For a given image, they construct a graph with nodes representing blocks and directed arcs weighted with the probability that the connected pair of blocks are contiguous. Finding k disjoint longest paths gives a candidate defragmentation of k files.

To calculate the arc weights, one approach suggests decoding each block separately, and using a probabilistic model to estimate the likelihood that the blocks’ contents follow each

5. Reconstruction of fragmented compressed data

other, by making assumptions about the encoded data. For example, a model for digital photographs might assume that sudden differences in image content and sharp edges are quite rare, so blocks with similar image content and smooth variations will be assigned a higher probability of being adjacent. For uncompressed text files, one approach applies prediction by partial matching [10], which uses a context model to predict the probability of observing a particular character given previous data, over several window sizes. These approaches are only applicable when it is possible to decode file information inside a block independently from the rest of the file, which is not the case in some compressed bitstream formats, where decoder desynchronisation is a problem (that is, when it is only possible to evaluate the probability of observing a particular part of the bitstream having decoded up to that point in the file). Even if it is possible to decode separate sections of the file, constructing a realistic probabilistic model can be difficult.

Having constructed a graph of the file, several methods are available for finding the shortest paths. The state of the art, introduced by Pal [77], uses sequential hypothesis testing to join blocks which are expected to be contiguous with high confidence, and constructs paths for all files simultaneously, allowing overlapping paths. When one path is complete, it discards all the other paths and removes the complete path's nodes from the graph, then repeats the procedure, until all files have been reconstructed.

Cohen [12] proposes an alternative model to deal with files that are not heavily fragmented. He uses 'discriminators' which detect whether a given bitstream is valid, and generalises the technique of finding header/footer byte sequences, by locating positions in the image which are 'positive constraints' (associated with known positions in the file, such as header data) and 'negative constraints' (positions known not to be in the file). His technique also tries to model the block allocation strategy of the filesystem, through so-called 'fragmentation models', that enforce assumptions about where data are likely to be located. He shows that his fragmentation models are accurate for hard disks. However, they do not allow for heavily fragmented files, as might be found in images from wear-levelled flash memories. He describes a general structure for defragmenters, where information from discriminators is fed back to the fragmentation model to generate new candidate fragmentation points.

Block classification

The cost of search-based defragmentation algorithms increases with the memory size measured in blocks: larger memories and those with fragmentation over smaller block sizes are more expensive to defragment. To reduce the cost, some techniques suggest using block classification algorithms to filter the set of blocks available to each file, to include only those which seem to contain the sought type of content [73].

Network traffic analysers use similar techniques to classify packets efficiently based on their payloads. Most techniques involve constructing histograms of byte values within a block, as

certain formats will have peaks at certain byte values (for example, ‘<’ and ‘>’ characters in ASCII/UTF-8 encoded HTML/XML files). Their performance can be improved by weighting different byte values based on how consistently they appear to be common over many files of the same type, and measuring frequencies of observing particular differences between adjacent byte values (the latter improvement giving a 99% classification performance on JPEG images in one experiment [48]). Statistical entropy can be used to distinguish broad classes of files. However, it is generally difficult to distinguish different compressed file types (and encrypted files) because they look like random byte sequences.

Syntax-checking parsers

A common feature of defragmentation algorithms in the literature is the use of syntax-checking parsers (also called validators, detectors or discriminators), that output whether a candidate bitstream could be part of one of the sought files. False positives occur when the parser accepts the bitstream but it could not be part of a file. If the parser rejects the bitstream despite its content being valid, this is a false negative.

It is acceptable for the parser to output false positives, because they can be eliminated later using a more thorough parser or by manual inspection. The parser should avoid false negatives because they are difficult to fix retrospectively. Parsers should be computationally efficient and report errors as soon as possible. They should use all internal error-checking features in the bitstream format.

The JPEG standard describes a way to insert integrity check values (called ‘restart markers’) at regular intervals in a stream. These allow decoders to restart decoding after corrupted data, and include two bit long sequence numbers, which help detect whether information might be missing. Karresand and Shahmehri [49] use these markers to defragment JPEG images. However, the markers are an optional part of the bitstream.

Custom-written format parsers are not commonly used. The alternative is to use general-purpose parsers for each file format, such as standard video players and image decoders, and detect when these parsers encounter an error.

This approach has several disadvantages. General-purpose parsers tend to attempt to recover from errors rather than reporting them, which means that errors are not reported as early as possible; early error detection is important because the location where errors are detected is a bound on the address of a fragmentation point, assuming the original file contains valid syntax. Some of the work done by these parsers might also be superfluous to the defragmentation problem. For example, if syntax checking is the only requirement, and the parsers go as far as producing the decompressed data, a lot of computation time has been wasted. Finally, general purpose parsers may have an interface that is not suitable for error detection. For example, they may not return the earliest bit offset in the image where they detected a syntax error.

5. Reconstruction of fragmented compressed data

Garfinkel [28] found that JPEG decompressors typically output several corrupted blocks after first finding an error, but would always correctly output at the end of decoding whether any errors had been found in the bitstream.

Cohen [13] modified `libjpeg` (the Independent JPEG Group codec [57]) to allow snapshotting/resuming decoding, then used this in conjunction with `fork` to decode from several fragmentation points in parallel.

The disadvantage of custom-written syntax-checking parsers is that they can be quite time-consuming to write and test. Our defragmentation tool tries to ameliorate this problem by accepting a syntax description written in a simple programming language, which we then process to produce a fast parser.

5.2.4 H.264/AVC error detection

Our defragmentation algorithm relies on the ability to filter out erroneous candidate bitstreams very efficiently. We use compressed bitstream syntax errors to identify which bitstreams are definitely not possible, and these are specified by means of a syntax flowgraph description, annotated with restrictions whose violation indicates a syntax error. To demonstrate our defragmentation algorithm, we wrote such a syntax description for H.264/AVC bitstreams. This subsection describes prior work on H.264/AVC syntax checking.

Prior work in error detection in compressed video streams has been directed towards video conferencing and streaming applications. In these scenarios, a client typically receives a sequence of packets from the server. The packets may be dropped, which leads to non-contiguous sequence numbers, or corrupted, which can be detected by testing a checksum value in the packet's header. Retransmission is often not practical, since it introduces unacceptable latency, so clients must deal with corrupted and missing packets.

Because video compression schemes use previously decoded data to predict later data, errors may propagate, so that a decoder reconstructs pictures that are inconsistent with the encoder's model. Errors can propagate spatially (within a picture) and temporally (to future pictures). Error concealment algorithms try to minimise the distortion produced by errors by detecting errors and recovering, using data known to be correct.

However, corrupted packets do not always need to be discarded entirely; bytes preceding the corruption are transmitted correctly and can be decoded usefully. Superiori, Nemethova and Rupp [96] use syntax error detection in H.264/AVC bitstreams to find a bound on the address of corruption in a video stream. An error's position only tells us the latest possible point at which bytes may be uncorrupted; the interval between occurrence and detection can be large.

Their error detection and concealment strategy outperforms simpler packet dropping and 'straight decoding' (where the decoder simply picks the closest value, or safest context, when decoding an invalid syntax element value). They classify syntax errors into three categories:

(1) codeword errors, where the next bitstring in the stream does not match any of the allowed bitstrings for the decoder’s current coding mode, (2) contextual errors, where decoding the value leads the decoder to enter an illegal state (for example, incrementing the macroblock address outside the bounds of the picture), and (3) out of range values, where the decoded value exceeds the allowed range for a syntax element (for example, a macroblock type is decoded which is not in the set of allowed values given the current slice type). Because their algorithm uses a full decoder (a modified version of the JM reference decoder [11]) they are able to detect errors which only arise after reconstructing pixel values. However, they do not detect all possible errors in the syntax, and in particular don’t support error detection in metadata.

5.3 The defragmentation problem

We represent a memory dump image \mathbf{f} as a vector of N bytes $f[i] \in \{0, \dots, 255\}$ ($0 \leq i < N$). Let the block size be b , so that the total number of blocks in the image is $B = \lceil N/b \rceil$. The unfragmented image \mathbf{g} has bytes $\mathbf{g}[i] = \mathbf{f}[\pi^{-1}(\lfloor i/b \rfloor) + (i \bmod b)]$ ($0 \leq i < N$), where the permutation mapping physical (fragmented) memory block indices onto logical (unfragmented) block indices is $\pi : \{0, \dots, B - 1\} \leftrightarrow \{0, \dots, B - 1\}$. We write $\mathbf{f} = P_\pi(\mathbf{g})$ to indicate that \mathbf{f} is the result of reordering the blocks of \mathbf{g} according to permutation π .

5.3.1 Syntax checkers

A syntax checker $\text{SYNTAXCHECK}(\mathbf{g}[o : o+l], c)$ is a function which takes a candidate bitstream as a vector of byte values (here consisting of the bytes from offset o to $o+l-1$ inclusive) and some decoding context c , and returns `TRUE` if the bitstream is error-free when decoded in the context c , and `FALSE` otherwise. We assume that bitstreams start at byte-aligned addresses.

The ideal syntax checker SYNTAXCHECK^* detects exactly those errors which can ever be detected (for example, by reference to a standardisation document).

The user must specify a syntax checking parser implementing the function $\text{SYNTAXCHECK}'$, which we can use to check whether a given bitstream is error-free. This function should provide an over-approximation of the set of valid bitstreams: it should never output `FALSE` when provided with a valid bitstream and sufficient context as input, which would be a false negative. It may output `TRUE` when the input bitstream is not error-free according to the standard, which is a false positive. We discuss how to handle false positives later.

5.3.2 Decoding contexts

If the syntax checking parser can reference contextual information decoded in other bitstreams, and this affects whether a given bitstream is valid, we can model the behaviour using the de-

5. Reconstruction of fragmented compressed data

coding context c , passed to the syntax checker. The special context \emptyset contains no information, and is used to decode bitstreams that do not rely on any contextual information. If a bitstream tries to read some context variable that is unavailable, this constitutes a syntax error.

$\text{AVAILABLECONTEXTS}(\mathbf{g}, (o, l))$ outputs the set of contexts that are available to the parser before parsing an unfragmented bitstream \mathbf{g} from byte offset o to $o + l - 1$. The set consists of the empty context and those contexts which can be built by parsing a sequence of non-overlapping bitstreams in the image, each modifying the previous bitstream's output context, without parsing any bytes in the range $\{o, o + 1, \dots, o + l - 1\}$.

More formally, we have

$$\begin{aligned} \text{AVAILABLECONTEXTS}(\mathbf{g}, (o, l)) = & \{\emptyset\} \cup \{c : \exists n, ((o_0, l_0, c_0), (o_1, l_1, c_1), \dots, (o_n, l_n, c_n)). \\ & (\text{SYNTAXCHECK}(\mathbf{g}[o_0 : o_0 + l_0], \emptyset) \\ & \wedge c_0 = \text{PARSE}(\mathbf{g}[o_0 : o_0 + l_0], \emptyset)) \\ & \wedge (\forall i \in \{1, \dots, n\}. \text{SYNTAXCHECK}(\mathbf{g}[o_i : o_i + l_i], c_{i-1}) \\ & \wedge c_i = \text{PARSE}(\mathbf{g}[o_i : o_i + l_i], c_{i-1})) \wedge c = c_n \\ & \wedge \text{NON-OVERLAPPINGEXTENTS}(((o, l), (o_0, l_0), \dots, (o_n, l_n))))\} \end{aligned}$$

where

$$\begin{aligned} \text{NON-OVERLAPPINGEXTENTS}(((o_0, l_0), (o_1, l_1), \dots, (o_n, l_n))) = \\ \forall i, j \leq n. (i = j) \vee ((o_i + l_i - 1 < o_j) \vee (o_j + l_j - 1 < o_i)). \end{aligned}$$

and $\text{PARSE}(\mathbf{g}[o : o + l], c)$ returns the context resulting from decoding the bitstream \mathbf{g} between offsets o and $o + l - 1$ inclusive in the context c .

We call the bitstreams which are parsed to build up a decoding context *configuration bitstreams*. Those bitstreams which can be read in any order, given a decoding context, are called *data bitstreams*, because they contain the main content of the file (for example, image/video data). For file formats where data bitstreams do not rely on a decoding context, there may be no configuration bitstreams².

For the purposes of our algorithm, the important distinction is that configuration bitstreams must be parsed in a given order, building up a decoding context, while data bitstreams can be parsed in any order as long as a complete decoding context is available.

²In our defragmentation tool, we provide a facility for the user to specify decoding contexts explicitly, in case configuration bitstreams are transmitted separately from data bitstreams. For H.264/AVC streams, the algorithm can search over common decoding contexts based on frame sizes and maximum frame numbers until it can parse slices successfully, which indicates that the chosen context may be correct.

5.3.3 Finding valid bitstreams and defragmentation

First considering unfragmented images, we can describe the set of all valid bitstreams in such an image \mathbf{g} as

$$\begin{aligned} \text{ALLVALIDBITSTREAMS}(\mathbf{g}) = \{ & (o, l) : \exists c. \text{SYNTAXCHECK}(\mathbf{g}[o : o + l], c) \\ & \wedge c \in \text{AVAILABLECONTEXTS}(\mathbf{g}, (o, l)) \} \end{aligned}$$

which is a set of pairs of (byte offset, bitstream duration in bytes) which index bitstreams without errors, according to SYNTAXCHECK.

Given a fragmented image \mathbf{f} and a syntax checker SYNTAXCHECK', our task is to find a permutation π^* which maximises the number of valid bitstreams in the re-ordered file:

$$\pi^* = \arg \max_{\pi} |\text{ALLVALIDBITSTREAMS}(\mathbf{P}_{\pi^{-1}}(\mathbf{f}))|$$

Note that when one or more filesystem blocks do not participate in any of the bitstreams, several permutations will achieve the maximum.

If all permutations are equally likely, and our algorithm returns exactly one permutation covering n blocks, the amount of information related to the order of blocks is $\log_2(n!) \approx (n \ln n - n) / \ln 2$ bits. This is over five kilobytes in a two megabyte file with 512 byte blocks, for example.

5.3.4 False positives

ALLVALIDBITSTREAMS will produce superset of the 'ground truth' set of bitstreams that an intact container/filesystem would indicate; it may contain false positives. The function SYNTAXCHECK' may erroneously declare bitstreams to be error-free when in fact they do cause an error according to SYNTAXCHECK*.

Another type of false positive is when a particular bitstream in the file is a valid bitstream, but is not part of a compressed file. The probability of this occurring is low when the bitstream syntax has many opportunities for error detection, and the bitstreams are sufficiently long. There is no way to distinguish these false positives from 'correct' bitstreams, unless we make further assumptions about the arrangement of bitstreams in the file. (A probabilistic model could be used to distinguish bitstreams which seem to be natural from valid but 'unnatural' bitstreams, but we concentrate on syntax rather than content analysis.)

5.4 Bitstream syntax description

The ideal syntax checking parser implementation for our application has the following properties:

5. Reconstruction of fragmented compressed data

- It is computationally efficient.
- It should have state which can be captured and cloned, so that the defragmenter can try multiple bitstream continuations after a block boundary. The state should contain the decoding context, allowing for inter-bitstream dependencies.
- It should be aware of the number of bits remaining in the current block. As well as notifying the caller of syntax errors, it should also notify the caller when there are too few bits available in the current block to parse a syntax element.
- It should be aware of the expected number of bits remaining in the stream, so that it can raise an error if it tries to read bits after the end of the stream, which constitutes a syntax error.

The language for specifying bitstream syntax should have convenient facilities for specifying constraints on values read from the bitstream, allow for easy enumeration of all permitted values, and allow for compact syntax specifications for new formats.

Our defragmentation tool generates an efficient syntax checker (modelled by the function `SYNTAXCHECK'`) in the C programming language, based on a text file provided by the user. We parse the text file to create a control flow graph, where nodes can read values of syntax elements from the bitstream, derive new values from them, check the values of variables (syntax element values and derived values) to detect errors, perform tests on variables and jump to other nodes. The text file format is inspired by the tabular syntax specification language in [45, Clause 7, syntax and semantics]. It is flexible enough to describe any format based on the concatenation of variable-length bitstrings.

For convenience, portions of the syntax flowgraph are separated into *syntax procedures*, which consist of groups of nodes, and function similarly to procedures in a programming language. Within a procedure, nodes can jump to the start of (call) other syntax procedures, but no recursive calls are allowed.

Our defragmentation algorithm runs the generated bitstream parser on candidate bitstreams, updating a *decoder state*. The parser will stop on detection of an error, a block boundary, or if it reaches the end of the bitstream syntax (indicating a successful decoding). The decoder state consists of: a dictionary of syntax element name/value pairs (containing the decoding context), a stack which tracks syntax procedure invocation, and values storing the current offset in the bitstream (in bits) and the number of bits remaining in the bitstream. This decoder state can be copied, so that it is possible to try resuming decoding at several different positions.

Section 5.4.1 describes how the bitstream syntax can be represented abstractly as a flowgraph. Section 5.4.2 shows an example of the mapping from a textual syntax description onto such a graph.

5.4.1 The bitstream syntax flowgraph

The flowgraph consists of nodes which have associated actions (reading a value from the bitstream, assigning a value to a variable, checking if a value is in range, ...), and directed arcs defining a successor relation between nodes.

```

Nodes = Read(successor ∈ Nodes, destination ∈ Variables, coding_mode ∈ CodingModes,
            value_restriction ∈ ValueRestrictions)
| Assign(successor ∈ Nodes, destination ∈ Variables, expression ∈ Expressions)
| Check(successor ∈ Nodes, expression ∈ BooleanExpressions)
| Test(true_branch_successor ∈ Nodes, false_branch_successor ∈ Nodes,
      expression ∈ BooleanExpressions)
| Call(successor ∈ Nodes, procedure ∈ Procedures, arguments ∈ Variables*)
| END

```

Every node (except END) has at least one successor.

Execution begins at a distinguished initial node called the *global entry point*.

Syntax procedures

Syntax procedures are collections of nodes determined by induction, forming a graph specifying control flow during parsing. Each collection contains an entry point, and for any node in the collection the syntax procedure also contains its successors (of which there is exactly one for every node type except END, which, as the final node in a syntax procedure, has no successors, and Test, which has two successors). The global procedure is formed starting with the global entry point. Call nodes have, in addition to a successor, a pointer to another node which is a *procedure entry point*, with the associated syntax procedure formed by induction.

At runtime, invocation of syntax procedures (by Call nodes) is tracked using a stack data structure. The stack is initially empty, and when control reaches a Call node, that node is pushed onto the stack and control flow passes to the relevant procedure entry point. Whenever an END node is reached, if the stack is non-empty, a node is popped from the stack and control passes to its successor. If the stack is empty, the flowgraph's execution is complete and it returns TRUE to indicate that parsing was successful.

There is a single global namespace for variables. When control reaches a Call node, we assign to each formal parameter the value of the corresponding actual parameter; when control reaches an END node, we assign back to each actual parameter the value of each formal parameter.

5. Reconstruction of fragmented compressed data

Flowgraph nodes

The set `Procedures` consists of those nodes which are procedure entry points.

The set `CodingModes` depends on the compression format. Its elements correspond to bijections between integer syntax element values and binary codewords. Common coding modes include: fixed length constants, constant length unsigned integer values with their most significant bits first, values from a variable length code tree given in tabular form³, and so on.

The set `Variables` depends on the compression format. Its elements are the names of syntax elements read by the parser, or named variables derived from these values, named constants and so on. Elements of syntax element arrays indexed using square bracket notation are also variables. Typical syntax elements in video coding include: flags to indicate whether features are enabled, transform coefficients, motion vector differences, and so on.

Expressions can be viewed as functions which take as input a mapping from `Variables` onto integers, and return values of a particular type. `BooleanExpressions` contains all expressions that return `TRUE` or `FALSE`. `Expressions` contains all expressions that return integers.

Value restrictions

$$\begin{aligned} \text{ValueRestrictions} = & \text{Range}(\textit{minimum} \in \text{Expressions}, \textit{maximum} \in \text{Expressions}) \\ & | \text{Set}(\textit{value_0} \in \text{Expressions}, \textit{value_1} \in \text{Expressions}, \dots) \end{aligned}$$

can encode a range or set of integer values. This is quite a limited way to specify restrictions on values. Nevertheless, it is sufficient to describe tests in the H.264/AVC standard, and branching and `Check` nodes can achieve more complicated checks if they are necessary. By providing this limited syntax, the defragmenter can easily generate all valid possibilities for a syntax element, which would be expensive for arbitrary Boolean expressions.

A node's action may cause the flowgraph to return `FALSE`, to indicate a syntax error.

The action of `Read` nodes is to invoke the reading function associated with their *coding_mode*, which is format-specific, and to return an integer value, which is checked according to the *value_restriction* and assigned to the variable *destination*. If an error is raised, either directly from the coding mode reading function, or from the value restriction, the flowgraph returns `FALSE`.

The action of `Assign` nodes is to evaluate *expression* in the global namespace and to assign the result to *destination*.

The action of `Check` nodes is to evaluate *expression* in the global namespace and return `FALSE` from the flowgraph if the result is not equal to *variable*. If the result is `TRUE`, execution continues.

³Code tables and other auxiliary data can be provided in as a Python module imported by the parser.

The action of **Test** nodes is to evaluate *expression* in the global namespace and pass execution to the *true_branch_successor* or the *false_branch_successor*, if the result is TRUE or FALSE, respectively.

As described above, **Call** nodes generate assignments from actual parameters onto formal parameters, push themselves onto the stack and pass execution to the procedure entry point indicated by *procedure*. If the stack is empty, **END** nodes cause the flowgraph to return TRUE. Otherwise, they generate assignments from formal parameters to actual parameters, pop their caller from the stack and pass execution back to its successor.

5.4.2 Textual representation of bitstream syntax

In our defragmenter implementation, users specify a description of the bitstream syntax flowgraph by means of a text file provided as input.

The following example code is an excerpt from the `seq_parameter_set_rbsp()` syntax procedure of an H.264/AVC Baseline profile parser. Both the text-based description and the syntax flowgraph it represents are shown. This portion of the syntax flowgraph sets the values of three syntax elements, each of which is a flag⁴.

```

read(frame_mbs_only_flag, u(1))
if (frame_mbs_only_flag == 0)
    read(mb_adaptive_frame_field_flag, u(1, require(0)))
else
    assign(mb_adaptive_frame_field_flag, 0)
read(direct_8x8_inference_flag, u(1))

```

The corresponding syntax flowgraph representation is

```

n0 = Read(n1, frame_mbs_only_flag, u(1), ∅)
n1 = Test(n2, n3, frame_mbs_only_flag == 0)
n2 = Read(n4, mb_adaptive_frame_field_flag, u(1), Set(0))
n3 = Assign(n4, mb_adaptive_frame_field_flag, 0)
n4 = Read(n5, direct_8x8_inference_flag, u(1), ∅)
...

```

where `u(1)` is the coding mode for 1-bit unsigned integers, which reads one bit from the input bitstream, and \emptyset is the empty value restriction. `Set(0)` is the value restriction allowing only the value 0.

⁴The values of the flags determine (1) whether field-based (interlaced) coding is allowed, (2) whether macroblocks in a given picture may be coded using either frame or field coding (MBAFF) and (3) set whether a particular prediction mode is allowed.

5. Reconstruction of fragmented compressed data

n_0 reads a single bit from the bitstream and assigns its value to the `frame_mbs_only_flag`. No syntax error is possible because the value restriction on this node is empty. n_1 tests the read value and moves control to either n_2 (if it is 0) or n_3 (if it is 1). n_2 may detect a syntax error if the value it reads from the stream is equal to 1. The potential error exists because valid bitstreams for our parser may not set the `mb_adaptive_frame_field_flag` to 1. n_3 assigns a default value of 0 to this syntax element.

5.5 H.264/AVC bitstream syntax checking

Our demonstration of the defragmentation algorithm uses a parser for H.264/AVC Baseline profile bitstreams. This section describes the format of these compressed video files, and evaluates the performance of our syntax checker.

Syntax element names are typeset like `nal_unit_type`, and syntax procedures like `nal_unit()`.

5.5.1 Assumptions about the video

We need only consider part of the H.264/AVC standard for this application, because the devices under consideration produce bitstreams with only a subset of all possible parameter selections. The standard specifies a set of named parameter choices (‘profiles’) and constraints on the stream (‘levels’): “Profiles and levels specify restrictions on bitstreams and hence limits on the capabilities needed to decode the bitstreams. Profiles and levels may also be used to indicate interoperability points between individual decoder implementations.” [45, Annex A].

We assume that the Baseline profile [45, Subclause A.2.1] is in use. The most important restrictions it places on the bitstream (in conjunction with its level constraints in [45, Subclause A.3.1]) are:

- Context-adaptive variable length coding (CAVLC) is used (arithmetic coding (CABAC) is not allowed). The stream consists of a concatenation of bitstrings based on integer (syntax element value) to bitstring mapping tables (coding modes).
- Frames may only contain frame macroblocks (i.e., interlacing is not allowed).
- The syntax element `level_prefix` shall not be greater than 15 (where present).
- The number of bits in each macroblock shall not exceed 3200.

File structure and containers

Like most compressed video formats, the H.264/AVC standard [45] specifies a bitstream syntax used to produce an ordered sequence of binary payloads, which are then embedded within a

structured file called a container. The binary payloads are called NAL (network abstraction layer) units. Several types of NAL units are specified, and the type is indicated in the bitstream by the value of the `nal_unit_type` syntax element. Two NAL unit types (`nal_unit_type` = 1 and `nal_unit_type` = 5, which contain picture data for instantaneous decoder refresh (IDR) slices and non-IDR slices, respectively) have picture data in the type of files we wish to defragment, and two other NAL unit types (`nal_unit_type` = 7 and `nal_unit_type` = 8, which contain configuration information in the form of sequence parameter settings (SPS) and picture parameter settings (PPS) respectively) have important metadata. These two collective types are *slice NAL units* and *configuration NAL units*, respectively. Slice NAL units are data bitstreams, and configuration NAL units are configuration bitstreams.

In addition to carrying compressed video bitstreams, containers also sometimes include interleaved audio data and indices to facilitate random access. The ISO base media file format [42] is one such container format, and has extensions for the MP4 file format [40] and encapsulation of H.264/AVC video bitstreams in an MP4 file [43]⁵.

MP4 files encode a tree of ‘boxes’. Each box is a 4 byte length tag⁶, which specifies the number of bytes occupied by the box contents, followed by a four ASCII character text identifier, which indicates the type of data contained in the box, and finally the contents (payload) of the box. A box payload may be one or more other boxes concatenated together, which are said to be nested within it. The first byte of the file is treated as the first byte of a root box payload.

This structured data format allows playback programs to read any metadata of interest very efficiently, by jumping over boxes that are not as important.

In MP4 files containing H.264/AVC video streams, a box identified with the string `avcC` has a payload containing the SPS and PPS NAL units, which are typically each about ten bytes long, along with some additional values. These additional values redundantly encode the H.264/AVC profile and level numbers as fixed-length integers. (The values are also present in the SPS payload.) The total number of SPS and PPS NAL units relating to the video stream is also stored in the `avcC` box payload [43, Subclause 4.1.5.1.1]. Another box, identified by `avc1`, encodes some redundant information about the width, height and colour depth of the video.

Several boxes contain information about the offsets and lengths (in bytes) of slice NAL units, but we do not read these during defragmentation. The `stsz` box specifies the sizes of slice NAL units. The `stco` and `stsc` boxes specifies the offsets (in bytes) of chunks of slice data in the file. These indices are used for random access within the large part of the file dedicated to storing video payload data.

The `mdat` box contains the slice NAL units, partitioned into separate groups called chunks. Each chunk is a concatenation of slice NAL units, each encoded as a four byte length tag

⁵The QuickTime (MOV) container is very similar to MP4. It is practically the same for our purposes.

⁶SPS and PPS NAL units have a 2 byte length tag prefix but are not MP4 boxes.

5. Reconstruction of fragmented compressed data

followed by the bytes which make up the NAL unit. Slice NAL units are always a whole number of bytes because they end with the `rsbsp_trailing_bits` syntax procedure, which outputs a one bit followed by zero or more zero bits until the bitstream pointer is byte-aligned. In video files with associated audio, the sound samples are also stored in the `mdat` box.

When chunks follow one another directly, all slice NAL units are effectively concatenated, and each is prefixed by a four byte length tag. We use the length tag specification and the fact that the NAL units are contiguous (in the logical, unfragmented file) in an optional optimisation step for our algorithm, described in section 5.6. In container formats that do not have length tags prefixing each NAL unit, the same optimisations may still be made if the lengths of NAL units can be found elsewhere.

The leftmost column of figure 5.1 shows an example file layout.

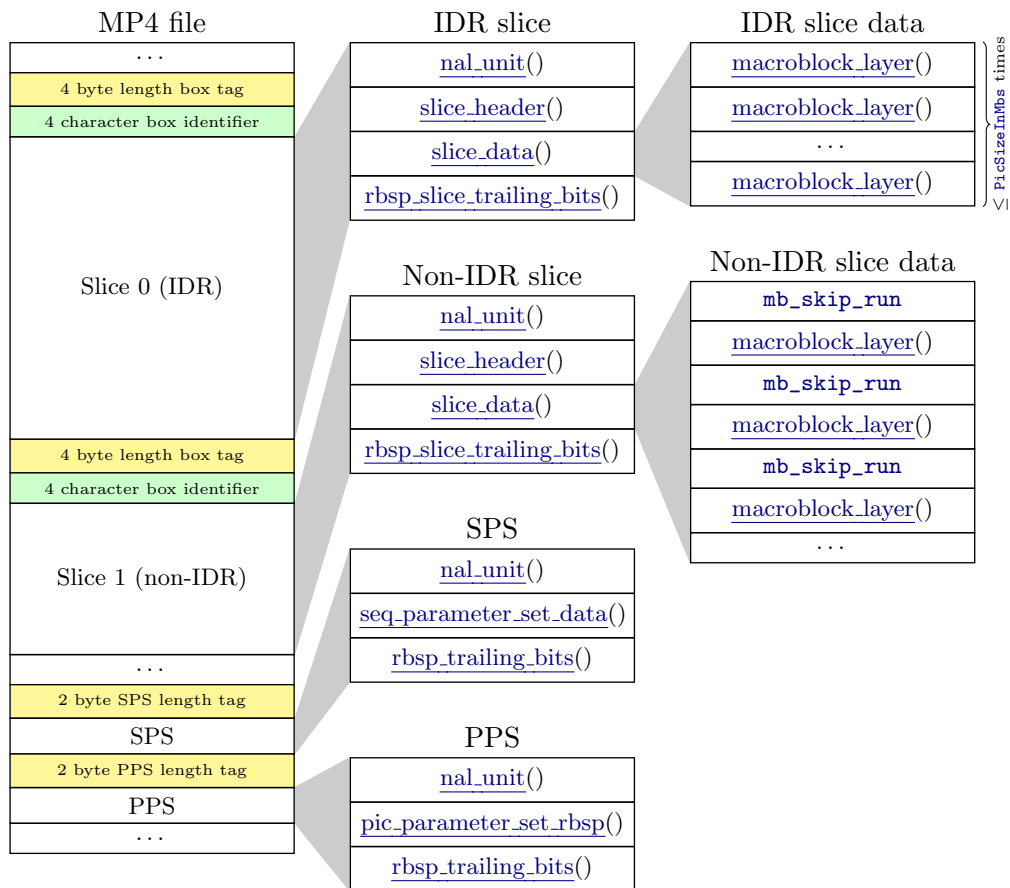


Figure 5.1: An example file layout showing H.264/AVC video bitstreams inside an MP4 container. File byte addresses increase down the page. The nesting structure of bitstream syntax procedures is shown on the right (see also subsection 5.5.3 and appendix B).

The defragmentation algorithm does not rely on details of the container format, but is faster when (1) we know the NAL unit lengths and (2) we know that NAL units follow one another directly. When audio information is interleaved between frames, we may still be able to join

adjacent NAL units by considering the length of audio data chunks. This involves tracking which NAL units are first in their group and are at byte offsets that are consistent with being separated from the previous group by the appropriate number of bytes. In our test files, we have observed that audio is interleaved between groups of frames. We can still take advantage of knowing that NAL units are adjacent within these groups.

5.5.2 Coding modes

H.264/AVC Baseline profile uses context-adaptive variable length coding (CAVLC), which uses only symbol coding modes. Context-adaptive binary arithmetic coding (CABAC) is available in other profiles.

Each coding mode specifies one or more mappings from bitstrings onto integer values. Which mapping is chosen may depend on the syntax element being decoded and the values of other syntax elements. The codewords are prefix-free, that is, no valid codeword is the prefix of another valid codeword.

For any given coding mode/parameter choice, invalid codewords up to a certain length can be found by decoding all possible bitstrings up to a maximum length and noting each bitstring that cannot be decoded.

For compactness, I typeset bitstrings with \square denoting 1 and \blacksquare denoting a 0 so that, for example, $\blacksquare\blacksquare\square$, represents the decimal number three as a 4-bit big-endian bitstring.

H.264/AVC's context-adaptive variable length coding (CAVLC) defines the following coding modes:

Unsigned integer in n bits


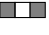
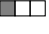





u(4)	Value
$\blacksquare\blacksquare\blacksquare\blacksquare$	0
$\blacksquare\blacksquare\blacksquare\square$	1
$\blacksquare\blacksquare\square\blacksquare$	2
...	...
$\square\square\square\blacksquare$	14
$\square\square\square\square$	15

This coding mode is indicated by $u(n)$. n is either a constant integer, in which case n bits are read and the result is interpreted as an unsigned integer with the most significant bit first, or the string 'v', in which case the number of bits to read is a function of some previously read values as specified in the semantics [45, Subclause 7.4].

5. Reconstruction of fragmented compressed data

$f(n)$ for some constant integer n denotes the fixed unsigned integer reading mode. The parser reads n bits from the stream, and the result must be equal to a constant associated with the syntax element. It is a syntax error if the constant does not equal the read value.

Order 0 exponential-Golomb coding

Bitstring	code_num	ue(v)	se(v)	me(v)	te(v)
	0	0	0		
	1	1	1	Mapping in [45, Subclause 9.1.2]	If range $x = 1$, decode as $!u(1)$ If range $x > 1$, decode as $ue(v)$
	2	2	-1		
	3	3	2		
	4	4	-2		
	5	5	3		
...		
	14	14	-7		
	15	15	8		
...		

Several coding modes use exponential-Golomb codewords, each with different mappings onto decoded values. The 3rd–6th columns of this table show these coding modes. ‘range x ’ is the maximum value that the syntax element x may take on, and is determined based on the decoding context, as specified in [45, Subclause 7.4].

There are four coding modes ($ue(v)$, $se(v)$, $me(v)$ and $te(v)$) which use order-0 exponential-Golomb codewords. The decoder counts the number of zero bits, l , present in the stream before the first one bit. Having read the one bit, it reads l further bits, interpreting them as an unsigned integer in l bits to read the value `code_num`, which is then mapped onto an integer for the particular coding mode in use (as described in the table).






The $me(v)$ coding mode depends on the values of `ChromaArrayType` and `coded_block_pattern`. These signal how colour information is represented in coded pictures, and which sub-blocks within a macroblock are coded, respectively.

Code tables

The coding mode $ce(v)$ decodes the bitstring in the stream according to a tabulated mapping associated with the syntax element. The standard includes codeword tables for the syntax elements `coeff_token`, `level_prefix`, `total_zeros` and `run_before`. These syntax elements appear in the syntax procedure dedicated to coding quantised transform coefficients, `residual_block_cavlc()`.

`coeff_token` uses [45, Subclause 9.2.1, table 9-5]. The mapping depends on the value of `nC`, which is calculated based on the availability, type and `total_coeff` value associated with the macroblocks above and to the left of the current macroblock in the slice.


For values of `nC` other than `nC = -1`, not all bitstrings are possible to decode, and can incur an error. Specifically, the following bitstrings cause an error:


Invalid bitstrings	
<code>nC = -1</code>	None
<code>nC = -2</code>	
$0 \leq nC < 2$	
$2 \leq nC < 4$	
$4 \leq nC < 8$	
$8 \leq nC$	


The value of `coeff_token` determines `total_coeff = GetTotalCoeff(coeff_token)` and `trailing_ones = GetTrailingOnes(coeff_token)`:

$$\text{GetTotalCoeff}(c) = \begin{cases} 0 & c = 0 \\ 1 & 1 \leq c < 3 \\ 2 & 3 \leq c < 6 \\ 3 + (c - 6)/4 & \text{otherwise,} \end{cases}$$

$$\text{GetTrailingOnes}(c) = \begin{cases} 0 & c = 0 \\ (c - 1) \bmod 2 & 1 \leq c < 5 \\ 2 & c = 5 \\ (c - 6) \bmod 4 & \text{otherwise.} \end{cases}$$

`level_prefix` is coded using unary notation [45, Subclause 9.2.2.1]. The stream contains `level_prefix` zeros followed by a one. In the Baseline profile, the value may not exceed 15, so all bitstrings starting  are invalid.

`maxNumCoeff` (an argument to `residual_block_cavlc`) determines which table(s) are used to decode `total_zeros`, out of [45, Subclause 9.2.3, tables 9-7, 9-8 and 9-9]. Within each table, the set of available codewords depends on `total_coeff`, derived from `coeff_token`. When `maxNumCoeff` $\notin \{4, 8\}$ and `total_coeff = 1`, any bitstring starting  is invalid.

The code table for `run_before` depends on the value of `zerosLeft` [45, Subclause 9.2.3, table 9-10]. When `zerosLeft > 6`, bitstrings starting  are invalid.

5. Reconstruction of fragmented compressed data

5.5.3 NAL unit syntax

As well as detecting errors caused by observing invalid codewords, we can also detect errors based on constraints specified in the semantics section [45, Subsection 7.4], which we include in the user-specified syntax flowgraph.

This section includes some representative and interesting sections of the syntax flowgraph in its textual representation, provided as input to the defragmentation tool.

For brevity, some syntax procedures are given in appendix B, and sections of syntax which are unused in Baseline profile streams are omitted.

Header syntax [45, Subclause 7.3.1, NAL unit syntax]

Every NAL unit starts with a one byte header, specified in [nal_unit\(\)](#):

```
# 7.3.1 NAL unit syntax
nal_unit()
  read(forbidden_zero_bit, f(1, require(0x00)))
  read(nal_ref_idc, u(2))
  read(nal_unit_type, u(5, require(1, 5, 6, 7, 8, 9, 10, 11)))
  assign(IdxPicFlag, 1 if nal_unit_type == 5 else 0)
  if (nal_unit_type == 14 || nal_unit_type == 20)
    read(svc_extension_flag, u(1, require(0)))
    # We do not support multi-view/scalable coding

  if (nal_unit_type == 5)
    check(nal_ref_idc, range(1, 3))
  if (nal_unit_type == 6 || nal_unit_type == 9 || nal_unit_type == 10
      || nal_unit_type == 11 || nal_unit_type == 12)
    check(nal_ref_idc, 0)

  # Clear the frame decoding context.
  assign(context_total_coeff, {})
  assign(context_mb_type, {})
```

This syntax procedure parses one byte primarily extracting the type of NAL unit. The NAL units denoted by each value of `nal_unit_type` are specified in [45, Table 7-1].

Picture slices that are completely independent of previously decoded pictures (called instantaneous decoding refresh (IDR) slices) have `nal_unit_type = 5` and `nal_ref_idc ≠ 0`. It is important to recover these NAL units because they are likely to contain useful information even when viewed separately from the rest of the stream.

Sequence parameter set RBSP syntax [45, Subclause 7.3.2.1]

The sequence parameter set is the first configuration NAL unit to be parsed. It sets the profile and level of the video, and configures its dimensions, the range of the `frame_num` syntax element and other important variables.

All later NAL units depend on the values of syntax elements in the SPS and PPS NAL units, so it is vital to locate these configuration NAL units.

7.3.2.1 Sequence parameter set RBSP syntax

```
seq_parameter_set_rbsp[category = 0]()
  seq_parameter_set_data()
  rbsp_trailing_bits()
```

Sequence parameter set data syntax [45, Subclause 7.3.2.1.1]**# 7.3.2.1.1 Sequence parameter set data syntax**

```
seq_parameter_set_data[category = 0]()
  read(profile_idc, u(8, require(66)))
  read(constraint_set0_flag, u(1))
  read(constraint_set1_flag, u(1))
  read(constraint_set2_flag, u(1))
  read(constraint_set3_flag, u(1))
  read(constraint_set4_flag, u(1, require(0)))
  read(reserved_zero_3bits, f(3, require(0x00)))
  read(level_idc, u(8, require(9, 10, 11, 12, 13, 20, 21, 22, 30,
    31, 32, 40, 41, 42, 50, 51)))
  read(seq_parameter_set_id, ue(v, require(0)))

  if (profile_idc == 100 || profile_idc == 110 || profile_idc == 122
    || profile_idc == 244 || profile_idc == 44 || profile_idc == 83
    || profile_idc == 86 || profile_idc == 118)
    # Omitted (not for Baseline profile)
  else
    assign(chroma_format_idc, 1)
    assign(separate_colour_plane_flag, 0)
    assign(ChromaArrayType, chroma_format_idc)
    assign(bit_depth_luma_minus8, 0)
    assign(bit_depth_chroma_minus8, 0)

    assign(BitDepthY, 8 + bit_depth_luma_minus8)
    assign(QpBdOffsetY, 6 * bit_depth_luma_minus8)
    assign(BitDepthC, 8 + bit_depth_chroma_minus8)
    assign(QpBdOffsetC, 6 * bit_depth_chroma_minus8)
```

5. Reconstruction of fragmented compressed data

```

read(log2_max_frame_num_minus4, ue(v, require(range(0, 12))))
read(pic_order_cnt_type, ue(v, require(range(0, 2))))
if (pic_order_cnt_type == 0)
    read(log2_max_pic_order_cnt_lsb_minus4, ue(v,
                                                require(range(0, 12))))
# Omitted [handlers for pic_order_cnt_type not equal to zero]

read(max_num_ref_frames, ue(v))
read(gaps_in_frame_num_value_allowed_flag, u(1, require(0)))
read(pic_width_in_mbs_minus1, ue(v))
read(pic_height_in_map_units_minus1, ue(v))

read(frame_mbs_only_flag, u(1))
if (frame_mbs_only_flag == 0)
    read(mb_adaptive_frame_field_flag, u(1, require(0)))
else
    assign(mb_adaptive_frame_field_flag, 0)

read(direct_8x8_inference_flag, u(1))
read(frame_cropping_flag, u(1))

# Derive SubWidthC, SubHeightC
if (chroma_format_idc == 1 && separate_colour_plane_flag == 0)
    assign(SubWidthC, 2)
    assign(SubHeightC, 2)
else if (chroma_format_idc == 2 && separate_colour_plane_flag == 0)
    assign(SubWidthC, 2)
    assign(SubHeightC, 1)
else if (chroma_format_idc == 3 && separate_colour_plane_flag == 0)
    assign(SubWidthC, 1)
    assign(SubHeightC, 1)

# Get the PicWidthInMbs/SamplesL/C.
if (chroma_format_idc == 0 || separate_colour_plane_flag == 1)
    assign(MbWidthC, 0)
    assign(MbHeightC, 0)
else
    assign(MbWidthC, 16 / SubWidthC)
    assign(MbHeightC, 16 / SubHeightC)
assign(PicWidthInMbs, pic_width_in_mbs_minus1 + 1)
assign(PicWidthInSamplesL, PicWidthInMbs * 16)
assign(PicWidthInSamplesC, PicWidthInMbs * MbWidthC)
assign(PicHeightInMapUnits, pic_height_in_map_units_minus1 + 1)
assign(PicSizeInMapUnits, PicWidthInMbs * PicHeightInMapUnits)
assign(FrameHeightInMbs, (2 - frame_mbs_only_flag) *

```



```
PicHeightInMapUnits)
```

```
# Omitted [cropping parameters]
```

```
# Omitted [VUI parameters]
```

Trailing bits syntax [45, Subclauses 7.3.2.10 and 7.3.2.11]

Each NAL unit ends with a trailing bits syntax procedure.

The padding bits that align the end of the bitstream to a byte boundary are another useful source of redundancy for error checking: the parser knows when it has reached the end of a slice bitstream already, and can search for the padding bits (in the event that it did not finish parsing exactly one bit before a byte boundary).

```
# 7.3.2.10 RBSP slice trailing bits syntax
rbbsp_slice_trailing_bits()
  rbsp_trailing_bits[category = *]()
  if (entropy_coding_mode_flag == 1)
    # Omitted [only used in non-Baseline profiles]

# 7.3.2.11 RBSP trailing bits syntax
rbbsp_trailing_bits[category = *]()
  read(rbsp_stop_one_bit, f(1, require(0x01)))
  while(not byte_aligned())
    read(rbsp_alignment_zero_bit, f(1, require(0x00)))
```

5.5.4 Error detection performance

Detecting syntax errors that occur due to incorrect block transitions (after discontinuities) is vital to the performance of our defragmentation algorithm. The parser cannot normally detect an incorrect block transition immediately. Syntax errors occur later due to the decoder's desynchronisation from the pattern of codeword boundaries, or errors in the context data stored in the decoder state. It is beneficial for our algorithm if an incorrect block transition is detected within the next disk block, as this avoids incurring the cost of an additional level of the search tree.

We ran experiments to measure the error detection performance of our H.264/AVC parser. Because our defragmentation algorithm relies on error detection to eliminate incorrect candidate block orderings, we measured the number of bytes parsed after a simulated incorrect block transition before an error was first detected.

Since the characteristics of the bitstream's content, especially the choice of coding features in the bitstream syntax, could affect the error detection performance, we used three bitstreams

5. Reconstruction of fragmented compressed data

from different sources: H.264/AVC video recorded on an Apple fourth generation iPod Touch (running iOS 4.0), a bitstream output by the x264 encoder version 0.104 (targeting the Baseline profile, using default options) and a file downloaded from the YouTube website⁷.

We ran the following experiment on each source video, to measure how quickly the parser could detect a syntax error due to a discontinuity. The block size was set to 512 bytes.

1. Load the unfragmented source bitstream. Parse the SPS and PPS configuration NAL units, giving a decoder state which is sufficient to parse any data NAL unit.
2. For each data NAL unit in the file, parse it up to the end of its initial block and complete the following steps:
3. Jump to a random offset in the file where at least the next 16 blocks' worth of bytes consists of data from an H.264/AVC data bitstream, simulating a discontinuity.
4. Parse from this point onwards until the parser returns. End of block conditions are ignored, and the parser is instructed to continue from its current offset in the file. If a syntax error is detected during parsing, note how many bits were parsed since the simulated discontinuity, and the type of error (that is, the syntax error being read when the error was detected) and stop parsing.
5. For each repetition required, go back to stage 3, using a new clone of the decoder's state after the initial block of this NAL unit.

In summary, we ran many decoder instances, each with a random block discontinuity, simulated by moving the bitstream pointer to a random location during decoding. We measured the number of bits each parser consumed between the discontinuity and the point where it detected a syntax error. We also recorded the syntax element being read at the time of the error.

The histograms in figures 5.2 (iPod source), 5.3 (x264 source) and 5.4 (YouTube source) summarise our results for the three test videos. Because the 'survival rate' of test decodes at each bit offset after a simulated block discontinuity is of interest, the histograms show for each possible post-discontinuity bit offset the number of decoders which will later detect an error (before the limit of 16 blocks of data has been parsed) on a log scale. The black line shows this value for all possible errors, and the other series each show the value for one type of error, as shown in the legend. At bit offset zero, the black line's position is the total number of errors detected (of all types), and the line drops as errors are detected. A steeper gradient at a given bit offset indicates that more of the decoders are detecting errors at this point. The black line

⁷Google have not made public details of their video encoding pipeline, but they seem to use x264 [29, 74], with customised encoding settings.

is the sum of all other series shown. The other series are plotted independently of each other. The legends show the percentage of all errors falling into each syntax error category.

In a search over all possible block orderings, larger block sizes give more bytes for error detection before requiring inspection of a new level in the search tree. The charts show that block sizes larger than 1024 bytes do not improve the detection performance substantially, and that a block size of 512 bytes already allows detection of a large proportion of the errors. They also show that some categories of syntax error are almost always found very close to the actual incorrect block transition, while others may be found several kilobytes later. The charts also show that there is significant variability in how soon errors are detected across data produced by different encoders and input video.

5. Reconstruction of fragmented compressed data

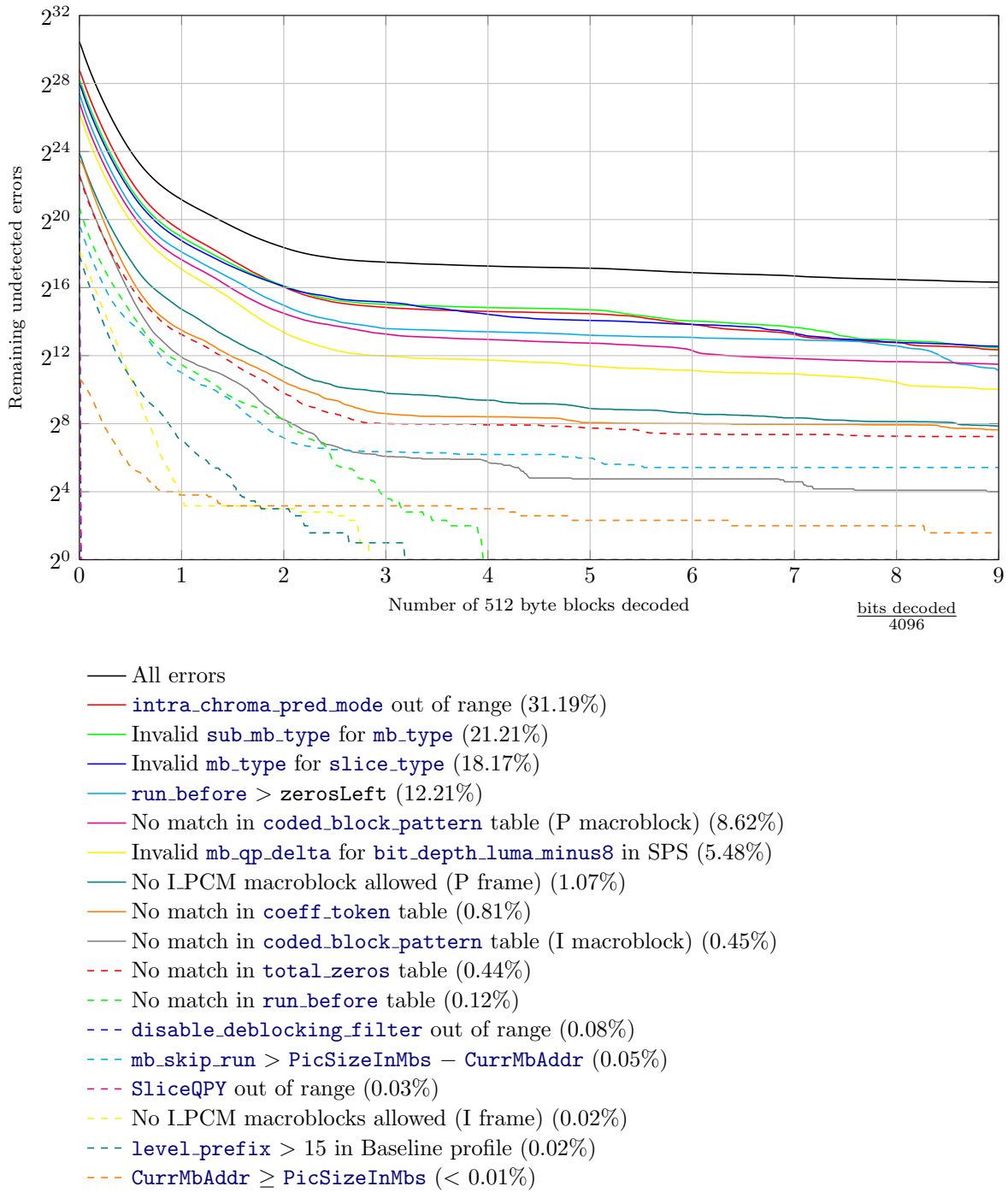


Figure 5.2: This chart shows the error detection performance over about 2.8 billion decodes, each with an incorrect block transition. Whenever the decoder detected an error, we noted its category and the current offset in the bitstream relative to the discontinuity. The top line (black) represents all types of error, while the other lines each represent one type of error, as described in the legend. Percentages in the legend show the proportion of all detected errors after 16×512 bytes.

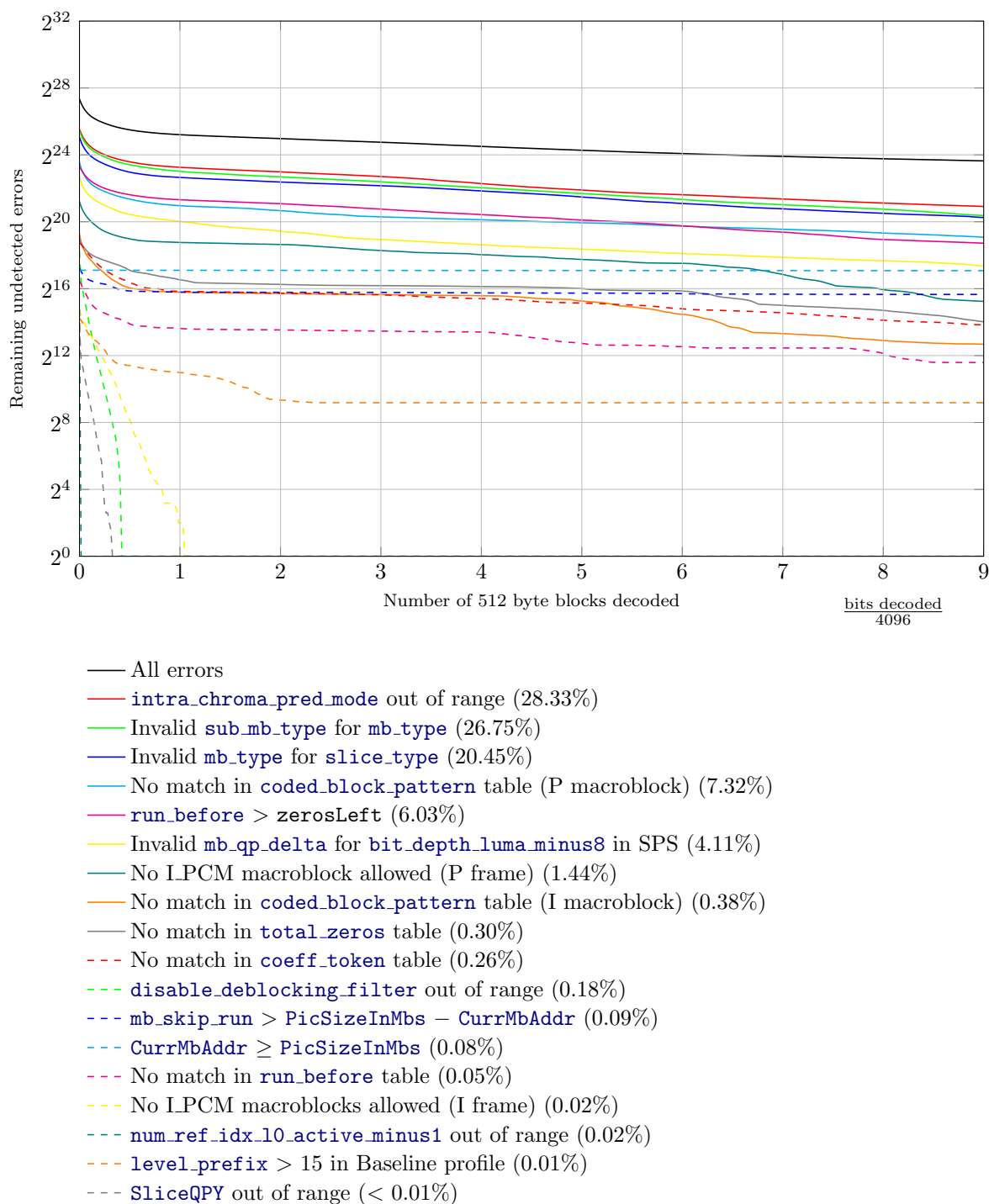


Figure 5.3: This chart shows the results of the same experiment with source video produced by the x264 codec.

5. Reconstruction of fragmented compressed data

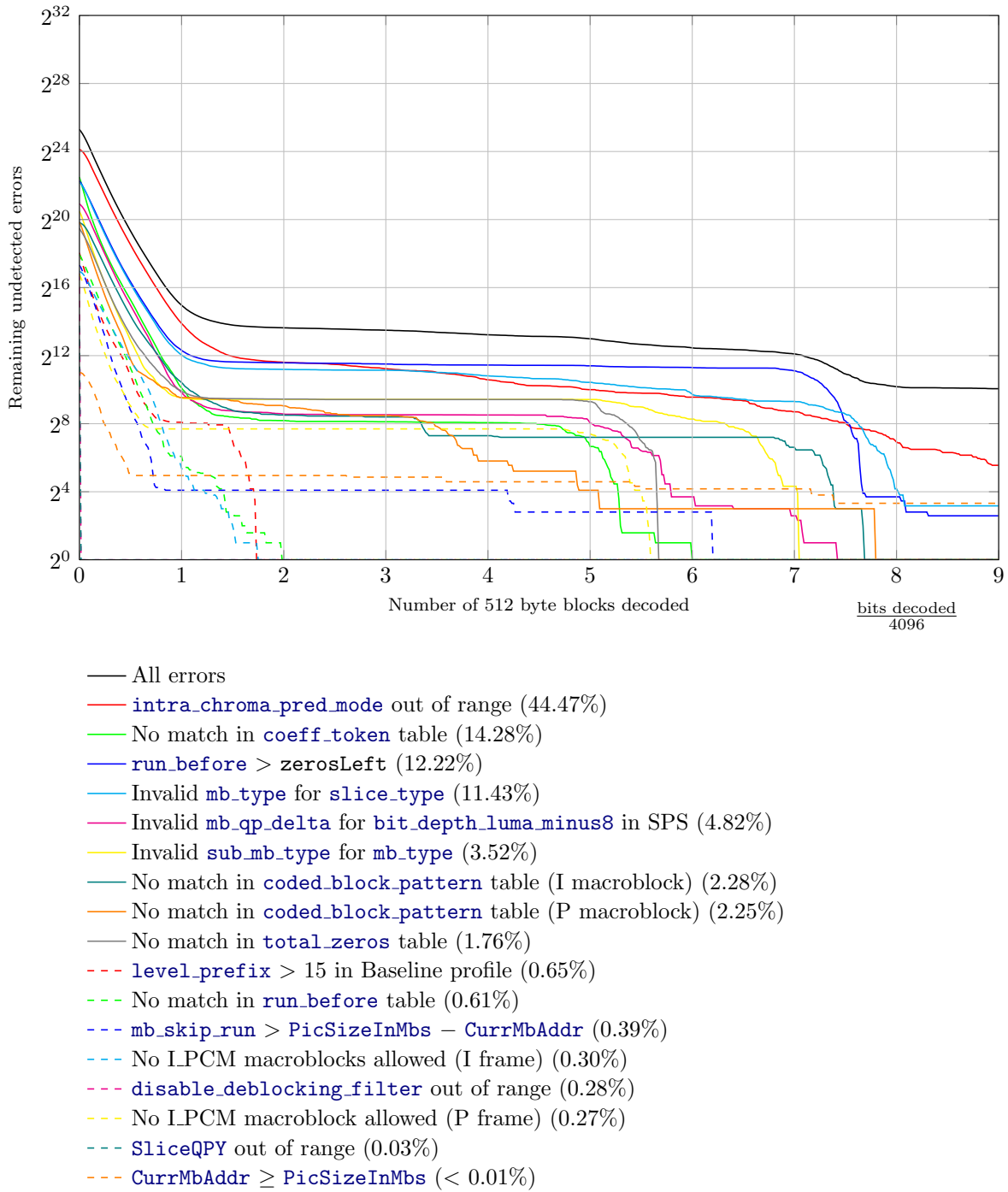


Figure 5.4: This chart shows the results of the same experiment with source video downloaded from the YouTube website.

As well as measuring error detection performance after a single incorrect block transition, we also gathered data about the effect of multiple discontinuities, in the same setup. At each possible block boundary (at integer multiples of 512 bytes), we copied the decoder state and

created a new decode operation which was identical except with an altered bitstream pointer, simulating a random discontinuity. Figure 5.5 shows the number of remaining undetected errors at each bit offset (using source video from the iPod), where each bifurcation of the line creates an upper line associated with a decode without a discontinuity and a lower line which continues decoding after a discontinuity. The latter line is always lower because additional discontinuities give new opportunities for error detection. Note that the top line of this chart is the same as the top line in figure 5.2, because only one discontinuity is simulated.

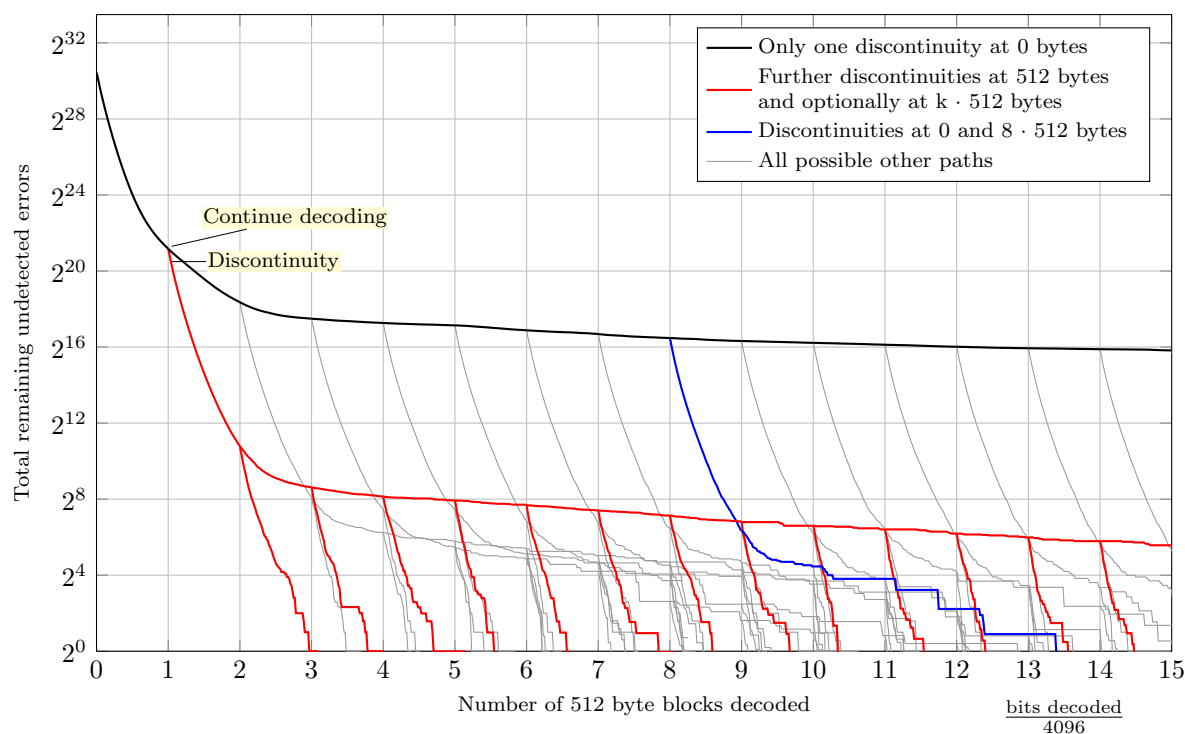


Figure 5.5: This chart shows how error detection performance varies with the number of incorrect block transitions. We ran about 2.8 billion decode operations, each with an initial incorrect block transition. At each subsequent multiple of 512 bytes, we copied the decoder state, allowing one parser to continue, while the other experienced an additional random jump (simulating another incorrect block transition). At each bit offset after the first transition, we plot the number of decoders on each branch for which no errors have yet been detected.

We observe that the same curve shape appears at all positions in 5.5 where discontinuities are simulated, and that larger block sizes improve the error detection rate per block, making the a search over candidate block orderings more efficient.

5.6 Fragmented bitstream recovery algorithm

This section describes our defragmentation algorithm, making use of the input bitstream syntax description and its corresponding parser.

Each bitstream (in the case of H.264/AVC, each NAL unit) can occupy one or more blocks. Each bitstream has an *initial block*, which contains its first byte, and a *final block*, containing its last byte. If a bitstream occupies any other blocks (apart from its initial and final blocks), these are called *intermediate blocks*.

If a bitstream does not extend past its initial block (that is, its initial and final blocks are the same), we say that it is *complete*, because no further searching is necessary.

We try to create *chains* of bitstreams, which are groupings of one or more bitstreams that are logically contiguous. In a chain, we know the final block index (in addition to the initial block index) for every bitstream except the last one.

Our defragmentation algorithm consists of the following stages:

1. Configuration bitstream parsing and data bitstream offset search

We compile a list of extents in the image that contain bytes which could constitute the first few bytes of a valid bitstream.

We first locate configuration bitstreams, then data bitstreams. To find bitstreams of a given type, we use the bitstream syntax flowgraph to generate the first few bytes of all valid bitstreams of the sought type, then look for offsets in the image which match these generated bitstrings.

We may find false positives, where the bitstream is valid but was not one of the bitstreams according to the container of the unfragmented file. There may also be false negatives, where we miss bitstreams whose first few bytes lie across a block boundary, as the candidate bitstream start byte sequences we generated and search for are not fragmented; stage 3 provides a solution in some cases.

We parse each configuration bitstream candidate fully, using a backtracking recursive search to make sure that we get an ordered sequence of non-overlapping, compatible configuration bitstreams. Subsection 5.6.2 describes this step in detail.

The result of this stage is a list of possible complete decoding contexts (called *post-configuration states*) and a list of byte offsets which may contain data bitstreams. The rest of the algorithm must be run for each possible post-configuration state⁸.

⁸In all our tests on H.264/AVC bitstreams, there was exactly one post-configuration state available, due to the compatibility restriction on configuration bitstreams: if one configuration bitstream is not correct, its parameters are likely to cause a syntax error in a later configuration bitstream, or the first data bitstream.

As an example, for H.264/AVC we search for sixteen 24-bit long bitstrings to find the SPS, and use this to search for a single possible 18-bit long bitstring to find the corresponding PPS. IDR slices are located using six 29 or 33-bit long bitstrings, and non-IDR slices using sixteen 27, 29 or 31-bit long bitstrings.

2. Data bitstream filtering

For each candidate data bitstream offset, we copy the post-configuration state into the parser and attempt to parse to the end of the block, which can eliminate some false positives.

As the probability of the parser having detected an incorrect block transition increases as we decode further from the discontinuity, we are likely to remove more false positives where bitstreams start near the beginning of their blocks. We are less likely to remove false positives which begin near the end of their blocks, because there are fewer opportunities to detect errors before the end of the block.

3. Data bitstream mapping (optional)

We can optionally map out the sequence of bitstream chains in the file, to help reduce false positives and false negatives by inferring the positions of bitstreams missed during the data bitstream offset search. This step can also reduce the search size in the next stage of the algorithm.

This stage is applicable if the container format has the following three properties: (1) we know the length of each bitstream, due to the presence of a length tag prefix, or other side information, (2) we know the number of bytes separating bitstreams in the container format, and (3) there is value near the start of each data bitstream which can be used to detect whether two bitstreams may be adjacent, such as a frame number which counts up modulo a certain maximum; I will call this value a *frame number*, encoded in the syntax element `frame_num`, with modulus `max_frame_num`. These are the corresponding read/derived syntax elements for H.264/AVC.

Since we know the frame number and byte offset of each possible bitstream, we can combine this information with the length and frame number of each other candidate bitstream to deduce which bitstreams are likely to be logically adjacent. This lets us infer the final block index for bitstreams with known successors, so that we now have a chain of bitstreams.

When the bitstreams do not form a single chain in the image, we can still form several independent chains, each with a final data bitstream that has an unknown last block index (if it extends past the end of its initial block).

4. Data bitstream block search

We know the initial block index for each data bitstream, and possibly its final block index. This stage uses an exhaustive search to find the indices of any intermediate

5. Reconstruction of fragmented compressed data

blocks between its initial and final blocks. To make the search more efficient, we filter the list of potential intermediate blocks to be tested using a map listing which blocks are known to be occupied by other bitstreams.

When the search for a bitstream is inconclusive, we store a tree data structure representing our knowledge about which sequences of blocks give valid bitstreams. The search proceeds to the next bitstream, but whenever we discover that a block is in fact occupied we recursively update all trees which reference the block. This may lead to the elimination of further blocks, causing a recursive update.

5. Output

Finally, we output the permutation of the file and a list of offsets in the permutation which produce valid bitstreams. If the user requests a playable file, we also output an elementary stream containing the bitstreams present in the defragmented file.

The chosen permutation is the one which maximises the number of bitstreams that can be decoded, because the algorithm initially finds all offsets which may contain valid bitstreams (with the help of stage 3), never eliminates a potentially valid offset, and finds a permutation of blocks which lets all the bitstreams be parsed. It therefore solves the problem described in section 5.3⁹.

5.6.1 Algorithm notation and objects

In the following algorithms we use Python-like lists, dictionaries, tuples and objects, and some Python syntax. We typeset objects of non-built-in types as **object**, and references to their members as **object.member**. Instances of built-in types are written as **variable**.

- A decoding context (which is a dictionary containing syntax element names and their values) is stored in **state.variables**, for some state object **state**. State objects also have an associated current node **state.node**, a stack which tracks syntax procedure invocation, and a **state.clone()** method that produces a copy of the state (as described in section 5.4).
- Flowgraph nodes are represented as objects, with each type of node including the members given in its definition (see subsection 5.4.1).

Read nodes also have a **node.generate(state, value_list)** method, which returns a list of (syntax element value, bitstring) tuples, pairing up each possible syntax element value in **value_list** with its binary encoding under the node's coding mode. **Read** nodes store information about restrictions on their values in the field **node.value_restriction**, which

⁹The only bitstreams which are missed by the algorithm are those where both (1) the initial bytes straddle a block boundary and (2) they do not lie directly after another bitstream. When the mapping stage does not find a single chain, false positives can cause the algorithm to fail to find bitstreams, because blocks may be marked as occupied when they are in fact available.

itself has a method `Node.value_restriction.get_possible_list(decoding_context)`, that returns the set of possibilities for the syntax element under the `decoding_context`. They also store the name of the syntax element they read in `node.destination`.

All nodes have a `node.run(state)` method, which executes their action (according to section 5.4), modifying `state`. Only `Read` nodes require access to the input bitstream.

- Finally, we introduce a new object type `bitstream_info`, which summarises the information we have regarding a bitstream, with the following members: `initial_block_index` stores the integer block index containing the start of the bitstream; `initial_block_byte_offset` stores the integer byte offset in the initial block; `final_block` stores the final block index, if it is known; `duration_bytes` stores the duration of the block in bytes, and `block_count` stores the number of blocks containing data from the bitstream; and `state_after_initial_block` stores a copy of the decoder's state after parsing the bitstream up to the end of its first block.

5.6.2 Configuration bitstream parsing and data bitstream offset search

Configuration bitstreams must be parsed in order, as the values of expressions in the bitstream syntax may depend on syntax elements parsed in an earlier configuration bitstream.

For each configuration bitstream, the user gives a list of requirements as a dictionary mapping syntax element names onto values, `known_variables`, and the defragmentation tool generates all bitstreams that meet the requirements, up to a certain named syntax element `last_node` (avoiding combinatorial explosion). The tool generates a list of all byte offsets in the image that contain one of the generated bitstreams. It parses each one in turn, and each time recursively finds the next configuration bitstream in order, using backtracking, until it has found a list of mutually compatible configuration bitstream sequences.

To generate all bitstreams conforming with the specified requirements, we use `GETALLBITSTREAMS(known_variables, last_node, decoding_context)` (algorithm 3), where `decoding_context` is the current decoding context (which may be \emptyset). It returns a list of pairs (`state`, `bitstring_list`), with each item representing one possible bitstring, which conforms to the requirements, and the decoder state after parsing it.

Having located the configuration bitstreams, we search for data bitstreams in the same manner, passing in the post-configuration state and each possible value of `frame_num` in `known_variables`.

5.6.3 Data bitstream filtering

We iterate over the list of candidate data bitstream offsets. For each offset, we put the parser in its post-configuration state and try to parse from the offset until the end of its block,

5. Reconstruction of fragmented compressed data

Algorithm 3 Get a list of valid streams of coded syntax element values.

`known_variables` is a dictionary mapping syntax element names to values. `last_node` is a syntax element name. `decoding_context` is a decoder state.

`HANDLESTACK(state)` checks whether the invocation stack in `state` is non-empty and `state.node` is END. If so, it pops the caller from the stack and updates `state.node` to point to the caller's successor.

```

function GETALLBITSTREAMS(known_variables, last_node, decoding_context)
    state_before ← new state based on decoding_context
    state_before.node ← global entry point node
    bitstream_list ← []
    GETBITSTREAMSRECURSIVE(state_before, [], bitstream_list, known_variables, last_
node)
    return bitstream_list
function GETBITSTREAMSRECURSIVE(state, syntax_element_sequence, bitstream_list,
known_variables, last_node)
    HANDLESTACK(state)
    new_states ← []
    previous_node ← state.node
    if state.node is a Read node then
        possibilities ← state.node.generate(state, [known_variables[state.node.destination]] if
known_variables.has_key(state.node.destination) else state.node.value_restriction.get_possi-
ble_list(state.variables))
        for (value, bitstring) in possibilities do
            s ← state.clone()
            s.variables[previous_node.destination] ← value
            new_states.append((s, bitstring))
    else
        state.node.run(state)
        if syntax error then
            return
        new_states ← [(state, None)]
    if previous_node is a Read node and previous_node.destination = last_node then
        bitstream_list.extend([(state, syntax_element_sequence + [bs]) for (state, bs) in
new_states])
    else
        for (s, bs) in new_states do
            GETBITSTREAMSRECURSIVE(s, syntax_element_sequence + [bs] if bs ≠ None
else syntax_element_sequence, bitstream_list, known_variables, last_node)

```

removing from the list any offsets where the parser detects a syntax error. Bitstreams which do not extend outside their starting block and parse fully are marked as completed, and do not proceed to the search stage.

The parser takes a decoding context and byte offset as input, and returns either `FALSE`, indicating that the bitstream is invalid, `TRUE`, indicating that the parser reached the end of the syntax flowgraph in this block without detecting any errors, or `ENDOFBLOCK`, which indicates that the parser cannot proceed because insufficient bits are available to finish parsing the bitstream before the end of the current disk block. (In the latter case, a valid decoder state is returned, which can be used to resume decoding with a candidate next block.)

The parser supports escaping. This operation is able to transform the stream by replacing a certain byte sequence with another (possibly shorter/longer) byte sequence whenever the parser encounters it. We implement this feature by storing a table of offsets in the image where the byte sequence appears, and performing transformations at any relevant offsets whenever the tool invokes the parser. One important implementation detail is that escape sequences over block boundaries in the image should be ignored, as the logical file may not be contiguous across the boundary; instead, we search and unescape those bytes which straddle the block boundary whenever the parser loads a candidate block pair (previous block, candidate block)¹⁰.

5.6.4 Data bitstream mapping (optional)

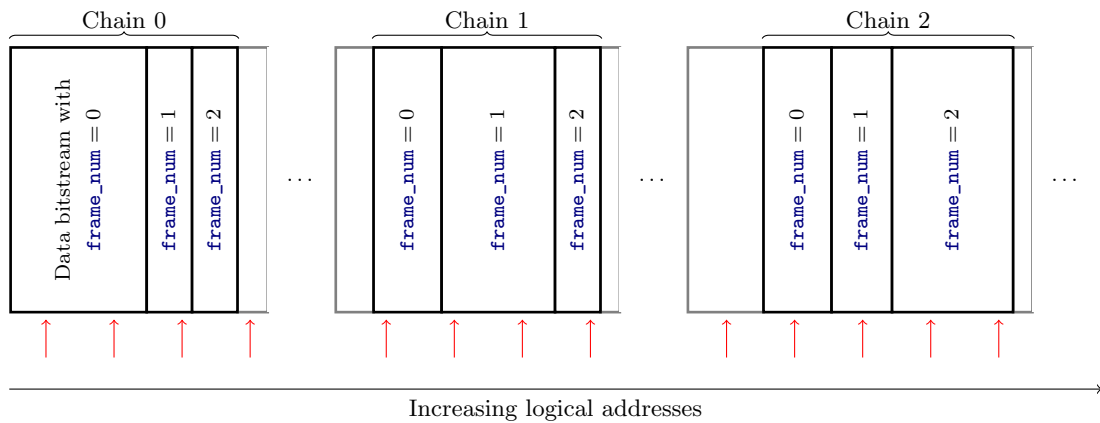
If this stage is omitted, the input to the next stage is the post-configuration state and a list of data bitstream start offsets. If this stage is carried out because assumptions can be made about the container, described earlier in this section, the input to the next stage is the post-configuration state and a list of data bitstream start offsets with associated end block indices and offsets.

1. Given a list of offsets in the file which contain syntactically correct data bitstreams (up to the end of their first blocks), the first step of building a map of the data bitstreams is to find groups of logically adjacent bitstreams (chains). In the first stage of the mapping algorithm, we group bitstreams with consecutive frame numbers into chains.

The figure shows an example file in logical order, part way through execution of this stage. Bitstreams are grouped up to `frame_num = 2`, and three chains are visible. `→` denotes a block boundary.

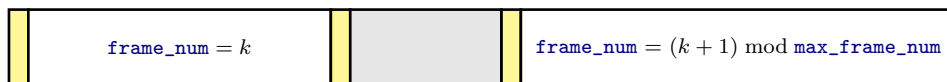
¹⁰In H.264/AVC, the decoder unescapes the three byte sequence `00 00 03` to the two byte sequence `00 00` [45, Subclause 7.3.1].

5. Reconstruction of fragmented compressed data

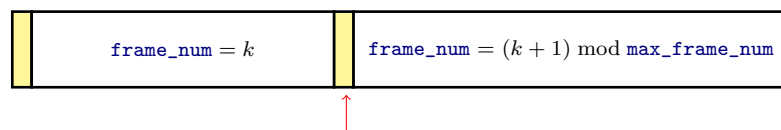


2. The following cases deal with some rare bitstream arrangements. Length tags are shown in yellow.

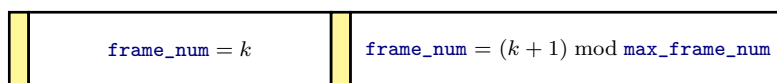
- Find bitstreams which are separated by another bitstream (shown in grey) that is not one of the sought types, but that can be parsed (for example, supplementary enhancement information (SEI) in H.264/AVC).



- If data bitstreams are prefixed by length tags, we find bitstreams between two chains, where the bitstream's length tag has one or more bytes on each side of a block boundary. We search for length tag values encoding bitstream lengths based on the start offset of the next chain with various numbers of intermediate blocks. For each candidate block pair containing the length tag, we see if it is possible to parse to the end of the block, and check its frame number.



3. Finally, we join chains where the last bitstream of the first chain and the first bitstream of the second chain have consecutive frame numbers, and the start byte offset of the first bitstream of the second chain matches the expected offset given the start byte offset and length of the last bitstream of the first chain.



We repeatedly apply these rules until the list of chains no longer changes.

Every bitstream is contained in exactly one chain. For those bitstreams which are not the final bitstream in their chain, we know their initial and final blocks. Otherwise, we know only the initial block.

5.6.5 Data bitstream block search algorithm

The next stage searches for each bitstream's unknown blocks. When a bitstream reaches the end of its initial block, we must check each possible next block as a potential continuation. We do this recursively, until the number of remaining bytes in the bitstream is less than or equal to the size of one block. At this point, if the bitstream's final block index is known due to mapping, we check that the parser returns TRUE within that block. If the parser does not return true, or the bitstream's final block index is unknown, we search all possible final blocks.

At any stage during the search, the list of unoccupied blocks contains all possible blocks except those which are occupied by an earlier block in the current search path, or another bitstream. The list of partially unoccupied blocks is the same, but also includes those blocks which are only partially occupied by another bitstream (when another bitstream starts part-way through the block).

To work out which sequences of blocks lead to valid, completely decoded bitstreams, we use the depth-first search described in algorithm 4, invoked with `FINDBLOCKS(bitstream_info, 1, (bitstream_info.initial_block_index, bitstream_info.state_after_initial_block))`, where `bitstream_info` holds the data bitstream's information (described in subsection 5.6.1). The algorithm produces a tree with block indices as nodes, representing all block orderings with error-free bitstreams, called a *possibility tree*. Every path from the root is the same length, passing through `bitstream_info.block_count - 1` nodes, where the initial block index is not included. Each path represents one possible ordering of blocks leading to a valid bitstream. When only one block ordering leads to an error-free bitstream, there is exactly one path through the tree. In this case, the blocks are marked as occupied, except for the initial block, which is usually partially occupied.

Making the search more efficient

We improve the search efficiency by using information about which blocks are definitely already occupied at a given point during the search. In particular, if we know that a bitstream has only one possible sequence of blocks, these blocks cannot contain another bitstream (unless they are initial/final blocks, occupied by the final/initial blocks of the other bitstream respectively).

To take advantage of this information, we calculate for each bitstream's possibility tree a list of block indices which are referenced on all paths from the root. These block indices are

5. Reconstruction of fragmented compressed data

Algorithm 4 Find all possible block orderings that parse the data bitstream `bitstream_info`.

`DECODE(previous_block_index, state, candidate_block_index)` sets up a new unescaped byte array containing data from `previous_block_index` and `candidate_block_index`, and resumes decoding using `state`. There are three possible results: (1) the bitstream ends successfully, (2) the bitstream decodes to the end of `candidate_block_index`, but more bits are required to continue decoding or (3) it detects a syntax error.

```

function FINDBLOCKS(bitstream_info, blocks_decoded_count, (previous_block_index, previous_state))
    if blocks_decoded_count = bitstream_info.block_count - 1 then
        if bitstream_info.final_block ≠ None then
            test_state ← previous_state.clone()
            DECODE(previous_block_index, test_state, bitstream_info.final_block)
            if no syntax error then
                return [(bitstream_info.final_block, None)]
        valid_final_blocks ← []
        for candidate_block_index in partially unoccupied blocks do
            DECODE(previous_block_index, previous_state.clone(), candidate_block_index)
            if no syntax error then
                valid_final_blocks.append((candidate_block_index, None))
        return valid_final_blocks
    else
        new_child_nodes ← []
        for candidate_block_index in unoccupied blocks do
            candidate_state ← previous_state.clone()
            DECODE(previous_block_index, candidate_state, candidate_block_index)
            if no syntax error and end of block then
                child_nodes ← FINDBLOCKS(bitstream_info, blocks_decoded_count + 1, (candidate_block_index, candidate_state))
                if child_nodes ≠ None then
                    new_child_nodes.append((candidate_block_index, child_nodes))
        if new_child_nodes = [] then
            return None
        else
            return new_child_nodes

```

unavailable for other bitstreams. For each always-referenced block index, we iterate over all other trees associated with bitstreams searched earlier, and prune those trees that reference it to remove the block. We then perform the same procedure recursively on any trees which were updated. Since we track which bitstreams might occupy each block, even if there are multiple possible paths for a bitstream at one point during execution, other bitstreams may later eliminate all but one path in the tree, leading to a single solution.

Because longer bitstreams have more blocks, meaning that there are more opportunities to branch, ordering the bitstreams by their duration in blocks can lead to an overall shorter search time: earlier bitstreams which are shorter will lead to the elimination of blocks, speeding up the search for intermediate blocks in later bitstreams.

If we can make assumptions about block ordering (for example, by understanding the wear-levelling scheme), we can speed up the search. For example, if we know that the image is likely to contain runs of contiguous blocks, we can prioritise searching block $n + 1$ after block n . This will produce a solution more quickly, but the solution may be incomplete, in that other paths could lead to valid bitstreams. It is necessary to explore every possible block after a discontinuity to guarantee finding the permutation which maximises the number of valid bitstreams.

5.7 Results

This section presents the results of testing the defragmentation algorithm on input data from various devices, with simulated fragmentation at four different block sizes. I use the IEC 27.2 binary prefix convention that n KiB = $n \cdot 1024$ bytes and n MiB = $n \cdot 1024^2$ bytes, and use B as the unit symbol for byte.

5.7.1 Input data

To test the performance of the defragmenter, we prepared several storage images. Each image has a different combination of source video data, fragmentation block size and amount of video data. Each image contains content from other files (including compressed PDF data and text) in addition to some source video data.

The blocks in each image are shuffled to simulate applying a randomised wear-levelling algorithm, which is the most challenging scenario. However, this shuffling does not affect the cost of the search, as our algorithm treats all possible block orderings in the same way. To successfully defragment a file, our tool needs to be provided with the fragmentation block size, or one of its integer divisors.

There are six source videos:

5. Reconstruction of fragmented compressed data

- 46 second clip recorded on a fourth generation Apple iPod Touch, with resolution 1280×720 pixels, with AAC-encoded audio and some motion (constant bitrate 10.6 Mbit/s);
- 74 second clip recorded on a fourth generation Apple iPod Touch, with resolution 1280×720 pixels, with AAC-encoded audio and little motion (constant bitrate 10.7 Mbit/s);
- 42 second clip recorded on a Canon Powershot SX 200 IS, with resolution 1280×720 pixels, with PCM-encoded audio and some motion (average bitrate 23.0 Mbit/s);
- 32 second clip recorded on a Canon Powershot SX 200 IS, with resolution 1280×720 pixels, with PCM-encoded audio and little motion (average bitrate 23.2 Mbit/s);
- 634 second clip downloaded from the YouTube website, with resolution 480×360 pixels, without audio (average bitrate 515 kbit/s); and
- the same 634 second clip, recompressed using the x264 encoder using the command-line options `--crf=21.0 --profile=baseline` (average bitrate 609 kbit/s).

We refer to these six videos as iPod (H), iPod (L), Canon (H), Canon (L), YouTube (H) and x264 (H) respectively.

We simulated fragmentation at block sizes of 4096, 2048, 1024 and 512 bytes. For each clip/block size combination we created two images, one small image with 10 MiB of video data and 2 MiB of other data (S), and one large image with 40 MiB of video data and 10 MiB of other data (L).

5.7.2 Data bitstreams

For each input image, we ran the defragmentation tool with the appropriate block size and recorded the number of data bitstreams recovered and their associated block sequences. We limited the maximum number of decoding operations to 500 million. Table 5.6 show for each source/block size/image size combination the number of data bitstreams reconstructed (in the ‘Correct’ column). Some defragmenters skipped bitstreams due to the upper limit on the number of decoding operations; the number of skipped bitstreams is given in the column entitled ‘Skipped’. The number of bitstreams where the algorithm was unable to eliminate all but one possible block ordering are listed in the ‘Multiple’ column.

CPU runtimes are quoted in order to give an approximate impression of the relative cost of the algorithm with different inputs (‘Time taken’). Each defragmenter ran on a machine in a cluster with CPU speeds of 1.8–2.2 GHz.

Error conditions

We also load the ground-truth block orderings generated when the image was shuffled, and compare the block sequences to identify the following error conditions:

- ‘Incorrect’ bitstreams have one single possible block ordering, but it is not the correct one;
- ‘Failed’ bitstreams have no possible block orderings;
- ‘Missed’ bitstreams are present in the image but were not located by the defragmenter; and
- ‘False +s’ (false positives) are bitstreams which are not present in the image but were found by the defragmenter.

False positives occur when the image contains extents that are valid bitstreams, but are not among the bitstreams originally indicated by the container format. False positives can cause failed bitstreams, because they cause their blocks to be marked as occupied (or partially occupied). They can also lead to incorrect bitstreams, when a bitstream has two possibilities, and the correct one is eliminated due to the block occupancy of a false positive; the only remaining possibility is incorrect. When the mapping stage has not found a complete chain containing all the bitstreams, those bitstreams at the start of a chain whose first few bytes lie across a block boundary will be missed.

Table 5.6 shows that the cost of the algorithm, measured in the number of parser invocations required, is much greater at smaller block sizes, and in larger images. Missed bitstreams are also more common in images with small fragmentation block sizes because there are more block boundaries.

Several defragmenter instances did not terminate. In all these cases, the intermediate block search did not parse even one data bitstream in the allotted time. In particular, the large images proved too expensive to defragment at block sizes less than 4096 bytes. Some images were too expensive to defragment even at this block size. Because these defragmenters did not even construct one bitstream given many hours of processing time, due high cost of the algorithm’s search stage, they seem to lie below the threshold of what is feasible to defragment even with great computational effort.

Among the defragmenters which terminated without reaching the limit of 500 million decodes, almost all data bitstreams were recovered successfully. The time taken varied quite widely, but for block sizes greater than 512 bytes many small images were defragmented in less than an hour.

The source of video data had a strong effect on the difficulty of defragmentation. For example, the 4 KiB fragmentation block size, large Canon (L) image took several days to defragment, while the same images with data from the iPod only took a couple of hours. This is because errors are detected more quickly in video produced by certain encoders (see subsection 5.5.4).

5. Reconstruction of fragmented compressed data

5.7.3 Proportion of data recovered successfully

Table 5.7 shows the amount of video data recovered from each image, and the percentage of all video data recovered. Among defragmenters that did not reach the limit of 500 million decodes, all but one defragmenter instance recovered more than 90% of the video data.

5.8 Analysis

The algorithm recovered more than 90% of the fragmented video bitstreams in the majority of our tests. Each sample storage image included a mixture of compressed non-video data and uncompressed data, alongside video data produced by one of three video compressors. We have therefore shown that the algorithm can recover a useful proportion of video in relatively small but realistic storage images, with randomly-permuted disk blocks.

The remaining, unrecovered bitstreams were not found due to their blocks being marked as occupied by false-positive bitstreams. We rely on eliminating blocks as we establish that they are part of bitstreams, and recursively update the tree that encodes candidate paths for each bitstream when we find that blocks are occupied. False positives disrupt this process, leading to blocks being marked as occupied erroneously.

The bitstream mapping heuristics described in subsection 5.6.4 try to use information about the layout of bitstreams to eliminate false positives. This process, called chaining, is important to the performance of our algorithm. Ideally, our algorithm should find a single chain containing all bitstreams present in the storage image.

Missed bitstreams (when the initial bytes straddle a block boundary, for example) make it impossible to merge sequential chains. Additionally, we are unable to apply chaining if we do not have length tags for each bitstream, and know how many bytes lie between them. As well as causing false positives, the computational cost of the search step of the algorithm is greater for bitstreams that are the last entry in their chain, as their final disk block is unknown.

The time cost of the algorithm is high, as it has to parse many disk blocks when searching for sequences of blocks that yield valid bitstreams. While we demonstrated that the algorithm performs well on fifty megabyte images, forensic investigators must sometimes handle multi-gigabyte images.

5.8.1 Possible extensions to the algorithm

The computational cost of our algorithm could be reduced by initially eliminating blocks containing non-random data. In real-world forensics scenarios, our algorithm needs to handle larger storage images. However, substantially more computing power will be available, a lot of blocks are likely to contain non-video data, and the distribution of bitstream lengths will

be similar to that of our test images. Therefore, our algorithm is not necessarily limited to small storage images.

The main search stage of our algorithm uses fast generated C code, while the initial bitstream location step is written in Python. The latter will need to be optimised to handle multi-gigabyte images.

Other improvements to our algorithm are likely to involve reducing the false-positive rate by locating all bitstreams and improving chaining. In our testing, bitstreams were sometimes missed when their initial bytes straddled a block boundary. These could be located by joining all possible pairs of blocks (at quadratic cost) and searching for bitstreams over each boundary.

By associating an estimated probability that a given bitstream is a false positive (based on the length of chain it participates in, for example), we could use backtracking to try removing potential false positives systematically. This would increase the computational cost of the algorithm.

The algorithm's performance is dependent on the encoder used to produce the data being defragmented. It would be interesting to measure how quickly errors can be detected on data output by a wider selection of encoders than the ones considered in subsection 5.5.4. This would help in establishing bounds on whether defragmentation is feasible for each encoder, based on how quickly errors are detected.

The error detection rate for a given bitstream forms a useful discriminator for encoder classification. It is possible to adapt our flowgraph-based parser to provide other suitable metrics: the subset of codec features used, or the amount of time spent parsing particular parts of the syntax, for example.

Our automatic defragmentation tool will be very useful at forensics labs, where many devices must be processed per day. The methodology is applicable to other file types where error detection is possible. Eventually it might be possible to defragment bitstreams from several codecs at the same time, thereby eliminating a larger proportion of blocks from consideration.

The technique of generating parsers based on a syntax specification has applications outside forensics. It could be used as a syntax validator on the input of potentially vulnerable video players, to filter out invalid bitstreams. The same methodology could also be used to generate intentionally invalid input for fuzz testing.

5.9 Conclusion

We demonstrated a general-purpose defragmentation algorithm for storage images containing compressed data bitstreams, relying on syntax errors to test whether a given sequence of candidate blocks could be contiguous, as part of a search algorithm. Using a bitstream syntax description for H.264/AVC Baseline profile bitstreams, we demonstrated the algorithm's

5. Reconstruction of fragmented compressed data

efficacy in locating and rebuilding compressed video bitstreams generated by a variety of devices.

Our algorithm is of practical use to forensic investigators. We have already applied it to a fragmented hard disk image from a CCTV system provided by the London Metropolitan Police Service, where it located several compressed bitstreams, outputting a valid elementary stream for viewing. Because manual reconstruction of compressed video is difficult and time-consuming, our automatic tool has the potential to improve the efficiency of practical evidence processing procedures substantially.

Source video	Block size	Image size	Correct	Multiple	Incorrect	Failed	Skipped	Missed	False +s	Time taken (h:m:s)
Canon (L)	4,096	L	398	1	0	25	0	3	7	119:55:59
iPod (H)	4,096	L	920	0	0	0	0	3	0	2:13:47
iPod (L)	4,096	L	745	0	0	0	0	4	0	2:11:38
x264 (H)	4,096	L	15773	11	0	6	0	33	18	36:33:22
YouTube (H)	4,096	L	18354	6	0	1	0	655	3	28:46:48
Canon (H)	4,096	S	103	0	0	2	0	3	3	7:41:10
Canon (L)	4,096	S	104	0	0	2	0	3	3	0:27:21
iPod (H)	4,096	S	234	0	0	0	0	2	0	0:11:31
iPod (L)	4,096	S	185	0	0	0	0	3	0	0:10:29
x264 (H)	4,096	S	4421	1	0	1	0	12	1	1:13:32
YouTube (H)	4,096	S	5031	1	0	0	0	40	2	1:37:26
iPod (H)	2,048	L	917	1	0	0	0	5	0	7:47:51
iPod (L)	2,048	L	737	4	0	0	0	7	0	6:53:33
x264 (H)	2,048	L	15731	25	0	21	0	48	0	14:06:56
YouTube (H)	2,048	L	18808	39	0	10	5	154	0	15:33:48
Canon (L)	2,048	S	98	0	0	8	0	2	13	0:44:41
iPod (H)	2,048	S	234	0	0	0	0	2	0	0:27:57
iPod (L)	2,048	S	183	0	0	0	0	4	0	0:27:26
x264 (H)	2,048	S	4426	0	0	2	0	15	2	0:50:17
YouTube (H)	2,048	S	5024	2	0	0	0	46	2	1:08:49
iPod (L)	1,024	L	256	488	0	0	478	4	0	11:16:09
x264 (H)	1,024	L	6785	8924	0	0	8828	94	0	13:04:23
YouTube (H)	1,024	L	8925	9878	0	1	9658	207	0	16:42:45
Canon (L)	1,024	S	94	1	0	10	0	3	15	2:05:18
iPod (H)	1,024	S	233	1	0	0	0	2	0	1:54:49
iPod (L)	1,024	S	183	1	0	0	0	3	0	1:36:40
x264 (H)	1,024	S	3036	1357	0	0	1236	29	0	7:47:00
YouTube (H)	1,024	S	4056	954	0	0	807	56	0	8:19:28
iPod (L)	512	S	178	5	0	0	3	4	0	11:07:32
x264 (H)	512	S	1563	2806	0	0	2691	55	0	8:37:44
YouTube (H)	512	S	1292	3699	0	0	3574	76	0	8:23:27

Figure 5.6: This table summarises the results of running the defragmenter on 12/50 MiB images with block sizes of 512, 1024, 2048 and 4096 bytes. The fourth to tenth columns show the number of data bitstreams falling into each category described in subsection 5.7.2.

5. Reconstruction of fragmented compressed data

Source video	Block size	Image size	Recovered (MiB)	Recovered (%)	Skipped	Time taken (h:m:s)
Canon (L)	4,096	L	36.31	93.24	0	119:55:59
iPod (H)	4,096	L	39.64	99.68	0	2:13:47
iPod (L)	4,096	L	39.65	99.65	0	2:11:38
x264 (H)	4,096	L	39.56	99.06	0	36:33:22
YouTube (H)	4,096	L	36.33	93.45	0	28:46:48
Canon (H)	4,096	S	9.47	96.02	0	7:41:10
Canon (L)	4,096	S	9.42	95.73	0	0:27:21
iPod (H)	4,096	S	9.90	99.67	0	0:11:31
iPod (L)	4,096	S	9.91	99.22	0	0:10:29
x264 (H)	4,096	S	9.89	99.17	0	1:13:32
YouTube (H)	4,096	S	9.55	95.67	0	1:37:26
iPod (H)	2,048	L	39.50	99.34	0	7:47:51
iPod (L)	2,048	L	39.27	98.77	0	6:53:33
x264 (H)	2,048	L	39.24	98.25	0	14:06:56
YouTube (H)	2,048	L	37.15	95.56	5	15:33:48
Canon (L)	2,048	S	8.86	90.83	0	0:44:41
iPod (H)	2,048	S	9.90	99.67	0	0:27:57
iPod (L)	2,048	S	9.81	98.53	0	0:27:26
x264 (H)	2,048	S	9.89	99.06	0	0:50:17
YouTube (H)	2,048	S	9.52	95.29	0	1:08:49
iPod (L)	1,024	L	9.51	23.92	478	11:16:09
x264 (H)	1,024	L	4.73	11.83	8828	13:04:23
YouTube (H)	1,024	L	7.04	18.12	9658	16:42:45
Canon (L)	1,024	S	8.54	87.52	0	2:05:18
iPod (H)	1,024	S	9.86	99.27	0	1:54:49
iPod (L)	1,024	S	9.81	98.55	0	1:36:40
x264 (H)	1,024	S	3.65	36.61	1236	7:47:00
YouTube (H)	1,024	S	5.57	55.82	807	8:19:28
iPod (L)	512	S	9.21	92.53	3	11:07:32
x264 (H)	512	S	0.75	7.53	2691	8:37:44
YouTube (H)	512	S	0.70	7.01	3574	8:23:27

Figure 5.7: The defragmentation algorithm normally recovers more than 90% of fragmented data.

Chapter 6

Conclusions

I have shown that it is possible to exploit the low-level details of compression schemes and their implementations to develop automatic tampering detection and evidence recovery algorithms that are applicable in scenarios involving compressed data.

Recompression is increasingly an issue for content producers and consumers, especially with the popularity of images and videos recorded on consumer devices and transmitted over the Internet. Understanding the detailed effects of recompression can be useful for developing algorithms that warn users about hidden recompression steps, maintain quality in data processing systems and reconstruct a document's processing history.

The copy-evident marking algorithm presented in chapter 3 adds a high-frequency pattern to a uniform region of an image, modulated with a message that is imperceptible in the original marked image, but becomes visible after recompression using particular known quality settings. Such an algorithm could be used to make a visible warning appear in lower quality copies of a marked original document, or to expose a hidden recompression step performed by an Internet service provider without relying on special software tools.

The presented copy-evident marking algorithm is still limited to uniform areas and a single, known recompression quality factor. However, a message that appears after recompression to one of several quality factors can be achieved by multiplexing several marks. The recompressed image's message is less visible when the image undergoes filtering operations (for example, due to browser content resizing).

It may be possible to extend our technique to marking non-uniform images or video data. Currently, the distortion introduced by the high frequency checkerboard pattern is too noticeable in marked photographs, but the effect may work better on very high resolution screens, or in situations where we know that down-sampling by a particular factor will take place. Video presents a particular challenge because the variation of quantisation factors due to rate control can be quite unpredictable. However, motion compensation may provide an alternative opportunity to introduce objectionable distortion in recompressed versions. The combination of

6. Conclusions

JPEG's chroma down-sampling operation with gamma correction might also allow for another approach.

In chapter 4, I presented a new type of compressor, designed to process bitmaps output by a JPEG decompressor. It recovers the set of all bitstreams that produce a given result on decompression by inverting the computations performed during decompression. As a side-effect, it also indicates any regions that have been modified since decompression, whenever the changes have destroyed JPEG's characteristic distortions.

The recompressor is necessarily matched with one particular decompressor implementation, as it uses a precise model of the decompressor's computations. Saturated pixel values are a particular problem for exact recompressors, because they are produced by clipping operations that discard information. In our results, we observed that images with many saturated pixels were more expensive to recompress.

The same methodology may be applicable with other formats, such as compressed audio or video data, but the functionality of complicated decompressors is likely to be difficult to model and invert for the purposes of exact recompression.

By not relying on probabilistic techniques, we can be confident in the results of the algorithms, but at the expense of greater computational cost.

In chapter 5, I demonstrated how to locate and rebuild fragmented compressed bitstreams, by taking advantage of restrictions on bitstream syntax to eliminate incorrect candidate bitstreams. Having proposed a general-purpose algorithm, I showed the practical applicability of the algorithm on H.264/AVC Baseline profile compressed video streams, using source video from a variety of devices.

The defragmentation algorithm has some limitations. Based on our results, it is clear that missed bitstreams are a common problem, and can lead to false positives, or streams with multiple possible block sequences. An initial search testing the boundary between each possible pair of blocks (at quadratic cost) to find bitstreams whose first few bytes straddle two blocks would help to ameliorate this problem. The mapping stage of the algorithm could be improved by using any available information about interleaved audio streams.

The algorithm is suitable for applying in real-world evidence-processing pipelines. The search stage is amenable to parallelisation. The current implementation is quite fast, using generated C code for the expensive search stage. Block classification algorithms (as described in subsection 5.2.3) can be used to reduce the size of input to our tool, which can make the search cheaper in filesystems with uncompressed data. Finally, our tool could be improved by providing bitstream syntax descriptions for a variety of different compressed formats beyond H.264/AVC. In particular, it would be interesting to investigate the feasibility of our approach with standards employing arithmetic coding.

The approach of generating bitstream parsers automatically from a syntax description may have applications outside forensic investigation. It could be used to generate and update soft-

ware video decoders without transmitting binaries. It may also be possible to prove assertions about compressed bitstream formats by analysis of the syntax flowgraph, or justify properties of decoding software generated based on the syntax description.

Our work on defragmentation raises several interesting questions regarding compressed bitstream resynchronisation, where a decoder has to resume decoding in the middle of a bitstream due to data loss or corruption. The structure of the H.264/AVC Baseline profile syntax leads to repeated codewords in heavily-compressed data, creating repetitions which might facilitate resynchronisation.

Appendix A

JPEG encoder quality selection

The two quantisation tables used to quantise DCT coefficients in luma and chroma blocks during JPEG compression are normally chosen based on a user-specified scalar quality factor. Below are the mappings used by two popular implementations: the Independent JPEG Group (IJG) codec [57] and Adobe Photoshop CS2 [37].

A.1 IJG encoder

A scalar quality factor in the range 1–100 is passed to the encoder. This is specified using a slider in the graphical user interface of the GNU Image Manipulation Program (GIMP) [72], or with the option `-quality` for the `cjpeg` tool.

The quantisation tables, \mathbf{Q}^Y and \mathbf{Q}^C , are then chosen by scaling the tables suggested in the standard [38, Tables K.1 and K.2], here denoted by \mathbf{K}^Y and \mathbf{K}^C , based on the user’s choice of quality factor $q \in \{1, \dots, 100\}$ using the following formula:

$$(\mathbf{Q}^c)_{u,v} = \begin{cases} \text{divround}((\mathbf{K}^c)_{u,v} \cdot \lfloor 5000/q \rfloor, 100) & 1 \leq q < 50, \\ \max(1, \text{divround}((\mathbf{K}^c)_{u,v} \cdot (200 - 2 \cdot q), 100)) & 50 \leq q \leq 100. \end{cases} \quad (\text{A.1})$$

If the baseline option is chosen, the compressor clips output values to the range $\{0, \dots, 255\}$. These tables quantise higher spatial frequencies more aggressively than the low frequencies, as they are less perceptually important.

A.2 Adobe Photoshop CS2

Adobe Photoshop CS2 contains another widely used JPEG encoder. The ‘save for web’ feature lets the user choose an integer in $\{0, 1, \dots, 100\}$, while the main ‘save as’ feature has thirteen options for ‘quality’ ranging from 0 to 12.

Considering the ‘save as’ feature in more detail, qualities 0–6 use 4:2:0 chroma down-sampling, while qualities 7–12 do not use chroma down-sampling (4:4:4). There does not appear to be a simple mapping from quality settings onto quantisation matrices. Figure A.1 shows what quantisation factors are used: each colour of line corresponds to a group of spatial frequencies which are quantised in the same way as the quality option varies. There is clearly no simple relationship as in the IJG encoder, so the mapping from quality options onto quantisation matrices may be based on user studies or a more complex psychophysical model.

A. JPEG encoder quality selection

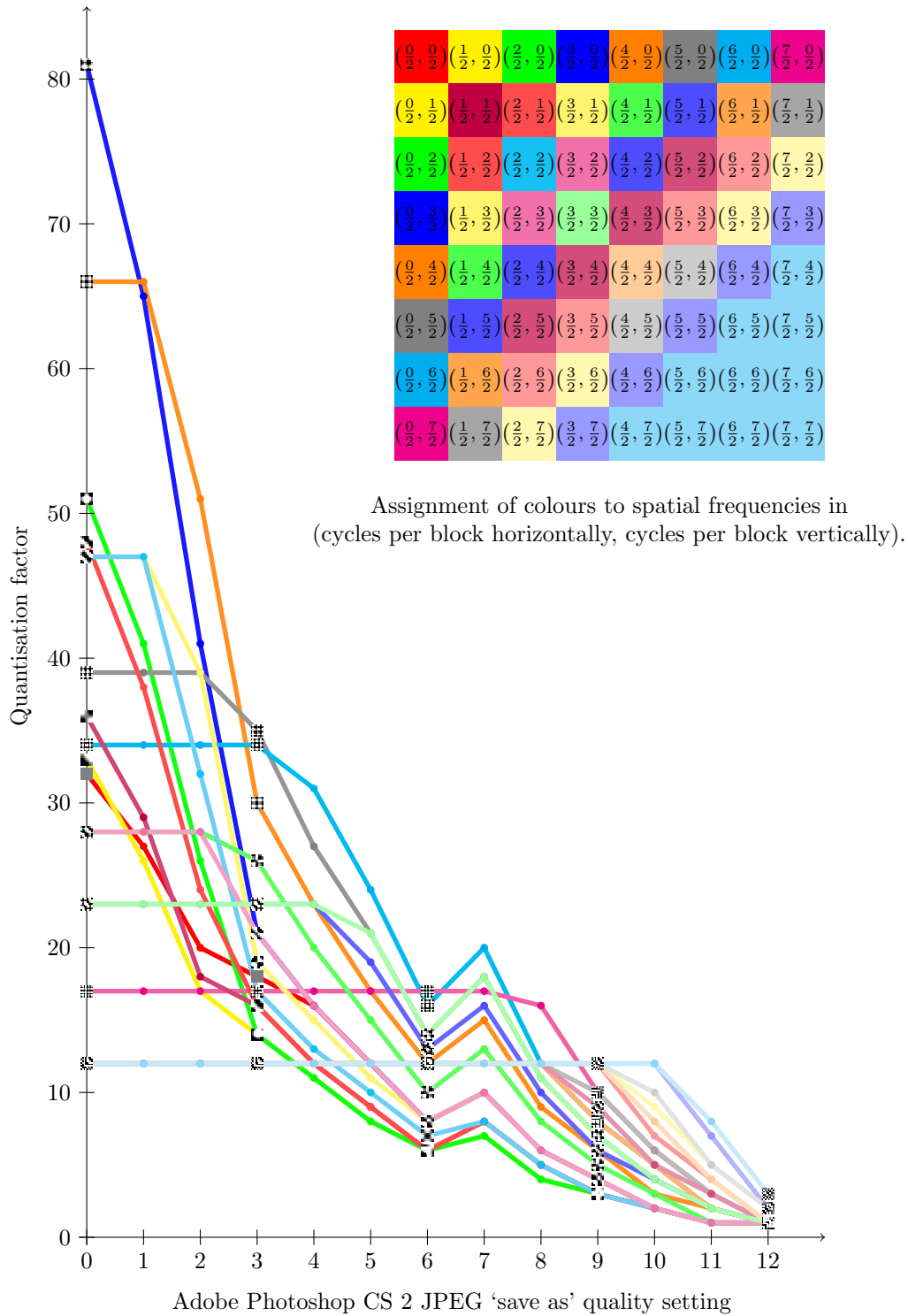


Figure A.1: Adobe Photoshop CS2 has thirteen options for JPEG image ‘quality’. This chart shows the mapping from qualities onto quantisation factors, grouping spatial frequencies which are quantised in the same way as quality is varied. Each 8×8 greyscale spatial domain block shows a sum of frequencies which are quantised equally.

Appendix B

H.264/AVC bitstream syntax

This appendix includes the bitstream syntax description for some less commonly-used parts of the H.264/AVC Baseline profile syntax than those given in subsection 5.5.3, which are also used by our defragmentation tool's parser.

Picture parameter set Rbsp syntax [45, Subclause 7.3.2.2]

```
# 7.3.2.2 Picture parameter set Rbsp syntax
pic_parameter_set_rbsp[category = 1]()
  read(pic_parameter_set_id, ue(v, require(range(0, 255))))
  read(seq_parameter_set_id, ue(v, require(range(0, 31))))
  read(entropy_coding_mode_flag, u(1, require(0)))
  read(bottom_field_pic_order_in_frame_present_flag, u(1, require(0)))
  read(num_slice_groups_minus1, ue(v, require(0), possible(range(0, 7))))
  if (num_slice_groups_minus1 > 0)
    # Omitted [multiple slices]
  read(num_ref_idx_l0_default_active_minus1,
        ue(v, require(range(0, 31))))
  read(num_ref_idx_l1_default_active_minus1,
        ue(v, require(range(0, 31))))
  read(weighted_pred_flag, u(1, require(0), possible(0, 1)))
  read(weighted_bipred_idc, u(2, require(0), possible(0, 1, 2)))
  read(pic_init_qp_minus26,
        se(v, require(range(-(26 + QpBdOffsetY), 25))))
  read(pic_init_qs_minus26,
        se(v, require(range(-26, 25))))
  read(chroma_qp_index_offset, se(v, require(range(-12, 12))))
  read(deblocking_filter_control_present_flag, u(1))
  read(constrained_intra_pred_flag, u(1))
  read(redundant_pic_cnt_present_flag, u(1, require(0)))
  if (more_rbsp_data())
```

B. H.264/AVC bitstream syntax

```
# Omitted [not present in baseline profile]
else
  assign(transform_8x8_mode_flag, False)
  assign(pic_scaling_matrix_present_flag, False)
  assign(second_chroma_qp_index_offset, chroma_qp_index_offset)
  rbsp_trailing_bits()
```

Slice layer without partitioning RBSP syntax [45, 7.3.2.8 Slice layer without partitioning RBSP syntax]

```
# 7.3.2.8 Slice layer without partitioning RBSP syntax
slice_layer_without_partitioning_rbsp()
  slice_header[category = 2]()
  slice_data[category = 2|3|4]()
  rbsp_slice_trailing_bits()
```

Slice header syntax [45, Subclause 7.3.3, slice header syntax] and associated syntax

```
# 7.3.3 Slice header syntax
slice_header[category = 2]()
  read(first_mb_in_slice, ue(v))
  if (nal_unit_type == 5)
    read(slice_type, ue(v, require(2, 7), possible(4, 9)))
  else
    read(slice_type, ue(v, require(0, 1, 5, 6), possible(3, 8)))
  read(pic_parameter_set_id, ue(v, require(range(0, 255))))
  if (separate_colour_plane_flag == 1)
    read(colour_plane_id, u(2, require(range(0, 2))))
  read(frame_num, u(v, bit_count(log2_max_frame_num_minus4 + 4)))
  if (frame_mbs_only_flag == 0)
    read(field_pic_flag, u(1, require(0), possible(1)))
    if (field_pic_flag)
      read(bottom_field_flag, u(1))
  else
    assign(field_pic_flag, 0)
  assign(MbaffFrameFlag, mb_adaptive_frame_field_flag &&
        (!field_pic_flag))
  if (IdrPicFlag == 1)
    read(idr_pic_id, ue(v, require(range(0, 65535))))
  assign(PicHeightInMbs, FrameHeightInMbs / (1 + field_pic_flag))
  assign(PicSizeInMbs, PicWidthInMbs * PicHeightInMbs)
  check(first_mb_in_slice, range(0, PicSizeInMbs - 1
    if !MbaffFrameFlag else
    PicSizeInMbs / 2 - 1))
  if (pic_order_cnt_type == 0)
```



```

read(pic_order_cnt_lsb,
     u(v, bit_count(log2_max_pic_order_cnt_lsb_minus4 + 4)))
if (bottom_field_pic_order_in_frame_present_flag == 1 &&
    field_pic_flag == 0)
    read(delta_pic_order_cnt_bottom, se(v))

if (pic_order_cnt_type == 1 &&
    delta_pic_order_always_zero_flag == 0)
    read(delta_pic_order_cnt[0], se(v))
if (bottom_field_pic_order_in_frame_present_flag &&
    (!field_pic_flag))
    read(delta_pic_order_cnt[1], se(v))

if (redundant_pic_cnt_present_flag)
    read(redundant_pic_cnt, ue(v))

if (IS_SLICE_TYPE_B(slice_type))
    read(direct_spatial_mv_pred_flag, u(1))
if (IS_SLICE_TYPE_P(slice_type) ||
    IS_SLICE_TYPE_SP(slice_type) ||
    IS_SLICE_TYPE_B(slice_type))
    read(num_ref_idx_active_override_flag, u(1))
if (num_ref_idx_active_override_flag == 1)
    read(num_ref_idx_l0_active_minus1,
         ue(v, require(range(0, 15
                             if !field_pic_flag else
                             31))))
    if (IS_SLICE_TYPE_B(slice_type))
        read(num_ref_idx_l1_active_minus1,
             ue(v, require(range(0, 15
                                 if !field_pic_flag else
                                 31))))
    else
        assign(num_ref_idx_l0_active_minus1,
               num_ref_idx_l0_default_active_minus1)
        if (IS_SLICE_TYPE_B(slice_type))
            assign(num_ref_idx_l1_active_minus1,
                   num_ref_idx_l1_default_active_minus1)

if (nal_unit_type == 20)
    ref_pic_list_mvc_modification()
else
    ref_pic_list_modification()

if ((weighted_pred_flag == 1 &&

```

B. H.264/AVC bitstream syntax

```
(IS_SLICE_TYPE_P(slice_type) ||
 IS_SLICE_TYPE_SP(slice_type)) ||
 (weighted_bipred_idc == 1 && IS_SLICE_TYPE_B(slice_type)))
pred_weight_table()
if (nal_ref_idc != 0)
  dec_ref_pic_marking()
if (entropy_coding_mode_flag == 1 &&
    (IS_SLICE_TYPE_I(slice_type) ||
     IS_SLICE_TYPE_SI(slice_type)))
  read(cabac_init_idc, ue(v))
read(slice_qp_delta, se(v))
assign(SliceQPY, 26 + pic_init_qp_minus26 + slice_qp_delta)
check(SliceQPY, range(-QpBdOffsetY, 51))
if (IS_SLICE_TYPE_SP(slice_type) ||
    IS_SLICE_TYPE_SI(slice_type))
  # Omitted [not in Baseline profile]

if (deblocking_filter_control_present_flag == 1)
  read(disable_deblocking_filter_idc,
       ue(v, require(range(0, 2))))
  if (disable_deblocking_filter_idc != 1)
    read(slice_alpha_c0_offset_div2, se(v))
    read(slice_beta_offset_div2, se(v))
if (num_slice_groups_minus1 > 0 && slice_group_map_type >= 3 &&
    slice_group_map_type <= 5)
  # Omitted [not in Baseline profile]
```

Slice data syntax [45, Subclause 7.3.4, slice data syntax]

7.3.4 Slice data syntax

```
slice_data()
if (entropy_coding_mode_flag == 1)
  # Omitted [not in Baseline profile]
assign(firstMbAddr, first_mb_in_slice * (1 + MbaffFrameFlag))
assign(CurrMbAddr, firstMbAddr)
assign(moreDataFlag, 1)
assign(prevMbSkipped, 0)
do
  if (!IS_SLICE_TYPE_I(slice_type) &&
      !IS_SLICE_TYPE_SI(slice_type))
    if (entropy_coding_mode_flag == 0)
      read(mb_skip_run,
           ue(v, require(range(0, PicSizeInMbs - CurrMbAddr))),
           2)
      assign(prevMbSkipped, (mb_skip_run > 0))
```

```

    for (i = 0; i < mb_skip_run; i++)
        check(CurrMbAddr, range(0, PicSizeInMbs - 1))
        if (IS_SLICE_TYPE_P(slice_type) ||
            IS_SLICE_TYPE_SP(slice_type))
            context_mb_type[CurrMbAddr] = MbTypes.P_Skip
        else
            context_mb_type[CurrMbAddr] = MbTypes.B_Skip
        assign(CurrMbAddr, NextMbAddress(CurrMbAddr))
    if (CurrMbAddr != firstMbAddr || mb_skip_run > 0)
        assign(moreDataFlag, more_rbsp_data())
else
    # Omitted [not in Baseline profile]

if (moreDataFlag)
    if (MbaffFrameFlag && (CurrMbAddr % 2 == 0 ||
        (CurrMbAddr % 2 == 1 && prevMbSkipped)))
        read(mb_field_decoding_flag, u(1) | ae(v), 2)
    else
        assign(mb_field_decoding_flag, field_pic_flag)
    check(CurrMbAddr, range(0, PicSizeInMbs - 1))
    macroblock_layer[category = 2|3|4]()

    assign(moreDataFlag, more_rbsp_data())
    if (!moreDataFlag)
        assign(CurrMbAddr, NextMbAddress(CurrMbAddr))

if (entropy_coding_mode_flag == 0)
    assign(moreDataFlag, more_rbsp_data())
else
    if (!IS_SLICE_TYPE_I(slice_type) &&
        !IS_SLICE_TYPE_SI(slice_type))
        assign(prevMbSkipped, mb_skip_flag)
    if (MbaffFrameFlag && CurrMbAddr % 2 == 0)
        assign(moreDataFlag, 1)
    else
        read(end_of_slice_flag, ae(v), 2)
        assign(moreDataFlag, !end_of_slice_flag)
    if (moreDataFlag)
        assign(CurrMbAddr, NextMbAddress(CurrMbAddr))
while (moreDataFlag)
    check(CurrMbAddr, PicSizeInMbs)

```

Macroblock layer syntax [45, Subclause 7.3.5]

7.3.5 Macroblock layer syntax

B. H.264/AVC bitstream syntax

```

macroblock_layer()
  read(mb_type, ue(v) | ae(v), 2)

  # Not from the standard. This creates unambiguous MB types.
  assign(u_mb_type, GetUniqueMbTypeFromMbType(mb_type, slice_type))

  # Store this in the decoding context.
  assign(context_mb_type[CurrMbAddr], u_mb_type)

  if (u_mb_type == MbTypes.IPCM)
    # Omitted [LPCM macroblock coding]
  else
    assign(noSubMbPartSizeLessThan8x8Flag, 1)
    if (u_mb_type != MbTypes.I_NXN &&
        MbPartPredMode(u_mb_type, 0, False) !=
          MbPartPredModes.Intra_16x16 &&
        NumMbPart(u_mb_type) == 4)
      sub_mb_pred[category = 2](u_mb_type)
      for (mbPartIdx = 0; mbPartIdx < 4; mbPartIdx++)
        if (u_sub_mb_type[mbPartIdx] != SubMbTypes.B_Direct_8X8)
          if (NumSubMbPart(u_sub_mb_type[mbPartIdx]) > 1)
            assign(noSubMbPartSizeLessThan8x8Flag, 0)
          else if (direct_8x8_inference_flag == 0)
            assign(noSubMbPartSizeLessThan8x8Flag, 0)
    else
      if (transform_8x8_mode_flag && u_mb_type == MbTypes.I_NXN)
        read(transform_size_8x8_flag, u(1) | ae(v), 2)
      else
        assign(transform_size_8x8_flag, 0)
      mb_pred[category = 2](u_mb_type)
    if (MbPartPredMode(u_mb_type, 0, False) !=
        MbPartPredModes.Intra_16x16)
      read(coded_block_pattern, me(v) | ae(v), 2)
      assign(CodedBlockPatternLuma, coded_block_pattern % 16)
      assign(CodedBlockPatternChroma, coded_block_pattern / 16)
      if (CodedBlockPatternLuma > 0 &&
          transform_8x8_mode_flag == 1 &&
          u_mb_type != MbTypes.I_NXN &&
          noSubMbPartSizeLessThan8x8Flag == 1 &&
          (u_mb_type != MbTypes.B_Direct_16X16 ||
           direct_8x8_inference_flag))
        read(transform_size_8x8_flag, u(1) | ae(v), 2)
      else
        assign(transform_size_8x8_flag, 0)
    else

```

```

assign(CodedBlockPatternLuma ,
        GetIntra16x16CodedBlockPatternLuma(u_mb.type))
assign(CodedBlockPatternChroma ,
        GetIntra16x16CodedBlockPatternChroma(u_mb.type))
if (CodedBlockPatternLuma > 0 ||
     CodedBlockPatternChroma > 0 ||
     MbPartPredMode(u_mb.type, 0, transform_size_8x8_flag) ==
     MbPartPredModes.Intra_16x16)
read(mb_qp_delta ,
      se(v, require(range(-(26 + QpBdOffsetY / 2),
                          25 + QpBdOffsetY / 2))) | ae(v), 2)
residual[category = 3|4](0, 15)

```

Macroblock prediction syntax [45, Subclause 7.3.5.1, Macroblock prediction syntax] and associated syntax

7.3.5.1 Macroblock prediction syntax

```

mb_pred[category = 2](u_mb.type)
if (MbPartPredMode(u_mb.type, 0, transform_size_8x8_flag) ==
     MbPartPredModes.Intra_4x4 ||
     MbPartPredMode(u_mb.type, 0, transform_size_8x8_flag) ==
     MbPartPredModes.Intra_8x8 ||
     MbPartPredMode(u_mb.type, 0, transform_size_8x8_flag) ==
     MbPartPredModes.Intra_16x16)
if (MbPartPredMode(u_mb.type, 0, transform_size_8x8_flag) ==
     MbPartPredModes.Intra_4x4)
for (luma4x4BlkIdx = 0; luma4x4BlkIdx < 16; luma4x4BlkIdx++)
  read(prev_intra4x4_pred_mode_flag[luma4x4BlkIdx],
       u(1) | ae(v))
  if (prev_intra4x4_pred_mode_flag[luma4x4BlkIdx] == 0)
    read(rem_intra4x4_pred_mode[luma4x4BlkIdx], u(3) | ae(v))
if (MbPartPredMode(u_mb.type, 0, transform_size_8x8_flag) ==
     MbPartPredModes.Intra_8x8)
for (luma8x8BlkIdx = 0; luma8x8BlkIdx < 4; luma8x8BlkIdx++)
  read(prev_intra8x8_pred_mode_flag[luma8x8BlkIdx],
       u(1) | ae(v))
  if (prev_intra8x8_pred_mode_flag[luma8x8BlkIdx] == 0)
    read(rem_intra8x8_pred_mode[luma8x8BlkIdx], u(3) | ae(v))
if (ChromaArrayType == 1 || ChromaArrayType == 2)
  read(intra_chroma_pred_mode ,
       ue(v, require(range(0, 3))) | ae(v))
else if (MbPartPredMode(u_mb.type, 0, transform_size_8x8_flag) !=
         MbPartPredModes.Direct)
for (mbPartIdx = 0; mbPartIdx < NumMbPart(u_mb.type); mbPartIdx++)
  if ((num_ref_idx_l0_active_minus1 > 0 ||

```

B. H.264/AVC bitstream syntax

```
mb_field_decoding_flag != field_pic_flag) &&
MbPartPredMode(u_mb_type,
                mbPartIdx, transform_size_8x8_flag) !=
MbPartPredModes.Pred_L1)
read(ref_idx_l0[mbPartIdx], te(v,
    bit_count(2 * num_ref_idx_l0_active_minus1 + 1
              if MbaffFrameFlag == 1 &&
                  mb_field_decoding_flag == 1 else
                  num_ref_idx_l0_active_minus1)) | ae(v))
for (mbPartIdx = 0; mbPartIdx < NumMbPart(u_mb_type); mbPartIdx++)
if (MbPartPredMode(u_mb_type,
                  mbPartIdx,
                  transform_size_8x8_flag) !=
MbPartPredModes.Pred_L0 &&
    (num_ref_idx_l1_active_minus1 > 0 ||
     mb_field_decoding_flag != field_pic_flag))
read(ref_idx_l1[mbPartIdx],
    te(v, bit_count(2 * num_ref_idx_l1_active_minus1 + 1
                    if MbaffFrameFlag == 1
                    && mb_field_decoding_flag == 1
                    else
                    num_ref_idx_l1_active_minus1)) | ae(v))
for (mbPartIdx = 0; mbPartIdx < NumMbPart(u_mb_type); mbPartIdx++)
if (MbPartPredMode(u_mb_type,
                  mbPartIdx,
                  transform_size_8x8_flag) !=
MbPartPredModes.Pred_L1)
for (compIdx = 0; compIdx < 2; compIdx++)
    read(mvd_10[mbPartIdx][0][compIdx], se(v) | ae(v))
for (mbPartIdx = 0; mbPartIdx < NumMbPart(u_mb_type); mbPartIdx++)
if (MbPartPredMode(u_mb_type,
                  mbPartIdx,
                  transform_size_8x8_flag) !=
MbPartPredModes.Pred_L0)
for (compIdx = 0; compIdx < 2; compIdx++)
    read(mvd_11[mbPartIdx][0][compIdx], se(v) | ae(v))

# 7.3.5.2 Sub-macroblock prediction syntax
sub_mb_pred[category = 2](u_mb_type)
for (mbPartIdx = 0; mbPartIdx < 4; mbPartIdx++)
    read(sub_mb_type[mbPartIdx], ue(v) | ae(v))

# Not from the standard. Derive an unambiguous sub_mb_type.
assign(u_sub_mb_type[mbPartIdx],
    GetUniqueSubMbTypeFromSubMbType(u_mb_type,
```

```

sub_mb_type[mbPartIdx]))
for (mbPartIdx = 0; mbPartIdx < 4; mbPartIdx++)
  if ((num_ref_idx_l0_active_minus1 > 0 ||
      mb_field_decoding_flag != field_pic_flag) &&
      u_mb_type != MbTypes.P_8X8Ref0 &&
      u_sub_mb_type[mbPartIdx] != SubMbTypes.B_Direct_8X8 &&
      SubMbPredMode(u_sub_mb_type[mbPartIdx]) !=
      SubMbPredModes.Pred_L1)
    read(ref_idx_l0[mbPartIdx],
        te(v, bit_count(2 * num_ref_idx_l0_active_minus1 + 1
            if MbaffFrameFlag == 1 &&
                mb_field_decoding_flag == 1 else
                num_ref_idx_l0_active_minus1)) | ae(v))
for (mbPartIdx = 0; mbPartIdx < 4; mbPartIdx++)
  if (SubMbPredMode(u_sub_mb_type[mbPartIdx]) !=
      SubMbPredModes.Pred_L0 &&
      u_sub_mb_type[mbPartIdx] != SubMbTypes.B_Direct_8X8 &&
      (num_ref_idx_l1_active_minus1 > 0 ||
      mb_field_decoding_flag != field_pic_flag))
    read(ref_idx_l1[mbPartIdx],
        te(v, bit_count(2 * num_ref_idx_l1_active_minus1 + 1
            if MbaffFrameFlag == 1 &&
                mb_field_decoding_flag == 1 else
                num_ref_idx_l1_active_minus1)) | ae(v))
for (mbPartIdx = 0; mbPartIdx < 4; mbPartIdx++)
  if (u_sub_mb_type[mbPartIdx] != SubMbTypes.B_Direct_8X8 &&
      SubMbPredMode(u_sub_mb_type[mbPartIdx]) !=
      SubMbPredModes.Pred_L1)
    for (subMbPartIdx = 0;
        subMbPartIdx < NumSubMbPart(u_sub_mb_type[mbPartIdx]);
        subMbPartIdx++)
      for (compIdx = 0; compIdx < 2; compIdx++)
        read(mvd_10[mbPartIdx][subMbPartIdx][compIdx],
            se(v) | ae(v))
for (mbPartIdx = 0; mbPartIdx < 4; mbPartIdx++)
  if (u_sub_mb_type[mbPartIdx] != SubMbTypes.B_Direct_8X8 &&
      SubMbPredMode(u_sub_mb_type[mbPartIdx]) !=
      SubMbPredModes.Pred_L0)
    for (subMbPartIdx = 0;
        subMbPartIdx < NumSubMbPart(u_sub_mb_type[mbPartIdx]);
        subMbPartIdx++)
      for (compIdx = 0; compIdx < 2; compIdx++)
        read(mvd_11[mbPartIdx][subMbPartIdx][compIdx],
            se(v) | ae(v))

```

Residual data syntax [45, Subclause 7.3.5.3, residual data syntax] and associated syntax

```

# 7.3.5.3 Residual data syntax
residual[category = 3|4](startIdx, endIdx)
# Set the component index explicitly for context calculation.
assign(iCbCr, 2)
residual_luma(i16x16DClevel, i16x16AClevel, level, level8x8,
             startIdx, endIdx)
assign(Intra16x16DClevel, i16x16DClevel)
assign(Intra16x16AClevel, i16x16AClevel)
assign(LumaLevel, level)
assign(LumaLevel8x8, level8x8)
if (ChromaArrayType == 1 || ChromaArrayType == 2)
    assign(NumC8x8, 4 / (SubWidthC * SubHeightC))
    for (iCbCr = 0; iCbCr < 2; iCbCr++)
        if ((CodedBlockPatternChroma & 3) && startIdx == 0)
            if (entropy_coding_mode_flag == 0)
                # Chroma DC level
                assign(nC, GetCoeffTokenNc(CtxBlockCats.ChromaDCLevel))
                residual_block_cavlc(ChromaDCLevel[iCbCr], 0,
                                   4 * NumC8x8 - 1, 4 * NumC8x8)
            else
                residual_block_cabac(ChromaDCLevel[iCbCr], 0,
                                   4 * NumC8x8 - 1, 4 * NumC8x8)
        else
            for (i = 0; i < 4 * NumC8x8; i++)
                assign(ChromaDCLevel[iCbCr][i], 0)
    for (iCbCr = 0; iCbCr < 2; iCbCr++)
        for (i8x8 = 0; i8x8 < NumC8x8; i8x8++)
            for (i4x4 = 0; i4x4 < 4; i4x4++)
                if ((CodedBlockPatternChroma & 2) && endIdx > 0)
                    if (entropy_coding_mode_flag == 0)
                        # Chroma AC level
                        assign(nC,
                            GetCoeffTokenNc(CtxBlockCats.ChromaACLevel))
                        residual_block_cavlc(
                            ChromaACLevel[iCbCr][i8x8 * 4 + i4x4],
                            max(0, startIdx - 1), endIdx - 1, 15)
                    else
                        residual_block_cabac(
                            ChromaACLevel[iCbCr][i8x8 * 4 + i4x4],
                            max(0, startIdx - 1), endIdx - 1, 15)
                else
                    for (i = 0; i < 15; i++)

```



```

        assign(ChromaACLevel[iCbCr][i8x8 * 4 + i4x4][i], 0)
else if (ChromaArrayType == 3)
    # Set explicitly for context calculation.
    assign(iCbCr, 0)
    residual_luma(i16x16DClevel, i16x16AClevel,
                 level, level8x8, startIdx, endIdx)
    assign(CbIntra16x16DClevel, i16x16DClevel)
    assign(CbIntra16x16AClevel, i16x16AClevel)
    assign(CbLevel, level)
    assign(CbLevel8x8, level8x8)

    # Set explicitly for context calculation.
    assign(iCbCr, 1)
    residual_luma(i16x16DClevel, i16x16AClevel,
                 level, level8x8, startIdx, endIdx)
    assign(CrIntra16x16DClevel, i16x16DClevel)
    assign(CrIntra16x16AClevel, i16x16AClevel)
    assign(CrLevel, level)
    assign(CrLevel8x8, level8x8)

# 7.3.5.3.1 Residual luma syntax
residual_luma(i16x16DClevel, i16x16AClevel, level, level8x8,
              startIdx, endIdx)
if (startIdx == 0 &&
    MbPartPredMode(u_mb_type, 0, transform_size_8x8_flag) ==
    MbPartPredModes.Intra_16x16)
    if (entropy_coding_mode_flag == 0)
        # Intra 16x16 DC level
        assign(nC,
              GetCoeffTokenNc(CtxBlockCats.iCbCrIntra16x16DClevel))
        residual_block_cavlc[category = 3](i16x16DClevel, 0, 15, 16)
    else
        residual_block_cabac[category = 3](i16x16DClevel, 0, 15, 16)
for (i8x8 = 0; i8x8 < 4; i8x8++)
    if (transform_size_8x8_flag == 0 ||
        entropy_coding_mode_flag == 0)
        for (i4x4 = 0; i4x4 < 4; i4x4++)
            if ((CodedBlockPatternLuma & (1 << i8x8)) != 0)
                if (endIdx > 0 &&
                    MbPartPredMode(u_mb_type, 0,
                                   transform_size_8x8_flag) ==
                    MbPartPredModes.Intra_16x16)
                    if (entropy_coding_mode_flag == 0)
                        # Intra 16x16 AC level
                        assign(nC, GetCoeffTokenNc(

```

```

        CtxBlockCats.iCbCrIntra16x16AClevel))
    residual_block_cavlc [category = 3](
        i16x16AClevel[i8x8 * 4 + i4x4],
        max(0, startIdx - 1), endIdx - 1, 15)
    else
        residual_block_cabac [category = 3](
            i16x16AClevel[i8x8 * 4 + i4x4],
            max(0, startIdx - 1), endIdx - 1, 15)
    else
        if (entropy_coding_mode_flag == 0)
            # Luma/Cb/Cr level
            assign(nC, GetCoeffTokenNc(CtxBlockCats.iCbCrLevel))
            residual_block_cavlc [category = 3|4](
                level[i8x8 * 4 + i4x4], startIdx, endIdx, 16)
        else
            residual_block_cabac [category = 3|4](
                level[i8x8 * 4 + i4x4], startIdx, endIdx, 16)
    else if (MbPartPredMode(u_mb_type,
        0, transform_size_8x8_flag) ==
        MbPartPredModes.Intra_16x16)
        for (i = 0; i < 15; i++)
            assign(i16x16AClevel[i8x8 * 4 + i4x4][i], 0)
    else
        for (i = 0; i < 16; i++)
            assign(level[i8x8 * 4 + i4x4][i], 0)
    if (entropy_coding_mode_flag == 0 &&
        transform_size_8x8_flag)
        for (i = 0; i < 16; i++)
            assign(level8x8[i8x8][4 * i + i4x4],
                level[i8x8 * 4 + i4x4][i])
    else if (CodedBlockPatternLuma & (1 << i8x8))
        if (entropy_coding_mode_flag == 0)
            # Level 8x8
            assign(nC, GetCoeffTokenNc(CtxBlockCats.iCbCrLevel8x8))
            residual_block_cavlc [category = 3|4](level8x8[i8x8],
                4 * startIdx, 4 * endIdx + 3, 64)
        else
            residual_block_cabac [category = 3|4](level8x8[i8x8],
                4 * startIdx, 4 * endIdx + 3, 64)
    else
        for (i = 0; i < 64; i++)
            assign(level8x8[i8x8][i], 0)

```

Residual block CAVLC syntax [45, Subclause 7.3.5.3.2, residual block CAVLC syntax]

```
# 7.3.5.3.2 Residual block CAVLC syntax
residual_block_cavlc[category = 3|4](coeffLevel, startIdxBlock,
                                     endIdxBlock, maxNumCoeff)

assign(coeffLevel, {})
assign(levelB, {})

for (i = 0; i < maxNumCoeff; i++)
    assign(coeffLevel[i], 0)

# This read requires nC to be set.
read(coeff_token, ce(v))
assign(total_coeff, GetTotalCoeff(coeff_token))
assign(trailing_ones, GetTrailingOnes(coeff_token))

# Cache total_coeff for context-adaptive reads later.
assign(context_total_coeff[
    CurrMbAddr * 16 * 3 + iCbCr * 16 + CurrentBlockIndex],
    total_coeff)

if (total_coeff > 0)
    if (total_coeff > 10 && trailing_ones < 3)
        assign(suffixLength, 1)
    else
        assign(suffixLength, 0)

for (i = 0; i < total_coeff; i++)
    if (i < trailing_ones)
        read(trailing_ones_sign_flag, u(1))
        assign(levelB[i], 1 - 2 * trailing_ones_sign_flag)
    else
        read(level_prefix, ce(v))
        assign(levelCode, (min(15, level_prefix) << suffixLength))

# Derive levelSuffixSize (9.2.2)
if (level_prefix == 14 && suffixLength == 0)
    assign(levelSuffixSize, 4)
else if (level_prefix >= 15)
    assign(levelSuffixSize, level_prefix - 3)
else
    assign(levelSuffixSize, suffixLength)

if (suffixLength > 0 || level_prefix >= 14)
```

B. H.264/AVC bitstream syntax

```

    if (levelSuffixSize > 0)
        read(level_suffix, u(v, bit_count(levelSuffixSize)))
    else
        assign(level_suffix, 0)
        assign(levelCode, levelCode + level_suffix)
    if (level_prefix >= 15 && suffixLength == 0)
        assign(levelCode, levelCode + 15)
    if (level_prefix >= 16)
        assign(levelCode, levelCode +
            (1 << (level_prefix - 3)) - 4096)
    if (i == trailing_ones && trailing_ones < 3)
        assign(levelCode, levelCode + 2)
    if (levelCode % 2 == 0)
        assign(levelB[i], (levelCode + 2) >> 1)
    else
        assign(levelB[i], (-levelCode - 1) >> 1)
    if (suffixLength == 0)
        assign(suffixLength, 1)
    if (abs(levelB[i]) > (3 << (suffixLength - 1)) &&
        suffixLength < 6)
        suffixLength++
    if (total_coeff < endIdxBlock - startIdxBlock + 1)
        read(total_zeros, ce(v))
        assign(zerosLeft, total_zeros)
    else
        assign(zerosLeft, 0)

    for (i = 0; i < total_coeff - 1; i++)
        if (zerosLeft > 0)
            read(run_before, ce(v, require(range(0, zerosLeft))))
            assign(run[i], run_before)
            assign(zerosLeft, zerosLeft - run_before)
        else
            assign(run[i], 0)

    assign(run[total_coeff - 1], zerosLeft)
    assign(coeffNum, -1)
    for (i = total_coeff - 1; i >= 0; i--)
        assign(coeffNum, coeffNum + run[i] + 1)
        assign(coeffLevel[startIdxBlock + coeffNum], levelB[i])

```

Bibliography

- [1] Stefano Barbato. ‘Recover’ utility.
<http://codesink.org/recover.html>.
- [2] Heinz H. Bauschke, Christopher H. Hamilton, Mason S. Macklem, Justin S. McMichael, and Nicholas R. Swart. Recompression of JPEG images by requantization. *IEEE Transactions on Image Processing*, 12(7):843–849, 2003.
- [3] Bryce E. Bayer. An optimum method for two-level rendition of continuous-tone pictures. *IEEE International Conference on Communications*, 1:11–15, 1973.
- [4] Frank Benford. The law of anomalous numbers. *Proceedings of the American Philosophical Society*, 78(4):551–572, 1938.
- [5] Joeri Blokhuis and Axel Puppe. DFRWS challenge 2010 – mobile forensics entry. Technical report, University of Amsterdam, July 2010.
- [6] Marcel Breeuwsma, Martien de Jongh, Coert Klaver, Ronald van der Knijff, and Mark Roeloffs. Forensic data recovery from flash memory. *Small Scale Digital Device Forensics Journal*, 1(1):1–17, 2007.
- [7] Brian Carrier. *File system forensic analysis*. Addison-Wesley Professional, 2005.
- [8] Eoghan Casey and Brian Carrier. Digital forensics research workshop.
<http://www.dfrws.org/>.
- [9] Mo Chen, Jessica Fridrich, and Miroslav Goljan. Digital imaging sensor identification (further study). *Proceedings of the SPIE: Security, Steganography, and Watermarking of Multimedia Contents*, 6505, February 2007.
- [10] John G. Cleary and Ian H. Witten. Data compression using adaptive coding and partial string matching. *IEEE Transactions on Communications*, 32(4):396–402, April 1984.
- [11] Video coding experts group. ITU-T recommendation H.264.2: Reference software for H.264 advanced video coding (JM reference software).
<http://www.itu.int/rec/T-REC-H.264.2/en>.

Bibliography

- [12] Michael I. Cohen. Advanced carving techniques. *Journal of Digital Investigation*, 4(3-4):119–128, 2007.
- [13] Michael I. Cohen. Advanced JPEG carving. *Proceedings of the 1st international conference on forensic applications and techniques in telecommunications, information, and multimedia*, pages 1–6, 2008.
- [14] Ingemar J. Cox, Matthew L. Miller, Jeffrey A. Bloom, Jessica Fridrich, and Ton Kalker. *Digital watermarking and steganography*. Morgan Kaufmann, 2008.
- [15] DataRescue. ‘PhotoRescue’ utility.
<http://www.datarescue.com/photorescue/>.
- [16] EASEUS. ‘EASEUS JPG/JPEG/PNG recovery’ utility.
<http://www.easeus.com/resource/jpg-jpeg-png-recovery-software.htm>.
- [17] Erik Reinhard, Erum Arif Khan, Ahmet Oğuz Akyüz, and Garrett M. Johnson. *Color Imaging: Fundamentals and Applications*. A K Peters/CRC Press, July 2008.
- [18] ETSI. 3GPP TS 26.244; Transparent end-to-end packet switched streaming service (PSS); 3GPP file format (3GP).
- [19] Zhigang Fan and Ricardo L. de Queiroz. Identification of bitmap compression history: JPEG detection and quantizer estimation. *IEEE Transactions on Image Processing*, 12(2):230–235, February 2003.
- [20] Hany Farid. Digital image ballistics from JPEG quantization. Technical Report TR2006-583, Department of Computer Science, Dartmouth College, 2006.
- [21] Hany Farid. Digital image ballistics from JPEG quantization: a followup study. Technical Report TR2008-638, Department of Computer Science, Dartmouth College, 2008.
- [22] Hany Farid. Exposing digital forgeries from JPEG ghosts. *IEEE Transactions on Information Forensics and Security*, 4(1):154–160, 2009.
- [23] Jessica Fridrich, Miroslav Goljan, and Rui Du. Steganalysis based on JPEG compatibility. *Proceedings of the SPIE: Multimedia Systems and Applications*, 4518:275–280, November 2001.
- [24] Dongdong Fu, Yun Q. Shi, and Wei Su. A generalized Benford’s law for JPEG coefficients and its applications in image forensics. *Proceedings of the SPIE: Security, Steganography, and Watermarking of Multimedia Contents*, 2007.
- [25] Eran Gal and Sivan Toledo. Algorithms and data structures for flash memories. *ACM Computing Surveys*, 37:2005, 2005.

- [26] Andrew C. Gallagher and Tsuhan Chen. Image authentication by detecting traces of demosaicing. *IEEE Computer Vision and Pattern Recognition Workshops (CVPRW)*, pages 1–8, 2008.
- [27] Simson L. Garfinkel. Forensic feature extraction and cross-drive analysis. *Journal of Digital Investigation*, 3:71–81, 2006.
- [28] Simson L. Garfinkel. Carving contiguous and fragmented files with fast object validation. *Journal of Digital Investigation*, 4:2–12, 2007.
- [29] Jason Garrett-Glaser. Flash, Google, VP8, and the future of internet video.
<http://x264dev.multimedia.cx/archives/292>.
- [30] Zeno Geradts and Rikkert Zoun. ‘Defraser’ utility.
<http://sourceforge.net/projects/defraser/>.
- [31] Miroslav Goljan, Jessica Fridrich, and Tomáš Filler. Large scale test of sensor fingerprint camera identification. *Proceedings of the SPIE: Media Forensics and Security*, 7254, February 2009.
- [32] Vivek K. Goyal. Theoretical foundations of transform coding. *IEEE Signal Processing Magazine*, 18(5):9–21, 2001.
- [33] Calvin Hass. ImpulseAdventure – JPEG compression quality from quantization tables.
<http://www.impulseadventure.com/photo/jpeg-quantization.html>.
- [34] Jürgen Herre. Content based identification (fingerprinting). *Lecture Notes in Computer Science 2770: Digital Rights Management*, pages 93–100, 2003.
- [35] Nicholas Zhong-Yang Ho and Ee-Chien Chang. Residual information of redacted images hidden in the compression artifacts. *Lecture Notes in Computer Science 5284: Information Hiding*, pages 87–101, 2008.
- [36] Golden G. Richard III. ‘Scalpel’ utility.
<http://www.digitalforensicssolutions.com/Scalpel/>.
- [37] Adobe Systems Incorporated. Adobe Photoshop CS2 program.
<http://www.adobe.com/products/photoshop>.
- [38] ISO/IEC. Digital compression and coding of continuous-tone still images: Requirements and guidelines, ITU-T recommendation T.81, ISO/IEC 10918-1, 1994.
- [39] ISO/IEC. Digital compression and coding of continuous-tone still images: Compliance testing, ITU-T recommendation T.83, ISO/IEC 10918-2, 1995.
- [40] ISO/IEC. MP4 file format, ISO/IEC 14496-14, 2003.

Bibliography

- [41] ISO/IEC. MPEG-4 Part 2: Visual, ISO/IEC 14496-2, 2004.
- [42] ISO/IEC. ISO base media file format, ISO/IEC 14496-12, 2008.
- [43] ISO/IEC. Advanced Video Coding (AVC) file format, ISO/IEC 14496-15, May 2010.
- [44] ISO/IEC. JPEG file interchange format, ISO/IEC FCD 10918-5, 2011.
- [45] ITU ISO/IEC. Advanced video coding for generic audiovisual services, ITU-T recommendation H.264, ISO/IEC 14496-10 Advanced Video Coding, 2010.
- [46] ITU. Studio encoding parameters of digital television for standard 4:3 and wide screen 16:9 aspect ratios, ITU-R recommendation BT.601, 1982.
- [47] JEITA. Exchangeable image file format for digital still cameras: Exif version 2.2, JEITA CP-3451, 2002.
- [48] Martin Karresand and Nahid Shahmehri. Oscar – file type identification of binary data in disk clusters and RAM pages. *Security and Privacy in Dynamic Environments*, pages 413–424, 2006.
- [49] Martin Karresand and Nahid Shahmehri. Reassembly of fragmented JPEG images containing restart markers. *European Conference on Computer Network Defense*, pages 25–32, 2008.
- [50] Andrew D. Ker. Resampling and the detection of LSB matching in colour bitmaps. *Proceedings of the SPIE: Security, Steganography, and Watermarking of Multimedia Contents*, 5681, March 2005.
- [51] Matthias Kirchner. Fast and reliable resampling detection by spectral analysis of fixed linear predictor residue. *ACM Multimedia and Security Workshop*, 2008.
- [52] Jesse Kornblum and Kris Kendall. ‘Foremost’ utility.
<http://foremost.sourceforge.net/>.
- [53] Jesse D. Kornblum. Using JPEG quantization tables to identify imagery processed by software. *Journal of Digital Investigation*, 5(Supplement 1):S21–S25, 2008.
- [54] Neal Krawetz. The hacker factor blog.
<http://www.hackerfactor.com/blog/>.
- [55] Neal Krawetz. A picture’s worth... *Black Hat Briefings USA*, 2007.
- [56] Markus G. Kuhn. Compromising emanations: eavesdropping risks of computer displays. Technical Report UCAM-CL-TR-577, University of Cambridge, Computer Laboratory, December 2003.

- [57] Thomas G. Lane. Independent JPEG Group library.
<http://www.ijg.org>.
- [58] Andrew B. Lewis. JPEG canaries: exposing on-the-fly recompression.
<http://www.lightbluetouchpaper.org/2011/02/04/jpeg-copy-evidence/>.
- [59] Andrew B. Lewis and Markus G. Kuhn. Towards copy-evident JPEG images. *Lecture Notes in Informatics*, P154:171; 1582–91, 2009.
- [60] Andrew B. Lewis and Markus G. Kuhn. Exact JPEG recompression. *Proceedings of the SPIE: Visual Information Processing and Communication*, 7543:27, 2010.
- [61] Bin Li, Yun Q. Shi, and Jiwu Huang. Detecting doubly compressed JPEG images by using mode based first digit features. *IEEE Workshop on Multimedia Signal Processing*, pages 730–735, 2008.
- [62] Weihai Li, Nenghai Yu, and Yuan Yuan. Doctored JPEG image detection. *Proceedings of the IEEE International Conference on Multimedia and Expo (ICME)*, pages 253–256, 2008.
- [63] Weihai Li, Yuan Yuan, and Nenghai Yu. Detecting copy-paste forgery of JPEG image via block artifact grid extraction. *Proceedings of the International Workshop on Local and Non-Local Approximation in Image Processing*, pages 121–126, 2008.
- [64] Weihai Li, Yuan Yuan, and Nenghai Yu. Passive detection of doctored JPEG image via block artifact grid extraction. *Signal Processing (EURASIP)*, 89(9):1821–1829, 2009.
- [65] Ching-Yung Lin and Shih-Fu Chang. A robust image authentication method surviving JPEG lossy compression. *Proceedings of the SPIE: Storage and Retrieval of Image/Video Databases*, 3312, 1998.
- [66] Zhouchen Lin, Junfeng He, Xiaoou Tang, and Chi-Keung Tang. Fast, automatic and fine-grained tampered JPEG image detection via DCT coefficient analysis. *Pattern Recognition (Pattern Recognition Society)*, 42(11):2492–2501, 2009.
- [67] Christoph Loeffler, Adriaan Ligtenberg, and George S. Moschytz. Practical fast 1-D DCT algorithms with 11 multiplications. *IEEE International Conference on Acoustics, Speech and Signal Processing*, 2:988–991, May 1989.
- [68] J. Luck and M. Stokes. An integrated approach to recovering deleted files from NAND flash data. *Small Scale Digital Device Forensics Journal*, 2(1):1941–6164, 2008.
- [69] Jan Lukáš, Jessica Fridrich, and Miroslav Goljan. Digital camera identification from sensor pattern noise. *IEEE Transactions on Information Forensics and Security*, 1(2):205–214, 2006.

Bibliography

- [70] Weiqi Luo, Jiwu Huang, and Guoping Qiu. JPEG error analysis and its applications to digital image forensics. *IEEE Transactions on Information Forensics and Security*, 5(3):480–491, September 2010.
- [71] David J. C. MacKay. *Information theory, inference, and learning algorithms*. Cambridge University Press, 2003.
- [72] Peter Mattis, Spencer Kimball, Manish Singh, et al. GNU image manipulation program. <http://www.gimp.org>.
- [73] Mason McDaniel and M. Hossain Heydari. Content based file type detection algorithms. *Hawaii International Conference on System Sciences (HICSS'03)*, 2003.
- [74] Mike Melanson. Google's YouTube uses FFmpeg. <http://multimedia.cx/eggs/googles-youtube-uses-ffmpeg/>.
- [75] Ramesh Neelamani, Ricardo L. de Queiroz, Zhigang Fan, and Richard Baraniuk. JPEG compression history estimation for color images. *Proceedings of the IEEE International conference on Image Processing (ICIP)*, 3:245–248, September 2003.
- [76] Anandabrata Pal and Nasir D. Memon. The evolution of file carving. *IEEE Signal Processing Magazine*, 26(2):59–71, 2009.
- [77] Anandabrata Pal, Husrev T. Sencar, and Nasir D. Memon. Detecting file fragmentation point using sequential hypothesis testing. *Journal of Digital Investigation*, 5:S2–S13, 2008.
- [78] Fabien A. Petitcolas. Watermarking schemes evaluation. *IEEE Signal Processing Magazine*, 17(5):58–64, 2002.
- [79] Fabien A. Petitcolas, Ross J. Anderson, and Markus G. Kuhn. Attacks on copyright marking systems. *Lecture Notes in Computer Science 1525: Information Hiding*, pages 218–238, 1998.
- [80] Fabien A. Petitcolas, Ross J. Anderson, and Markus G. Kuhn. Information hiding – a survey. *Proceedings of the IEEE, special issue on protection of multimedia content*, 87(7):1062–1078, July 1999.
- [81] Tomáš Pevný and Jessica Fridrich. Detection of double-compression in JPEG images for applications in steganography. *IEEE Transactions on Information Forensics and Security*, 3(2):247–258, 2008.
- [82] Alessandro Piva and Mauro Barni. The first BOWS contest: break our watermarking system. *Proceedings of the SPIE: Security, Steganography, and Watermarking of Multimedia Contents*, 6505, February 2007.

- [83] Better JPEG plug in. Lossless resave plug-in for Adobe Photoshop and Adobe Photoshop Elements.
<http://www.betterjpeg.com/jpeg-plug-in.htm>.
- [84] Marie-Charlotte Poilpré, Patrick Perrot, and Hugues Talbot. Image tampering detection using Bayer interpolation and JPEG compression. *e-Forensics 2008*, 2008.
- [85] Alin C. Popescu and Hany Farid. Statistical tools for digital forensics. *Lecture Notes in Computer Science 3200: Information Hiding*, pages 128–147, 2004.
- [86] Alin C. Popescu and Hany Farid. Exposing digital forgeries in color filter array interpolated images. *IEEE Transactions on Signal Processing*, 53(10):3948–3959, 2005.
- [87] Zhenhua Qu, Weiqi Luo, and Jiwu Huang. A convolutive mixing model for shifted double JPEG compression with application to passive image authentication. *IEEE International Conference on Acoustics, Speech and Signal Processing*, pages 1661–1664, 2008.
- [88] Carlos Salazar and Trac D. Tran. A complexity scalable universal DCT domain image resizing algorithm. *IEEE Transactions on Circuits and Systems for Video Technology*, 17(4):495–499, April 2007.
- [89] David Salomon. *Data compression: the complete reference (4th edition)*. Springer, 2007.
- [90] Gerald Schaefer and Michal Stich. UCID – an uncompressed colour image database. *Storage and Retrieval Methods and Applications for Multimedia 2004*, 5307:472–480, 2004.
- [91] Mathias Schlauweg, Torsten Palfner, Dima Pröfrock, and Erika Müller. The Achilles’ heel of JPEG-based image authentication. *Proceedings of the International Conference on Communication, Network and Information Security*, 499:1–6, 2005.
- [92] Sijbrand Spanenburg. Optically and machine-detectable copying security elements. *Proceedings of SPIE: Conference on Optical Security and Counterfeit Deterrence Techniques*, 2659:76–96, 1996.
- [93] Sijbrand Spanenburg. Developments in digital document security. *Proceedings of the SPIE: Conference on Optical Security and Counterfeit Deterrence Techniques*, 3973:88–98, January 2000.
- [94] Matthew C. Stamm, Steven K. Tjoa, W. Sabrina Lin, and K. J. Ray Liu. Anti-forensics of JPEG compression. *IEEE International Conference on Acoustics, Speech and Signal Processing (ICASSP)*, pages 1694–1697, 2010.
- [95] Jian Sun, Lu Yuan, Jiaya Jia, and Heung-Yeung Shum. Image completion with structure propagation. *ACM Transactions on Graphics (TOG)*, 24(3):861–868, 2005.

Bibliography

- [96] Luca Superiori, Olivia Nemethova, and Markus Rupp. Performance of a H.264/AVC error detection algorithm based on syntax analysis. *Journal of mobile multimedia*, 3(1):314–330, March 2007.
- [97] Andrey N. Tikhonov and Vasiliy Y. Arsenin. *Solutions of ill-posed problems*. V. H. Winston & Sons, Washington D.C., 1977.
- [98] Ronald van der Knijff (Netherlands Forensic Institute). 10 good reasons why you should shift focus to small scale digital device forensics. DFRWS 2007.
- [99] Rudolf L. van Renesse. Hidden and scrambled images – a review. *Proceedings of the SPIE: Conference on Optical Security and Counterfeit Deterrence Techniques*, 4677:333–348, January 2002.
- [100] Rudolf L. van Renesse, editor. *Optical Document Security*. Artech House, 3rd edition, 2005.
- [101] X-pire! GmbH. ‘X-pire’ website.
<http://www.x-pire.de/>.
- [102] Shuiming Ye, Qibin Sun, and Ee-Chien Chang. Detecting digital image forgeries by measuring inconsistencies of blocking artifact. *Proceedings of the IEEE International Conference on Multimedia and Expo*, pages 12–15, 2007.
- [103] Bin B. Zhu, Jeff Yan, Qiuji Li, Chao Yang, Jia Liu, Ning Xu, Meng Yi, and Kaiwei Cai. Attacks and design of image recognition CAPTCHAs. *Proceedings of the 17th ACM conference on computer and communications security*, pages 187–200, 2010.